Universidade de Aveiro
Departamento de
Eletrónica, Telecomunicações e Informática
2016

Ricardo Dias
Fernandes

Transmissão de Energia sem Fios Baseada em Acoplamento Elétrico Ressonante

Ricardo Dias
Fernandes

Transmissão de Energia sem Fios Baseada em Acoplamento Elétrico Ressonante

Wireless Power Transmission Based on Resonant Electrical Coupling

Tese apresentada à Universidade de Aveiro para cumprimento dos requisitos necessários à obtenção do grau de Doutor em Engenharia Eletrotécnica, realizada sob a orientação científica do Doutor Nuno Miguel Gonçalves Borges de Carvalho, Professor Catedrático do Departamento de Eletrónica, Telecomunicações e Informática da Universidade de Aveiro, e sob a co-orientação científica do Doutor João Nuno Pimentel da Silva Matos, Professor Associado do Departamento de Eletrónica, Telecomunicações e Informática da Universidade de Aveiro.

Apoio financeiro da Fundação para a Ciência e a Tecnologia (FCT), no âmbito da bolsa de doutoramento com a referência SFRH/BD/69392/2010.

O júri

presidente

Doutor Casimiro Adrião Pio
Professor Catedrático da Universidade de Aveiro

vogais

Doutor Mateo Burgos Garcìa
Professor Catedrático, Departamento de Señales Sistemas y Radiocomunicaciones, Universidade Politécnica de Madrid - Espanha

Doutor Rafael Ferreira da Silva Caldeirinha
Professor Coordenador, Departamento de Engenharia Eletrotécnica, Escola Superior de Tecnologia e Gestão do Instituto Politécnico de Leiria

Doutor João Nuno Pimentel da Silva Matos
Professor Associado da Universidade de Aveiro (co-orientador)

Doutor Rui Manuel Escadas Ramos Martins
Professor Auxiliar da Universidade de Aveiro

Doutor Luís Manuel de Sousa Pessoa
Investigador, INESC TEC - Instituto de Engenharia de Sistemas e Computadores - Tecnologia e Ciência, Porto

Agradecimentos

Aos meus orientadores, prof. Nuno Borges Carvalho e prof. João Nuno Matos, pela atitude positiva e incentivo, e pelas muitas oportunidades que tive nos últimos anos, em particular a visita à Universidade do Colorado, Boulder,
à prof. Zoya Popović pela orientação nessa visita,
aos colegas de grupo em Aveiro e em Boulder,
ao Instituto de Telecomunicações,
ao Departamento de Eletrónica, Telecomunicações e Informática e à Universidade de Aveiro,
à ação COST IC1301,
à Fundação para a Ciência e a Tecnologia (FCT),
ao Luís Rodrigues,
à Ana Azevedo e ao Bruno Andrade,
aos meus padrinhos,
à minha mãe,
ao meu pai (1949 - 2015),
e em especial à Carina,
o meu mais sincero obrigado.

Palavras-chave

Transmissão de energia sem fios, ressonância, acoplamento capacitivo ressonante, acoplamento elétrico ressonante, acoplamento híbrido ressonante, acoplamento indutivo, acoplamento magnético ressonante.

Resumo

Contidos neste documento estão resultados teóricos e experimentais relacionados com a viabilidade do uso de acoplamento elétrico ressonante como um método de transferência de energia sem fios através de distâncias não negligenciáveis. Conforme mostrado, o acoplamento elétrico ressonante é notavelmente semelhante ao acoplamento magnético ressonante em vários aspetos. No entanto, enquanto que o acoplamento magnético ressonante é atualmente um método de transferência de energia sem fios com uma presença muito forte na literatura, o acoplamento elétrico ressonante não é. A ausência de material relacionado com acoplamento elétrico ressonante, em conjunto com o potencial de atingir um compromisso equilibrado entre características críticas, tais como eficiência, distância, simplicidade, tamanho e capacidade de transferência de potência, foram as principais motivações para considerar este tópico específico. A possibilidade de combinar de forma construtiva acoplamento elétrico ressonante e acoplamento magnético ressonante é também abordada. Uma revisão do estado da arte da transferência de energia sem fios, não só em termos de publicações científicas, mas também em termos de adoção do mercado e normas internacionais, é incluída neste documento.

Keywords Wireless power transfer, resonance, resonant capacitive coupling, resonant electrical coupling, resonant hybrid coupling, inductive coupling, resonant magnetic coupling.

Abstract Contained in this document are theoretical and experimental results related to the feasibility of resonant electrical coupling as a method of wirelessly transferring power across non-negligible distances. As shown, resonant electrical coupling is remarkably similar to resonant magnetic coupling in several aspects. However, while resonant magnetic coupling is currently a method of wirelessly transferring power with a very strong presence in the literature, resonant electrical coupling is not. The lack of material related to resonant electrical coupling, together with the potential of achieving a balanced trade-off between critical features such as efficiency, distance, simplicity, size and power transfer capability, were the main motivations for considering this specific topic. The possibility of constructively combining resonant electrical coupling and resonant magnetic coupling is also addressed. A review of the state of the art of wireless power, not only in terms of scientific publications but also in terms of market adoption and international standards, is included in this document.

Contents

List of Figures

List of Tables

Chapter 1

Introduction and objectives

1.1 Summary

One of the most desirable attributes in wireless power transfer is distance. After all, spatial freedom is what makes wireless power truly wireless. Significant progress was made in this aspect just a few years ago, with the use of strongly coupled magnetic resonances. A distance of up to several times the dimensions of the devices involved can be achieved with this technology. This was an extremely important breakthrough. Unsurprisingly, many papers in the literature are based on strongly coupled magnetic resonances directly or indirectly. Most of the papers listed in the literature review included in chapter 2 are based on strongly coupled magnetic resonances, for instance. In contrast, only a few publications related to the use of electrical resonance for wireless power transfer currently exist in the literature. Capacitive coupling is generally perceived as something useful at very short distances but not more than that. Contained in this document is a study of the potential use of electrical resonance for the transfer of power across non-negligible distances, performed with the main goal of achieving results in the order of those obtained with resonant magnetic coupling. An analysis of the circuit that is currently most widely used to represent strongly coupled magnetic resonances is given in chapter 3. A similar analysis is presented in chapter 4 for resonant electrical coupling. Furthermore, the possible constructive combination of electrical and magnetic resonances is also considered in the same chapter. A proof of concept of resonant electrical coupling is presented in chapter 5. Most of the material contained in chapters 4 and 5 is published in [1], [2], [3] and [4]. A summary of each one of these papers is given in the next section of this chapter, immediately after this introductory text. A brief description of the technologies most often considered in wireless power transfer is presented afterwards.

1.2 Contributions

In following list of papers, [1], [2], [3] and [4] are directly related to electrical resonance. The subject of [5] and [6] is ultra-wide band pulse generation. The subject of [7] and [8] is the design of a battery-free programmable RFID tag. Lastly, [9] and [10] are related to the generation of signals with high peak-to-average power ratios.

[1] Most of the results presented in chapters 3, 4 and 5 are also in the paper "Resonant Electrical Coupling: Circuit Model and First Experimental Results", in a more condensed form. This paper is an extension of [2], in which novel experimental results obtained with an RF-to-DC converter and a comparison between electrical resonance and magnetic resonance are added and some parts of the analytical analysis of resonant electrical coupling are simplified. The most important aspect in this paper is the practical demonstration of wireless power transfer based on resonant electrical coupling across non-negligible distances and considering non-optimal orientations.

[2], [3] The first relevant results achieved in the study of electrical resonance are published in the papers "Behavior of resonant electrical coupling in terms of range and relative orientation" and "Wireless Power Transmission Based on Resonant Electrical Coupling". These papers contain an analysis of the circuit model considered for resonant electrical coupling and some preliminary experimental results obtained with a network analyzer. The most important aspect in these papers is the use of resonant electrical coupling for the purpose of wireless power transfer across non-negligible distances, as an alternative to resonant magnetic coupling.

[4] In the paper "Constructive combination of resonant magnetic coupling and resonant electrical coupling", the possibility of constructively combining electrical and magnetic resonances is proposed. A comparison between magnetic coupling only, electrical coupling only and several hybrid combinations is provided in the paper. The conclusion of this paper is that efficiency can be increased by combining magnetic coupling and electrical coupling. This conclusion is based on circuit theory.

[5] In the paper "Low-power ultra-wide band pulse generator based on a PIN diode" a low-power ultra-wide band pulse generator is proposed. This pulse generator is designed to produce a positive unipolar pulse for each high-to-low (1.8 V to 0) transition received from the passive RFID tag described in [7]. Very importantly, the power needed to activate the pulse generator is extracted from the trigger signal, eliminating the need for a separate supply voltage. The main novelty in this paper is the generation of an ultra-wide band pulse from a very limited power supply.

[6] A possible application of the pulse generator from [5] is described in the book chapter "Unconventional RFID systems". In this application an RFID tag receives power from nearby power transmitters and generates pulses that are then detected by ultra-wide band receivers placed in known locations. The position of the tag can be estimated based on the differences between the pulse arrival times reported by each of the receivers.

[7] Entitled "Design of a Battery-free Wireless Sensor Node", this is the publication where the development of the RFID tag used in [5] is described in most detail. The tag is battery-free, fully programmable, relatively small-sized and contains a pin interface of 26 pins for programming, debugging and testing new hardware.

[8] The paper "Design of a Battery-free Wireless Sensor Node" is a summary of [7].

[9] The subject of "Increasing the Range of Wireless Passive Sensor Nodes using Multisines" is the delivery of power to the RFID tag from [7] using multisines instead of the typical pure sinusoidal signals. As reported in the paper, significantly longer distances can be achieved with the same average power.

[10] The improvement reported in [9] is mainly caused by the relatively high peak-to-average power ratio that can be achieved with multisines. In the paper "Boosting the Efficiency: Unconventional Waveform Design for Efficient Wireless Power Transfer", multisines and other methods of producing high peak-to-average power ratios are considered.

1.3 Methods of wirelessly transferring power

The following sub-sections contain brief descriptions of the methods of wirelessly transferring power typically mentioned in the literature. These methods are inductive coupling, resonant magnetic coupling, capacitive coupling, lasers and microwaves. The first three methods are non-radiative or near-field and the last two methods are radiative or far-field. Inductive coupling, resonant magnetic coupling and microwaves are the most popular methods. In many papers, including review papers such as [11], these are in fact the only methods considered. Sometimes, for instance in [12], capacitive coupling and lasers are also mentioned but usually just briefly.

1.3.1 Inductive coupling

As mentioned in [12], the discovery of electromagnetic induction is generally credited to Michael Faraday, in 1831. At the fundamental level, electromagnetic induction is the production of a voltage across a closed circuit placed in a time-varying magnetic field or moving through a stationary magnetic field. It is common practice to denote this voltage, or electromotive force, by the letter

ϵ. Mathematically, the relationship between ϵ and a magnetic field B can be written as

$$\epsilon = -d\phi_B/dt, \tag{1.1}$$

in which ϕ_B represents the magnetic flux enclosed by the circuit. As can be seen in the equation, the voltage induced is directly proportional to the rate of change of the magnetic flux enclosed by the circuit. In particular, no voltage is generated if there is no change in the magnetic flux. In practical implementations the previously mentioned closed circuit is usually a coil and the magnetic field is usually generated by connecting a second coil of approximately the same dimensions to an oscillator, creating a time-varying magnetic field. Inductive coupling is the name given to the coupling between the two coils. Other names are sometimes used, such as magnetic coupling or simply induction. If the coils are properly aligned and in close proximity most of the flux generated by the transmitter coil is picked up by the receiver coil, resulting in a higher induced voltage. As the distance between the coils is increased the amount of flux that no longer passes through the receiver coils also increases, as shown in figure 1.1. As this leakage flux increases, the induced voltage decreases. The rate at which the induced voltage decreases with distance is very high and the coupling drops to zero typically after just a few milimeters. This is generally accepted as the single most critical limitation of inductive coupling.

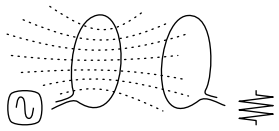

Figure 1.1: Graphical illustration of inductive coupling, in which dashed lines are used to represent magnetic field lines.

Over time, inductive coupling has been used in many different applications. Electrical transformers are a good example of the usefulness of inductive coupling. Many smart cards also make use of inductive coupling. One of the first systems of this kind was the FeliCa card mentioned in [11]. This card was proposed and sold by Sony in 1995. Electric toothbrushes, for instance, are typically recharged using inductive coupling. In this case the power connector can be eliminated and the process of recharging the toothbrush becomes much more convenient. In addition, both the toothbrush and the charger can be hermetically sealed. As a result, the problems of wear and tear in the connector and water seeping into the toothbrush and causing damage to internal components can be effectively solved. These are very strong advantages of inductive coupling in comparison to a wired connection. Another very useful application of inductive coupling is induction cooking. As mentioned in [12], induction cookers are faster, safer, more controllable and more energy-efficient than traditional stovetops. Induction cookers consist of a stovetop with one or more coils. Once a pot is placed on the stovetop and the latter is turned on, a time-varying magnetic field is created by the coils. Due to the internal resistance of the pot, the induced currents cause heat to be dis-

sipated. It is the pot itself that heats up, not the stovetop. More recent applications of inductive coupling include charging pads for tablets, smartphones and smartwatches. Specific examples of some of these applications are given in chapter 2.

1.3.2 Resonant magnetic coupling

Published in 2007, [13] is one of the first publications related to the use of strongly coupled magnetic resonances and also the most important. In this paper, a group of researchers led by Prof. Marin Soljačić reports the transfer of 60 W to an incandescent light bulb across a distance of 2 meters with an efficiency of 40%. These numbers were achieved using only two helical coils measuring 60 cm in diameter and 20 cm in height and two smaller single-turn loops, arranged as shown in figure 1.2. As mentioned at the beginning of this chapter, distance is something highly valued in wireless power transfer so a very reasonable efficiency at a distance of several times the diameter of the helical coils is obviously something important, especially when combined with such a simple apparatus. Although only a small part of the magnetic flux generated by the first helical coil is effectively picked up by the second helical coil due to distance, an efficient power transfer is still possible if those coils resonate at the same frequency and have very high Qs (quality factors), in the order of 950 at 9.9 MHz in this particular case. In short, the coupling strength depends on both the magnetic coupling coefficient and Q, not just the former. The first helical coil is inductively coupled to the source loop, which is in turn connected to an oscillating circuit. Similarly, the second helical coil is inductively coupled to the load loop, which is connected to a resistive load. Some related theoretical work published shortly before [13] can be found in [14]. Moreover, a more detailed version of the material published in [13] can be found in [15]. Applications of resonant magnetic coupling in consumer electronics, medical devices, electric vehicles, lighting and the military are shown in [16].

Since a high magnetic coupling coefficient is not required in strongly coupled magnetic resonances, a single transmitter can simultaneously deliver power to multiple receivers of different sizes, as pointed out in [17]. In addition, distance can be significantly extended through the use of resonant repeaters. In one of the applications shown in [16], for instance, multiple resonant repeaters are used in the design of light fixtures that seemingly float in mid-air. Specific examples of the transfer of power from a single transmitter to multiple receivers, transmitters and receivers of different sizes and resonant repeaters are given in chapter 2.

1.3.3 Capacitive coupling

Capacitive coupling is currently perceived as only suitable for extremely short distances, typically less than a millimeter. Clear evidence of this fact can be found for instance in the list of papers related to this technology published in the last few years contained in [18]. Wireless power transfer based on capacitive coupling usually consists of two pairs of conductive plates, or electrodes, as

Figure 1.2: Graphical illustration of strongly coupled magnetic resonances, consisting of two single-turn loops and two helical coils.

shown in figure 1.3. Assuming a small distance d between the electrodes, the capacitance C between each pair can be expressed as

$$C = \epsilon A/d, \tag{1.2}$$

in which ϵ represents the electric permittivity of the material between the electrodes and A represents the area of the electrodes. As pointed out in [19], there are some potential advantages of capacitive coupling in relation to inductive coupling. The first advantage is the flexibility in the design of the electrodes, which can be be made in shapes designed to best fit the place where they are supposed to be installed. Coils can also be made in different shapes but the flexibility is lower. Another advantage is that electrodes generate less heat than coils, which is particularly important at higher power levels. This is also an advantage if the electrodes have to be installed near components sensitive to temperature, such as batteries. Lastly, electrodes can be made very thin, thinner than flat coils.

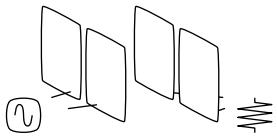

Figure 1.3: Graphical illustration of capacitive coupling, consisting of two pairs of electrodes.

1.3.4 Lasers

Even though some of the features of laser are unique and useful for wireless power transfer, there are also heavy drawbacks involved which limit the use of lasers to a very narrow range of applications. As mentioned in [12], safety is one of the major concerns since laser radiation is hazardous. Permament injuries such as blindness can result from exposure to laser beams. Significant distances are achievable due to the low dispersion loss but a very precise alignment between the transmitter and the photovoltaic receiver is required at all times, as well as an unobstructed line of sight. In addition, suitable atmospheric conditions are also required as absorption and scattering by clouds, fog or rain can cause significant losses. It is mainly due to these drawbacks that the use of lasers in wireless power transfer is limited.

1.3.5 Microwaves

One of first major milestones in the use of microwaves for wireless power transfer was in 1964 and consisted in the flight of a rotary-wing aircraft powered solely by a microwave beam. In this case, an electric motor was used to generate the necessary motion for the rotor blades to produce lift. An array of rectennas installed on the aircraft was used receive and rectify incoming microwaves in order to deliver 200 W to the motor. Although the vertical flight was constrained to a few centimeters due to the fact that the aircraft was tethered, an experiment of this kind had never been achieved in the past. Using the same aircraft, a continuous flight of 10 hours at an altitude of approximately 15 meters was demonstrated a few months later. Several other milestones were achieved in the following years, as detailed in [20] and [21] by William C. Brown. In particular, over 30 kW were transferred over a distance of approximately 1.6 km in 1975, from a large parabolic antenna to an array of rectennas. Never had so much power been transferred over such a large distance before using microwaves. Significant drawbacks of this technology such as size, weight and cost were also clearly exposed in this demonstration. Frequencies between 2.4 and 2.5 GHz or close were used in all the major milestones reported in [20] and [21].

Interest in transferring large amounts of power across long distances was at that time mainly motivated by the concept of beaming solar energy harvested by satellites to Earth using microwaves introduced in 1968 by Peter Glaser, in [22]. Compared to sunlight, microwaves are less affected by water droplets suspended in the atmosphere, due to the longer wavelengths. As a result, thick clouds and heavy rainfall are less of a problem. Additionally, there is plenty of sunlight available for the satellites to harvest. On the other hand, solar panels suffer much more degradation in space than they do on the planet, meaning more maintenance. Also, in order to gather massive quantities of energy, the satellites must be significantly large. Several satellites of this kind have been proposed since 1968, as mentioned in [23], but none of them have been effectively launched into orbit. Major technical, regulatory and conceptual issues must be solved before that happens.

Currently, passive RFID is probably the most widely known application of microwaves in wireless power transfer. Although only a small fraction of the power radiated by an RFID reader is received by each tag, resulting in a very low efficiency, many tags can be simultaneously powered. Easily delivering power from one source to multiple low-power receivers is a very important and unique advantage of microwaves. In addition, distances of several meters and fast data transfer rates can be achieved under appropriate conditions. In addition, tags can be made small, very thin, and sometimes physically flexible since most of the complexity can be shifted to the reader. Over time, microwaves have also been used occasionally in various other applications, such as powering miniature airplanes, electric cars, and transferring power from airships to ground, as shown in [24].

1.4 Early history of wireless power

Experiments on wireless power transfer date back to the famous gigantic coil wound around a 60 m mast with a 1 m diameter copper ball positioned at the top built by Nikola Tesla in 1899. A potential in the order of 10^8 V was produced at the sphere as a result of resonating the coil at 150 kHz with 300 kW, as documented in [20]. Such a high potential resulted in very long and very visible discharges from the sphere. Although there is no clear record of how much of this power was radiated into space and whether any significant part of it was collected at a distant point, there is an abundance of unsupported claims. One of the most popular claims is the lighting of 200 50 W incandescent lamps located 42 km away reported for instance in [25]. A patent for a second iteration of the previously described structure filed in 1902 can be seen in [26]. Such structure would mainly consist of a large coil and a massive 30 m diameter copper electrode shaped like a doughnut placed at the top of a 47 m high wooden tower. Construction was started but never completed due to the lack of funding. Concepts of critical importance in this project such as oscillating voltages and currents, capacitor charging and discharging, magnetic induction and resonators are still widely used.

Chapter 2

State of the art

2.1 Summary

A review of the recent developments in the field of wireless power transfer is given in this chapter. A snapshot of the current state of the art based on a group of selected papers is presented in the first part of the chapter. Subjects related to intellectual property, market adoption and standardization are addressed afterwards.

2.2 Selected publications

Several variations of the original apparatus from figure 1.2 have been proposed, in a clear effort to maximize spatial freedom. Examples of these variations, as well as recent proposals related to inductive coupling and capacitive coupling are included in the following list.

[27] In this paper, resonant magnetic coupling is used for wirelessly delivering power from a coil with a diameter of 30 cm to two smaller coils with diameters of 1.3 cm each, simultaneously. A resonant frequency of 8.3 MHz is used, which is slightly lower than [13]. More importantly, the same resonant frequency is achieved at both the transmitter and receiver coils by terminating them with lumped capacitors. An identical self-resonant frequency may be very difficult to obtain if the coil dimensions are drastically different, and this case is a good example of that, hence the use of lumped capacitors. Another important aspect reported in the paper is that bringing the two receivers into close proximity results in a significant degradation of efficiency due to frequency splitting, which is difficult to predict, especially in the case of more than one receiver. Chapter 3 contains more detailed information about frequency splitting. Means for tracking frequency shifts and continuously retuning the lumped capacitances are therefore critical when multiple receivers exist.

[28] In this paper, resonant magnetic coupling is also used for transferring power from a single larger transmitter coil to two smaller receivers, as in [27]. Contrary to [27], the same resonant frequency is achieved in both the larger coil and the smaller coils by tuning parameters such as diameter, number of turns and spacing between consecutive turns, rather than using lumped capacitors. Lumped capacitors are still used in the coils connected to the power supply and the loads, though. A slightly lower resonant frequency of 6.5 MHz and larger diameters of approximately 1.13 m and 30 cm and are used. An increase in the overall efficiency when both receivers are simultaneously powered can be seen in the paper, especially at higher distances, in comparison to the scenario in which each receiver is considered in isolation. An important fact is that in this case the receivers are placed one on each side of the large coil in order to maximize the distance between them and consequently minimize the frequency splitting and degradation in efficiency mentioned in [27]. Power levels upwards of 25 W delivered to each of the receivers are reported in the paper. Some additional information related to this paper is given in [29], by the same authors.

[30] Apart from the usage of flat coils instead of helical coils, there are no major differences between the apparatus reported in this paper and [13]. However, in this case a model based on passive circuit elements is used instead of the coupled-mode theory originally used in [13] and in other related papers such as [14], [28] and [29]. As concluded in [31], the two approaches are equivalent if the Qs are high but the model based on circuit theory remains valid for lower Qs whereas the coupled-mode theory does not. This detail is also mentioned in [28], although briefly. A very important property of strongly coupled magnetic resonances highlighted in the paper currently under consideration is that a nearly constant efficiency can be obtained at up to a certain distance if a suitable tuning mechanism is implemented. Two tuning methods are described in the paper, one based on frequency adaptation and a second one based on the adjustment of the distance between the receiver coil and the load coil. Further information on the previously mentioned property is given in chapter 3. Axial misalignment can also be compensated, although not in extreme cases such as when the receiver is perpendicular to the transmitter, as clearly shown in the paper. A review paper related to the previously mentioned subjects, by the same authors, can be found in [32].

[33] In this case the efficiency is tuned by varying the distance between the receiver coil and the load coil, as in [30], and also the distance between the source coil and the transmitter coil. Significant efficiency improvements of 46.2% and 29.3% at 60 cm and 1 m, respectively, are reported. More importantly, the reason for normally using a higher number of turns in the transmitter and receiver coils than in the source and load coils is also mentioned in the paper. With such turn ratios, the source and load resistances are converted to larger effective resistances in parallel to the transmitter and receiver coils, respectively.

[34] In this paper, an additional flat coil is inserted between the transmitter and receiver coils, which in this case are helical coils as in [13]. Both a coaxially arranged configuration and a perpendicularly arranged configuration are considered. The results reported in the paper show that the addition of an intermediate coil results in an increase in efficiency which remains consistent as the distance between the transmitter and receiver coils is changed. A substantial increase in efficiency is reported in the paper in the case of a coaxially arranged intermediate coil, which clearly demonstrates that in strongly coupled magnetic resonances the insertion of an additional coil between the transmitter and receiver coils results in an improvement, despite the fact of that coil not being physically connected to anything. Naturally, the intermediate coil must be resonant at the same frequency of the transmitter and receiver coils. A significant increase in efficiency is still achieved if the intermediate coil is arranged perpendicularly, although not as high as in the case of a coaxially arranged intermediate coil due to the non-optimal orientation.

[35] Another variation of [13] is reported in this paper, in which the receiver coil is removed. Not many details are provided in the paper, but the idea is still worth mentioning because it represents a trade-off between inductive coupling and strongly coupled magnetic resonances in terms of simplicity of the receiver, alignment, distance and need for tuning, which may be useful in some applications.

[36] An implementation of strongly coupled magnetic resonances based on open-circuited resonant shielded loops is reported in this paper. The open-circuit termination of the loops creates a capacitance which allows the loops to resonate, in this case at a relatively high frequency in the order of 37 MHz. An efficiency of 41.8% is achieved at a distance of 35 cm between two circular single-turn loops with a diameter of approximately 21.4 cm. This is an important result since the loops are geometrically simple and compact, more compact than [13] or [30], for instance. An efficiency of 36.5% is achieved at a higher distance of 56 cm by using ten turns instead of one for both the transmitter and the receiver. Matching networks are used to match the shielded loops to the source and the load in both cases. Information related to the planar implementation of resonant shielded loops can be found in [37], by the same authors.

[38] This paper can be considered as an extension of [34] in the sense that not one but up to six intermediate coils are used. Interestingly, maximum efficiency is not obtained when the coils are all equally spaced but rather when the distances from the transmitter coil to the first intermediate coil and from the last intermediate coil to the receiver coil are slightly smaller than the other distances. As pointed out in the paper, this phenomenon might be explained by the fact that the transmitter and receiver coils are the only ones coupled to only one adjacent coil instead of two. Several other arrangements are presented, such as curved,

circular, splitting of one path into two, merging of two paths into one and selection of a certain path over another based on detuning. These arrangements can be used to control how power flows in a highly flexible manner. The light fixtures that seemingly float in mid-air mentioned in sub-section 1.3.2, for instance, make use of the properties described in this paper. As a last note, resonant frequencies between 505 kHz and 530 kHz are used in this case, which is significantly lower than what is typically used in strongly coupled magnetic resonances.

[39] In this paper, a significant increase in efficiency is reported as a result of placing a slab of metamaterial between the transmitter and receiver coils. The metamaterial acts as a lens, focusing the magnetic field and consequently increasing the coupling between the coils, and thus distance. A metamaterial is an artificial material composed of engineered structures typically much smaller in size than the wavelength under consideration. Unique properties not normally found in natural materials can be otained with these materials, such as the negative magnetic permeability which is fundamental in this case, for instance. A variation of [38] is also reported in this paper, in which all the coils are on the same plane, rather than coaxially aligned. A demonstration of a toy train moving on an oval-shaped track using the previously mentioned arrangement is also presented.

[40] This is the first paper in this list in which capacitive coupling is considered instead of a magnetic coupling. In this case the focus is the transfer of power from the road infrastructure to electric cars through their tires, taking advantage of the fact that the latter are in principle always in physical contact with the road. As pointed out in the paper, the absence of an air gap potentially results in a lower electromagnetic field leakage compared to a power transfer from the road to the bottom of the car based on strongly coupled magnetic resonances. In the scenario envisioned in this paper, power is delivered from a pair of conductive lines installed under the surface of the road to the steel belts normally found inside commercially available tires, using the high electric permittivity of rubber to increase coupling and thus also efficiency, either in motion or when the car is stopped. A demonstration of this concept using two tires placed on top of concrete blocks is reported in the paper. Two other demonstrations using toy cars of different sizes are also reported.

[41] In this paper, the source, transmitter, receiver and load coils typically used in strongly coupled resonances are replaced by sets of three concentric orthogonal loops, in which the source and load loops are placed inside the transmitter and receiver loops, respectively. The purpose of this design is to minimize the drop in efficiency that occurs when a optimal orientation is not used, such as in the case when the transmitter and receiver coils are perpendicular to each other reported in [30]. A more stable efficiency can be obtained with the orthogonal loops at the cost of more complexity and volume for both the transmitter and receiver, in

comparison to the flat design proposed in [30], for instance. A simpler, less effective version with two concentric orthogonal coils is also mentioned in the paper. A related paper can be found in [42], where the main difference is that the receiver is located inside the transmitter.

[43] In this case, strongly couped magnetic resonances are used in an application where the medium is salt water, rather than air. Although not many details are given, it is concluded that efficiencies of approximately 80% can be obtained at distances in the order of 15 cm and that salt water introduces a loss of about 15% compared to air. A demonstration of the powering of an halogen lamp across a distance of 26 cm is shown, using a plastic container filled with water placed between the transmitter and receiver. In the application envisioned, the receiver would be installed in an autonomous underwater vehicle and the transmitter would be installed in an underwater charging station, providing an alternative to the use of wet-mate connectors and the possibility to automate the charging process.

[44] In this case the transmitter consists of a flat conductive surface and the receiver consists of a tightly wound coil connected to an incandescent light bulb. In order to deliver power to the conductive surface, one of the terminals of an oscillating circuit is connected to the mentioned conductive surface and the other terminal is electrically grounded. As mentioned in the paper, the power transfer is not wireless in the conventional sense of the word since one of the terminals of the coil is in direct contact with the conductive surface. However, the circuit is completed wirelessly using the stray capacitance that surrounds the coil. Power is transferred at the frequency at which the coil resonates with the stray capacitance, in this case in the order of 2 MHz. This is an important example of two-dimensional spatial freedom, since the receiver can be placed anywhere in the conductive surface and still receive power. A demonstration of the transfer of 50 W at an efficiency of 83% from a conductive surface measuring 25 cm by 25 cm to two incandescent light bulbs of 25 W each is reported in the paper. As a last note, a physical contact between the transmitter and the receiver is not absolutely necessary and an efficiency in the order of 80% can still be obtained with gaps of up to 3 cm, as mentioned by the same authors in [45].

[46], [47], [48] These papers and [2] are similar in the sense that the use of resonant electrical coupling as a method for wirelessly transferring power is the main topic addressed in all of them. Additional information about this subject is given in chapters 4 and 5.

[49] This paper provides an example of the use of coils terminated with capacitors in a scenario where the receiver coil is moving in relation to the transmitter coil. In this particular case the application is the transfer of power to a computer mouse from the mouse pad directly underneath, meaning a small gap. The mouse only receives power when the receiver coil is aligned with the transmitter coil installed in the center of the mouse pad so a super-capacitors

is installed in the receiver to act as a buffer. As reported in the paper, a fully charged supercapacitor is enough to power the computer mouse for 13 minutes and takes only 10 seconds to charge. With these values the receiver only needs to be aligned with the transmitter 1% of the time to guaranty a continuous operation, which is something significant. In both this paper and [44] the goal is to achieve two-dimensional spatial freedom, but the strategies used are quite different. A frequency of 120 kHz is used in this case. An extended version of this paper focused on the communication between the mouse pad and the mouse can be found in [50].

[51] A receiver designed to be compatible with both inductive wireless power transfer at 100 kHz and resonant wireless power transfer at 6.78 MHz is reported in this paper. The receiver consists of two coils arranged concentrically, each one optimized for each of the previously mentioned frequencies. Efficiencies of 84% in inductive mode and 82% in resonant mode are mentioned in the paper for an output power level of 2.5 W. The choice of frequencies is related to the support of both the Qi standard, based mainly on inductive coupling, and the standard from Power Matters Alliance, based on resonant magnetic coupling. An extended version of the paper currently under analysis can be found in [52]. Additional information related to the subject of standardization in wireless power is provided in sub-section 2.3.2.

[53] As in [35], in this paper the receiver is also composed by a single coil instead of two. The size and simplicity of the receiver are very important properties in this particular case because the goal is to wirelessly deliver power to hearing aids, which are very small devices. The transmitter is unique in the sense that the transmitter coil is designed to have the shape of a bowl. Such shape is used in order to make the position of the hearing aid in the bowl less relevant in the efficiency of the power transfer. The receiver coil is fully embedded into the hearing aid but the rechargeable battery and communication modules are not, due to size constraints. In this case ferrite sheets are used in the receiver coil to improve coupling. As reported in the paper, the battery in the hearing aid can be charged with an efficiency of approximately 30% in most locations within the bowl if the receiver coil is in a parallel arrangement. In a perpendicular arrangement the efficiency is lower but it is still possible to charge the battery except for a dead zone near the center of the transmitter coil. It is important to notice that even though most of the transmitted power is not received by the hearing aid and thus lost, this power loss is not critical due to the low power levels involved. This is a clear example of convenience over efficiency.

[54] The subject of this paper is the capacitive transfer of power to an electrical vehicle using a docking station that adapts to the shape of the electrical vehicle. As the vehicle pulls into the docking station, two conducting foils adhered to the surface of the bumper press against the foam on the charging area, bringing the surfaces together and improving coupling due

to the reduction of the air gap. As mentioned in the paper, there is a possibility for multiple vehicle charging as the conductive strips in the charging station can be extended along the length of a wall, for instance. There is no direct contact between the bumper of the vehicle and the charging station as the latter is covered by an insulation layer. The insulation layer also works as a dielectric material which helps to increase capacitance. A demonstration of a power transfer to an electric vehicle with an efficiency of 83% at 540 kHz is reported in the paper.

[55] As in [54], this paper also contains a variation of the typical use of capacitive coupling. In this case the receiver is implemented using multiple small hexagonal cells paired with individual half-bridge rectifiers instead of the usual two plates. The transmitter is implemented using severals strips of alternating polarity instead of the usual two plates. The reason for this approach is to increase coupling and therefore two-dimensional spatial freedom, as in [44].

[56] A charger designed to simultaneously deliver power to a smartphone and a smartwatch using magnetic resonance at 6.78 MHz is described in this paper. The charger is shaped as a vertical cylinder, with turns in the middle of the cylinder to provide power to the watch and turns at the top to provide power to the smartphone. It is more intuitive to charge a smartwatch with this design than with the more typical planar chargers as the shape of a smartwatch is not suitable to a planar charging pad, hence the cylindrical design. A ferrite sheet is used to shield the electronic components at the base of the charger. An efficiency of 48% is reported in the paper for the case in which the smartphone and the smartwatch are charged at a rate of 5 W and 1.15 W, respectively.

[57] The topic of simultaneous delivery of power to multiple receivers is also the focus of this paper. In this case the concepts of frequency tracking, power tracking and adaptive impedance matching are used to dynamically tune up to five receivers and the transmitted signal for optimal power delivery, including the case in which different power levels are needed by each receiver. The transmitter consists of an array of five coils over which the receivers are supposed to be placed, in close proximity. The ability to prioritize and isolate specific receivers using time-division multiplexing is demonstrated in the paper by sequentially powering each one of the receivers while detuning all the others.

[58] Long helical coils with a relatively small cross-section in an orientation perpendicular to the typical coaxial orientation are reported in this paper. Both the form factor of the coils and their orientations are different from what is normally seen in other papers, such as [30]. Another difference is that in this case stepped magnetic cores significantly longer than the coils are used in order to intensify the magnetic field by a factor of about 50, according to what is reported in the paper. The purpose of the stepped core is to minimize core loss for a given amount of ferrite material, as mentioned in the paper. Efficiencies of 29%,

16% and 8% for output power levels of 1403, 471 and 209 W for distances of 3, 4 and 5 meters are reported in the paper, at 20 kHz. Efficiencies of 46%, 31%, 15% and 6% for distances of 2, 3, 4 and 5 meters and an output power of 5 W are also reported in the paper, at 105 kHz. The use of cores limits the operating frequency due to losses, hence the low frequencies. An additional paper related to this subject can be found in [59], where two coils with magnetic cores arranged in an orthogonal manner are used instead of one in order to achieve omnidireccional power transfer, thus using a strategy similar to [41].

[60] In this last paper, a variation of [13] in which the source and load coils are coupled to the transmitter and receiver coils, respectively, using lumped transformers with ferrite cores instead of air. This approach results in a more compact size, as in [36]. Since the couplings between the source coil and transmitter coil and between the receiver coil and the load coil are not as critical as the coupling between the transmitter and receiver coils, a reasonable efficiency can still be achieved at a reasonable distance. A power transfer of 10 W with an efficiency of 80.2% at a distance of 13 cm is reported in the paper, at 500 kHz. As in [58], in this case the frequency is also limited due to the use of cores.

Many different proposals with the goal of enhancing spatial freedom can be found in the literature. A significant part of these proposals consists of variations of the original apparatus of resonant magnetic coupling, such as simultaneous wireless power transfer to several receivers of different sizes and the use of additional objects placed between the transmitter and the receiver to increase distance. These additional objects can be resonators or layers of metamaterials. In the case of additional resonators, interesting arrangements have been proposed to control power flow, such as straight, curved, circular, splitting of one path into two or merging of two paths into one. The use of concentric orthogonal coils with the goal to minimize drops in efficiency caused by non-optimal orientations has also been proposed in different configurations, including for instance the case in which the receiver is placed inside the transmitter. Several proposals also exist in the topic of two-dimensional spatial freedom, based on single-contact wireless power transfer, energy buffering as an alternative to complete coverage, and the use of capacitive coupling based on multiple cells paired with individual rectifiers.

2.3 Current state of wireless power in society

As mentioned in [61], wireless power is currently in the process of transitioning from a technology to an industry. The desire to simplify and add a new level of convenience to the powering and charging of electronic devices is driving the consumer expectation for wireless power. Several products are already on the market and the number of patents related to wireless power has increased significantly over the last few years, as described in the next sub-section. The second sub-section contains information related to the standardization of wireless power.

2.3.1 Market adoption

Two of the most influential patents in the field of wireless power are clearly [62] and [63]. These patents were filed shortly before [13], by the same authors, and refer to the same apparatus. These patents are currently part of the portfolio of Witricity, a company formed at that time that has experienced a tremendous growth in the last few years. Many other patents were filed by Witricity in the meantime but the two patents previously mentioned are the most critical. Additionally, a patent closely related to the system proposed in [30] can be found in [64]. Very importantly, [65] is a patent related to resonant electrical coupling. From the point of view of circuit topologies, the material in this patent is related to chapter 4. No other related publications were found in the literature. Some patents related to plain capacitive coupling also exist, such as [66]. Some more detailed information related to this patent can be found in [19], including the potential advantages of capacitive coupling listed in sub-section 1.3.3. Patents related to the use of inductive coupling also exist, such as [67], for instance. In this particular example, a set of coils is installed in the front of a vehicle in the space where the license plate is usually placed. The charging process is initiated when the vehicle is parked near a charging station equipped with a similar set of coils. Since the gap between the transmitter and receiver is small, the sizes of the coils can also be small and potentially less expensive. This is a variation of the typical inductive charging where coils are mounted on the underside of the vehicle and the ground. Interest in wireless vehicle charging has already been expressed be several car manufacturers, such as BMW in [68], for instance. According to [69], most of the patenting activity is in inductive coupling and in application areas related to smartphones, cameras, laptops and computers. Furthermore, a large number of patents in the field of wireless power is owned by either Samsung, Qualcomm or LG. Some of the largest smartphone manufacturers have already started to integrate wireless charging features in their flagship devices as early as 2013. Some examples are the Lumia 830 from Nokia, the Galaxy S4 from Samsung, the Droid DNA from HTC and the Nexus 4 from LG and Google. In addition, Intel seems to be preparing the first completely wireless computer for 2016. In a different industry, IKEA has announced the launch of bedside tables, lamps and desks with wireless chargers built-in. Lastly, various wireless power kits such as [70] and [71] were recently launched in the market.

2.3.2 International standards

A single, universal standard supporting multiple power needs and supported by a wide range of brands makes total sense in wireless power, as pointed out in [72], in order to avoid a fragmented industry. While this goal has not been achieved yet, significant progress has been made in the last few years. The Wireless Power Consortium was the first standardization group formed. As mentioned in [12], this group was formed in December 2008 by several companies such as Texas Instruments, Philips and Sanyo. Following the Wireless Power Consortium, the Power Matters Alliance and the Alliance for Wireless Power were also formed. By June 2013 the numbers of

members of these groups had increased to over 140, over 80 and over 40, respectively, as reported in [73]. By January 2014 these numbers had further increased to over 180, over 100 and over 60, as reported in [74]. Very recently, the Power Matters Alliance and the Alliance for Wireless Power have merged into a single organization under the name AirFuel Alliance. As of December 2015, the number of members of the Wireless Power Consortium and the AirFuel Alliance are 230 and 195, respectively. As can be seen by these data, the number of companies interested in wireless power has been increasing significantly. In fact, it is not unusal for companies to support all groups, rather than just one. Wireless Power Consortium is traditionally more associated with inductive coupling and AirFuel Alliance is mainly based on strongly coupled magnetic resonances.

Chapter 3

Resonant magnetic coupling

3.1 Summary

This chapter contains a circuit analysis of strongly coupled magnetic resonances based on the circuit model generally accepted in the literature as the equivalent. Although in [13], [15] and [14] this method is described using coupled-mode theory, circuit theory is currently more widely used. Several realizations of the circuit are presented using typical parameters reported in the literature as reference.

3.2 Circuit model

Even though relatively simple, the model shown in figure 3.1 is accurate and also the most widely used in the literature. The main objectives in this analysis are to obtain compact, manageable mathematical expressions for comparison with the analysis presented in chapter 4. Matching the circuit of figure 3.1 to the diagram of figure 1.2 is straightforward since each loop in the circuit corresponds to a coil in the diagram. In [13], R_1, R_2, R_3, R_4, C_2 and C_3 are all parasitic elements. In contrast, C_1 and C_4 are actual capacitors added to the single-turn loops to ensure that they resonate at the frequency at which the helical coils self-resonate. It is important to note that in many publications, [13] included, the couplings between the source and transmitter coils and between the receiver and load coils are described as inductive but in reality are resonant due to the added capacitors. The source and load resistances are represented by R_I and R_O, respectively, and V_I is the input voltage. As for magnetic couplings, L_1 is coupled to L_2, L_2 is coupled to L_3 and L_3 is coupled to L_4. Using M to represent mutual inductance and j as the imaginary unit it

is possible to write

$$(R_I + R_1 + jwL_1 - j/[wC_1])I_1 + jwM_{12}I_2 - V_I = 0 \tag{3.1}$$

$$jwM_{12}I_1 + (R_2 + jwL_2 - j/[wC_2])I_2 + jwM_{23}I_3 = 0 \tag{3.2}$$

$$jwM_{23}I_2 + (R_3 + jwL_3 - j/[wC_3])I_3 + jwM_{34}I_4 = 0 \tag{3.3}$$

$$jwM_{34}I_3 + (R_4 + jwL_4 - j/[wC_4])I_4 + V_O = 0 \tag{3.4}$$

$$R_O I_4 - V_O = 0. \tag{3.5}$$

Solving (3.2) for I_1 and substituting in (3.1) gives

$$K_1 I_2 + jwM_{23}Z_1 I_3 + jwM_{12}V_I = 0, \tag{3.6}$$

in which

$$Z_1 = R_I + R_1 + jwL_1 - j/(wC_1) \tag{3.7}$$

$$Z_2 = R_2 + jwL_2 - j/(wC_2) \tag{3.8}$$

and

$$K_1 = Z_1 Z_2 + w^2 M_{12}^2 \tag{3.9}$$

or, using the magnetic coupling coefficient k_{12},

$$K_1 = Z_1 Z_2 + w^2 k_{12}^2 L_1 L_2, \tag{3.10}$$

since

$$M_{12} = k_{12}\sqrt{L_1 L_2}. \tag{3.11}$$

Solving (3.3) for I_2 and substituting in (3.6) gives

$$(K_1 Z_3 + w^2 M_{23}^2 Z_1)I_3 + jwM_{34}K_1 I_4 - w^2 M_{12}M_{23}V_I = 0, \tag{3.12}$$

in which

$$Z_3 = R_3 + jwL_3 - j/(wC_3). \tag{3.13}$$

Solving (3.4) for I_3 and substituting in (3.12) gives

$$(K_1 K_2 + w^2 M_{23}^2 Z_1 Z_4 - R_O[K_1 Z_3 + w^2 M_{23}^2 Z_1])I_4 + jw^3 M_{12}M_{23}M_{34}V_I + (K_1 Z_3 + w^2 M_{23}^2 Z_1)V_O = 0, \tag{3.14}$$

in which

$$Z_4 = R_O + R_4 + jwL_4 - j/(wC_4) \tag{3.15}$$

and

$$K_2 = Z_3 Z_4 + w^2 M_{34}^2 \tag{3.16}$$

or, equivalently,

$$K_2 = Z_3 Z_4 + w^2 k_{34}^2 L_3 L_4, \tag{3.17}$$

since

$$M_{34} = k_{34}\sqrt{L_3 L_4}. \tag{3.18}$$

Solving (3.5) for I_4 and substituting in (3.14) gives

$$V_O/V_I = -jw^3 R_O M_{12} M_{23} M_{34}/(K_1 K_2 + w^2 M_{23}^2 Z_1 Z_4). \tag{3.19}$$

Considering

$$M_{23} = k_{23}\sqrt{L_2 L_3}, \tag{3.20}$$

(3.19) can be rewritten as

$$V_O/V_I = -jw^3 R_O k_{12} k_{23} k_{34} L_2 L_3 \sqrt{L_1 L_4}/(K_1 K_2 + w^2 k_{23}^2 L_2 L_3 Z_1 Z_4). \tag{3.21}$$

Using the operator $\Re\{\}$ to represent "real part of", the relationship between average power, voltage and current is given by

$$P = \Re\{V I^*\}/2. \tag{3.22}$$

In the case of R_O, (3.22) can be rewritten as

$$P_O = |V_O|^2/(2R_O) \tag{3.23}$$

because R_O is purely real. The power source (composed by V_I and R_I) is able to supply at most

$$P_A = |V_I|^2/(8R_I), \tag{3.24}$$

considering the case of a matched load. Using (3.23) and (3.24) the available power gain can be written as a function of the voltage gain obtained in (3.21) as

$$P_O/P_A = 4R_I |V_O/V_I|^2/R_O. \tag{3.25}$$

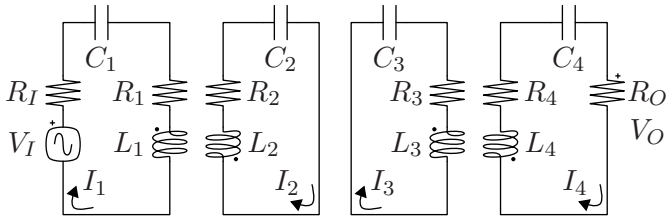

Figure 3.1: Circuit model most widely used in the literature to represent resonant magnetic coupling. Each loop in this circuit corresponds to the coil in the same relative position in figure 1.2.

The response of this model as a function of frequency for k_{23} equal to 0.002, 0.005, 0.008, 0.011, 0.017, 0.02, 0.03, 0.06, 0.11 and 0.18 considering the parameters listed in table 3.1 is illustrated in figures 3.2 and 3.3. The reference values were selected based on the values typically found in the literature, in particularl [30]. For k_{23} equal to 0.002 only a very small fraction of the power generated at the transmitter is received by the load. As k_{23} is increased the available power gain also increases and a resonant behavior can be clearly observed. In figure 3.2 the frequency at which the maximum gain is obtained is the same in all cases. Also, for k_{23} equal to 0.017, which is still a low value, the gain is already almost at 0.6. This is a very important aspect and is what best distinguishes resonant magnetic coupling from inductive coupling, where high magnetic coupling coefficients are required for high efficiency. As can be seen in figure 3.3, the resonant frequency splits into two as k_{23} is increased from 0.02 to 0.03. Increasing k_{23} further (up to 0.18 in this analysis) results in a larger separation between resonances. The splitting is approximately symmetrical. A very interesting property of resonant magnetic coupling is that the maximum gain remains very stable after the splitting occurs. Therefore, for a certain range of magnetic coupling coefficients, or distances, there is essentially no variation in gain.

Table 3.1: Reference parameters used in the analysis of the model represented in figure 3.1.

Parameter	Value
R_I, R_O	50 Ω
R_1, R_4	2 Ω
R_2, R_3	10 Ω
C_1, C_4	140 pF
C_2, C_3	5 pF
L_1, L_4	1 μH
L_2, L_3	28 μH
k_{12}, k_{34}	0.1

The ideal scenario in resonant magnetic coupling is when R_1, R_2, R_3 and R_4 are reduced to zero or, equivalently, when the Qs tend to infinity. Since there are no resistive losses, the maximum gain reaches 1, and in this case with k_{23} as low as 0.02, as can be seen in figure 3.4. A maximum gain of 1 means that all the power available in the transmitter is effectively delivered to the load. Compared to the reference figures 3.2 and 3.3, the resonances are sharper. This means that such a system would be very sensitive to detuning. It can be clearly seen in this case that Q plays a major role in the power transfer.

The effect of doubling L_3 and reducing the value of C_3 by the same ratio is shown in figure 3.5. Compared to the reference, the maximum gain increases by about 0.05. However, it is reasonable to expect that an increase in L_3 would most likely result in an increase of R_3 and that would

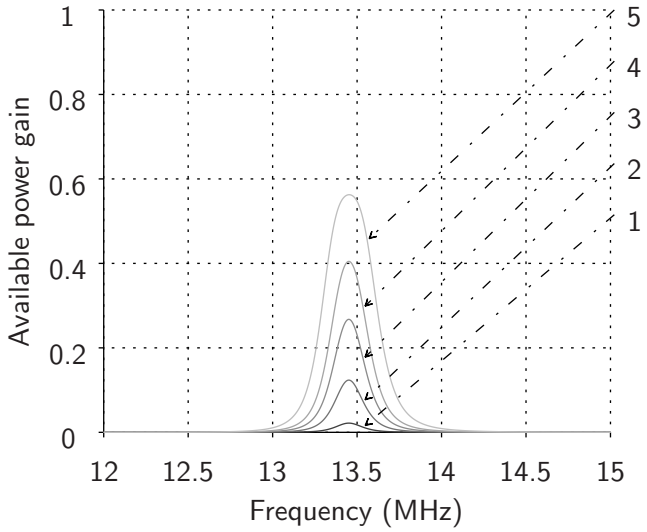

Figure 3.2: Available power gain as a function of frequency for k_{23} equal to 0.002 (curve 1), 0.005, 0.008, 0.011 and 0.017 (curve 5), calculated using (3.21) and (3.25), considering the parameters listed in table 3.1.

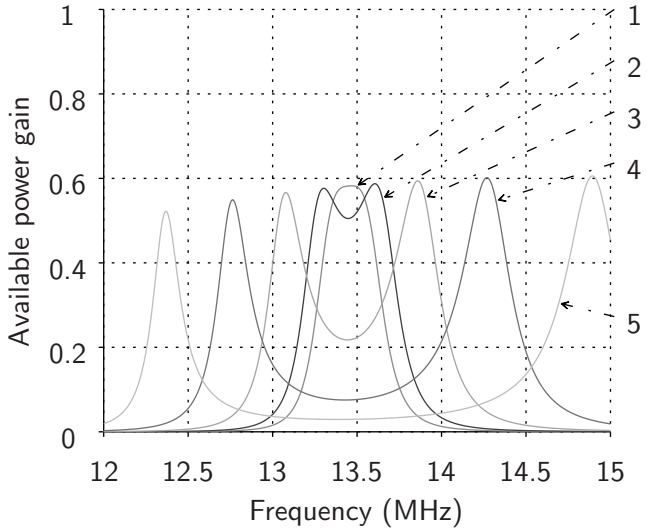

Figure 3.3: Available power gain as a function of frequency for k_{23} equal to 0.02 (curve 1), 0.03, 0.06, 0.11 and 0.18 (curve 5), calculated as described in the caption of figure 3.2.

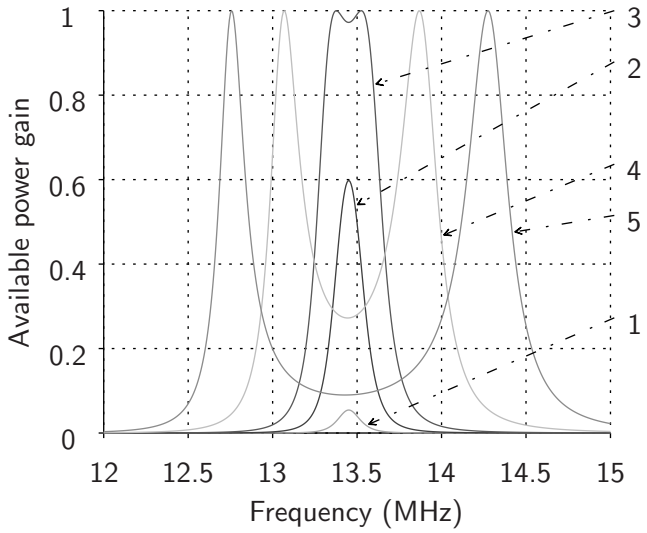

Figure 3.4: Available power gain as a function of frequency for k_{23} equal to 0.002 (curve 1), 0.008, 0.02, 0.06 and 0.11 (curve 5), calculated as described in the caption of figure 3.2, but with R_1, R_2, R_3 and R_4 all reduced to 0.

reduce the gain. In conclusion, the results are not much different from the reference. The opposite case, in which C_3 is doubled and L_3 is reduced by the same ratio is presented in figure 3.6. A decrease of about 0.1 in maximum gain compared to the reference can be observed in this case. However, a lower L_3 would most likely result in a lower value of R_3, which in turn would increase the maximum gain. In conclusion, as shown in figures 3.5 and 3.6, resonant magnetic coupling seems to be compatible with different values of L_3 and C_3, as long as their product, and therefore the resonant frequency, do not change.

If however the product does change, a significant decrease of maximum gain can be observed. In this case L_3 was reduced by just 5%. As can be seen in figure 3.7, for k_{23} values below 0.011 the gain is negligible. Furthermore, two resonant frequencies are observed even at lower k_{23} values. Higher values of k_{23} are required for achieving a maximum gain close to the reference.

Finally, figure 3.8 shows the effect of increasing k_{34} from 0.1 to 0.3. The result is an increase of maximum gain to 0.65, which is about 0.1 higher than the reference. This particularly high gain is obtained for k_{23} equal to 0.06. At all the other k_{23} values the gain is lower than the reference. Also, no frequency splitting is observed in this case. In conclusion, the gain can be optimized for a certain k_{23} (or equivalently distance) by adjusting k_{34}. Although not shown, adjusting k_{12} yields similar results.

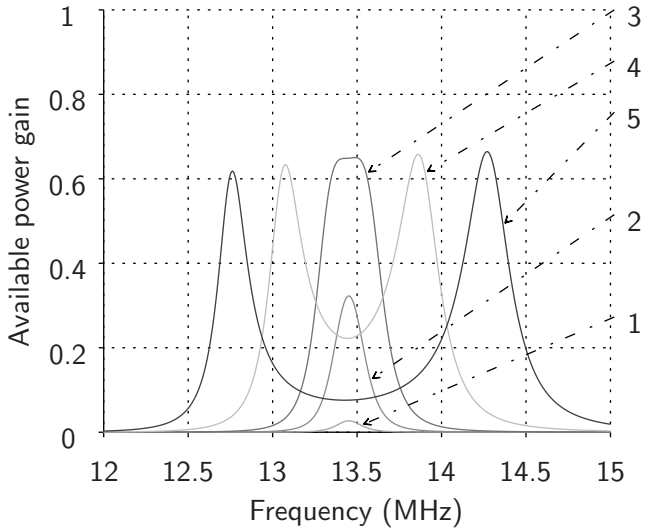

Figure 3.5: Available power gain as a function of frequency for k_{23} equal to 0.002 (curve 1), 0.008, 0.02, 0.06 and 0.11 (curve 5), calculated as described in the caption of figure 3.2, but with L_3 increased to 56 μH (twice the reference value) and C_3 reduced to 2.5 pF (half the reference value).

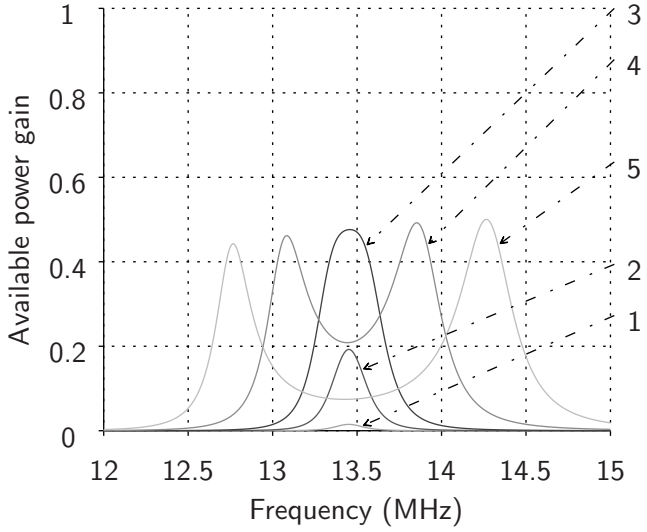

Figure 3.6: Available power gain as a function of frequency for k_{23} equal to 0.002 (curve 1), 0.008, 0.02, 0.06 and 0.11 (curve 5), calculated as described in the caption of figure 3.2, but with L_3 reduced to 14 μH (half the reference value) and C_3 increased to 10 pF (twice the reference value).

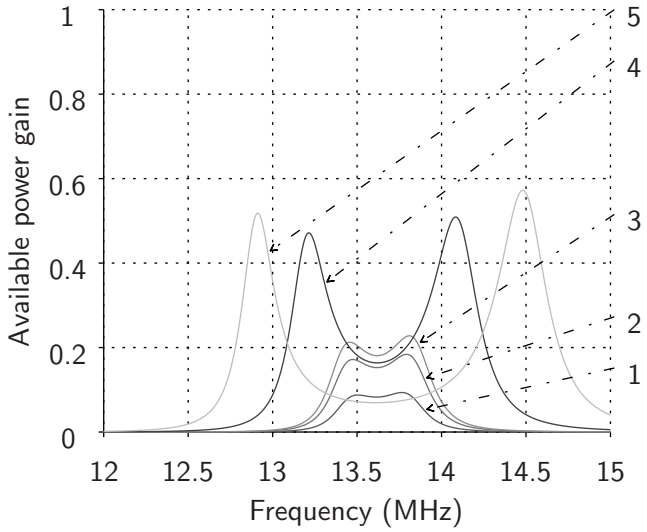

Figure 3.7: Available power gain as a function of frequency for k_{23} equal to 0.011 (curve 1), 0.017, 0.02, 0.06 and 0.11 (curve 5), calculated as described in the caption of figure 3.2, but with L_3 reduced to 26.6 μH (-5%).

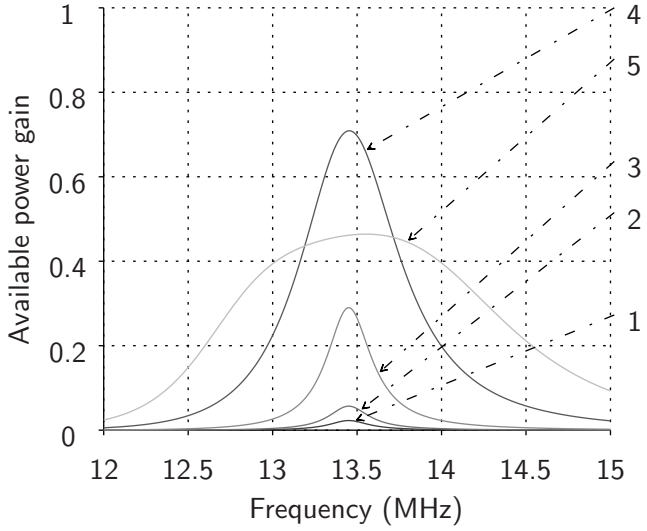

Figure 3.8: Available power gain as a function of frequency for k_{23} equal to 0.005 (curve 1), 0.008, 0.02, 0.06 and 0.11 (curve 5), calculated as described in the caption of figure 3.2, but with k_{34} increased from 0.1 to 0.3.

Chapter 4

Resonant electrical coupling

4.1 Summary

In the first part of this chapter a study of resonant electrical coupling based on circuit theory is presented. A proof of concept is considered afterwards, based on the conclusions obtained from the theoretical analysis. In the last part of the chapter the possibility of constructively combining resonant magnetic coupling and resonant electrical coupling is considered.

4.2 Feasibility study

In the next sub-section an analysis of the circuit selected to represent resonant electrical coupling is presented. This analysis follows a similar procedure to the procedure used in chapter 3 for resonant magnetic coupling. A slightly different circuit considered during the initial part of this study is mentioned in the second sub-section. In the last sub-section some parasitic capacitances that may be important in some implementations of the selected circuit are analyzed.

4.2.1 Selected circuit model

In this part, resonant electrical coupling is analyzed based on the circuit model presented in figure 4.1. The main purpose of the analysis is to link specific parameter variations to specific output variations. In the model, the power source is represented by the voltage source V_I plus the resistance R_I and the load is represented by R_O. The capacitive coupling between the source and the load is represented by C_3 and C_4. The remaining capacitances C_1 and C_2 are included in the model to resonate with L_1 and L_2, respectively. Lastly, the losses in L_1 and L_2 are taken into account in R_1 and R_2. If C_3 and C_4 are considered as an admittance two-port network

(highlighted in the figure by the dashed lines) it is possible to write

$$(R_I + R_1 + jwL_1)I_3 + jwM_{12}I_4 + V_1 - V_I = 0 \tag{4.1}$$
$$I_1 - I_3 + jwC_1V_1 = 0 \tag{4.2}$$
$$I_2 + I_4 + jwC_2V_2 = 0 \tag{4.3}$$
$$jwM_{12}I_3 + (R_2 + jwL_2)I_4 - V_2 + V_O = 0 \tag{4.4}$$
$$R_OI_4 - V_O = 0 \tag{4.5}$$
$$I_1 - Y_{11}V_1 - Y_{12}V_2 = 0 \tag{4.6}$$
$$I_2 - Y_{21}V_1 - Y_{22}V_2 = 0, \tag{4.7}$$

in which

$$Y_{11} = jwC_3C_4/(C_3 + C_4) \tag{4.8}$$
$$Y_{12} = -Y_{11} \tag{4.9}$$
$$Y_{21} = -Y_{11} \tag{4.10}$$
$$Y_{22} = Y_{11}. \tag{4.11}$$

Solving (4.6) for I_1 and substituting in (4.2) gives

$$I_3 - K_1V_1 - Y_{12}V_2 = 0, \tag{4.12}$$

in which

$$K_1 = Y_{11} + jwC_1. \tag{4.13}$$

Solving (4.7) for I_2 and substituting in (4.3) gives

$$I_4 + Y_{21}V_1 + K_2V_2 = 0, \tag{4.14}$$

in which

$$K_2 = Y_{22} + jwC_2. \tag{4.15}$$

Solving (4.14) for V_2 and substituting in (4.12) gives

$$K_2I_3 + Y_{12}I_4 - K_3V_1 = 0, \tag{4.16}$$

in which

$$K_3 = K_1K_2 - Y_{12}Y_{21}. \tag{4.17}$$

Substituting (4.14) also in (4.4) gives

$$jwM_{12}I_3 + (R_2 + jwL_2 + 1/K_2)I_4 + Y_{21}V_1/K_2 + V_O = 0. \tag{4.18}$$

Solving (4.16) for V_1 and substituting in (4.1) gives

$$(Z_1 + K_2/K_3)I_3 + (Y_{12}/K_3 + jwM_{12})I_4 - V_I = 0, \tag{4.19}$$

in which

$$Z_1 = R_I + R_1 + jwL_1. \tag{4.20}$$

Substituting (4.16) also in (4.18) gives

$$(Y_{21}/K_3 + jwM_{12})I_3 + (R_2 + jwL_2 + 1/K_2 + Y_{12}Y_{21}/[K_2K_3])I_4 + V_O = 0. \tag{4.21}$$

Solving (4.5) for I_4 and substituting in (4.21) gives

$$R_O(Y_{21}/K_3 + jwM_{12})I_3 + (Z_2 + 1/K_2 + Y_{12}Y_{21}/[K_2K_3])V_O = 0, \tag{4.22}$$

in which

$$Z_2 = R_O + R_2 + jwL_2. \tag{4.23}$$

Substituting (4.5) also in (4.19) gives

$$(Z_1 + K_2/K_3)I_3 - V_I + (Y_{12}/K_3 + jwM_{12})V_O/R_O = 0. \tag{4.24}$$

Solving (4.22) for I_3 and substituting in (4.24) gives

$$V_O/V_I = R_O(Y_{21} + jwM_{12}K_3)/(jwM_{12}[Y_{12} + Y_{21}] - w^2M_{12}^2K_3 + Y_{12}Y_{21}Z_1Z_2 - [1 + K_1Z_1][1 + K_2Z_2]). \tag{4.25}$$

Considering

$$M_{12} = k_{12}\sqrt{L_1L_2}, \tag{4.26}$$

(4.25) can be rewritten as

$$V_O/V_I = R_O(Y_{21} + jwk_{12}\sqrt{L_1L_2}K_3)/(jwk_{12}\sqrt{L_1L_2}[Y_{12} + Y_{21}] - w^2k_{12}^2L_1L_2K_3 + Y_{12}Y_{21}Z_1Z_2 - [1 + K_1Z_1][1 + K_2Z_2]). \tag{4.27}$$

The available power gain can be calculated with (3.25) as before, but in this case using the voltage gain from (4.27) instead of (3.21).

The response of this model as a function of frequency for C_3 equal to 0.02, 0.05, 0.09, 0.14, 0.24, 0.27, 0.35, 0.54, 0.81 and 1.2 pF considering the parameters listed in table 4.1 is illustrated in figures 4.2 and 4.3. It is important to note that no magnetic coupling is considered between the inductances L_1 and L_2 in this part, which means that the source and the load are assumed to be only coupled capacitively through C_3 and C_4. The parameters from table 4.1 are similar to the parameters used in the analysis presented in chapter 3. Lastly, C_4 is always considered equal to C_3.

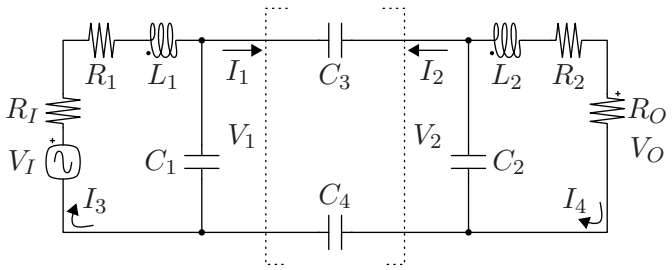

Figure 4.1: Circuit model considered in the study of resonant electrical coupling. The left and right parts of the circuit are coupled by C_3 and C_4.

Table 4.1: Reference parameters used in the analysis of the model represented in figure 4.1.

Parameter	Value
R_I, R_O	50 Ω
R_1, R_2	12 Ω
C_1, C_2	5 pF
L_1, L_2	28 μH
k_{12}	0

Figures 4.2 and 4.3 are similar to figures 3.2 and 3.3 in several aspects. For lower values of C_3, in this case 0.02 pF, only a very small of the available power is effectively received by the load. As C_3 is increased the available power gain also increases and a resonant behavior can be observed. This behavior is generally the same as in resonant magnetic coupling. The most significant difference is that in this case the resonant frequency decreases slightly as C_3 is increased. For C_3 equal to 0.24 pF, which is still a small value, the gain is already slightly above 0.6. The difference in peak gain is not critical since obtaining an equal gain in both cases is simply a matter of slightly adjusting the resistive elements. This is what best distinguishes resonant electrical coupling from capacitive coupling. As C_3 is further increased from 0.27 to 0.35 pF the resonant frequency splits into two. Continuing to increase C_3 (up to 1.2 pF in this case) results in a wider spacing between resonances. Unlike in resonant magnetic coupling, however, the splitting is highly asymmetrical, as the upper resonant frequency barely moves. The maximum gain remains very stable after the splitting occurs. Thus, for a range of C_3 values, or distances, the variation in gain is minimal.

Figure 4.4 shows the ideal scenario in which R_1 and R_2 are reduced to zero or, equivalently, when the Qs tend to infinity. Without the losses caused by the resistive components the maximum gain reaches 1, in this case with C_3 as low as 0.27 pF. A maximum gain of 1 means that all the power available in the transmitter is effectively delivered to the load. In this case the sensitivity to detuning is more significant. Since the resonances are sharper, the tuning has to be better in

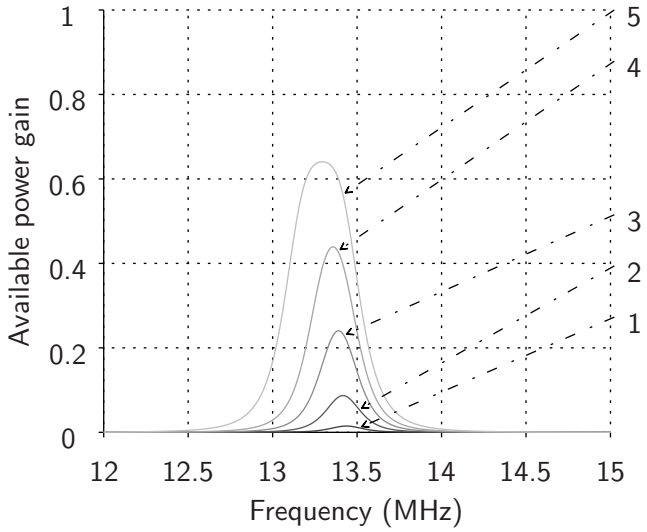

Figure 4.2: Available power gain as a function of frequency for C_3 equal to 0.02 (curve 1), 0.05, 0.09, 0.14 and 0.24 pF (curve 5), calculated using (4.27) and (3.25), considering the parameters listed in table 4.1.

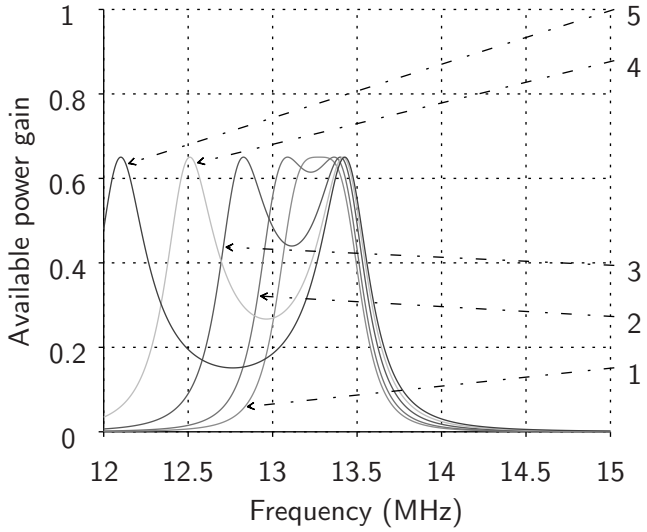

Figure 4.3: Available power gain as a function of frequency for C_3 equal to 0.27 (curve 1), 0.35, 0.54, 0.81 and 1.2 pF (curve 5), calculated as described in the caption of figure 4.2.

order to avoid substantial losses in efficiency. It can be clearly seen in this case that Q plays a major role in the power transfer, just as in resonant magnetic coupling.

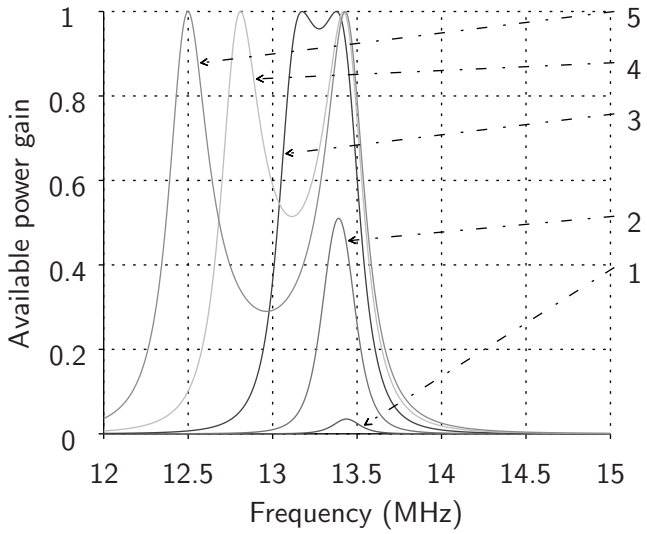

Figure 4.4: Available power gain as a function of frequency for C_3 equal to 0.02 (curve 1), 0.09, 0.27, 0.54 and 0.81 pF (curve 5), calculated as described in the caption of figure 4.2, but with R_1 and R_2 reduced to 0.

The effect of doubling L_2 and reducing the value of C_2 by the same ratio is shown in figure 4.5. As can be seen in the figure, the gain increases faster than the reference as C_3 is increased and stabilizes at approximately the same value. The splitting, however, begins sooner and the resonances are sharper. In this case there is a significant difference in gain between the two resonances, with the upper resonance not reaching the maximum gain reached by the lower resonance. As shown in figure 4.6, if both L_1 and L_2 are doubled and C_1 and C_2 reduced to half this difference in gain is no longer observed.

The opposite case of figure 4.5, in which L_2 is reduced to half and C_2 is doubled is presented in figure 4.7. In this case the gain increases at a slower rate. The curve corresponding to C_3 equal to 0.02 pF is replaced by 0.05 pF because the gain is negligible at 0.02 pF. As shown in figure 4.8, if both L_1 and L_2 are reduced to half and C_1 and C_2 are doubled the behavior becomes slighly more symmetrical. In this case the rate at which the gain increases is even lower. The curve corresponding to C_3 equal to 0.02 pF is replaced by 0.14 pF due to negligible gain.

Finally, figure 4.9 shows the effect of reducing L_2 by 5%. For C_3 values below 0.05 pF the gain is negligible. Furthermore, two resonant frequencies are observed even at lower C_3 values. Higher values of C_3 are required for achieving a maximum gain close to the reference. In resonant magnetic coupling the gain degradation caused by an equivalent mismatch is similar.

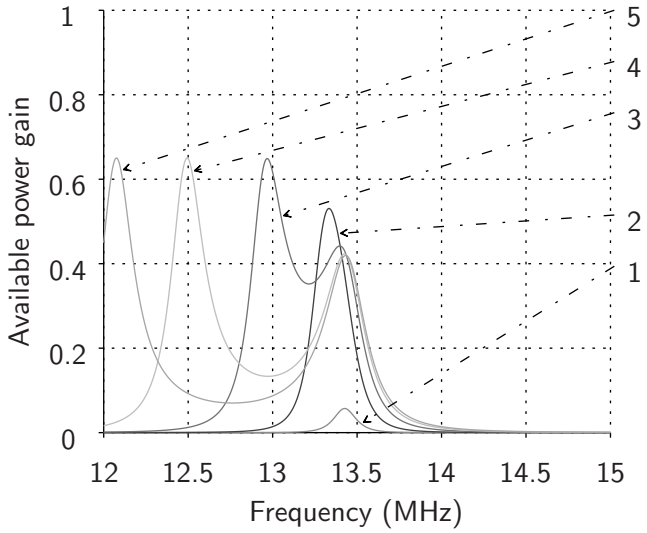

Figure 4.5: Available power gain as a function of frequency for C_3 equal to 0.02 (curve 1), 0.09, 0.27, 0.54 and 0.81 pF (curve 5), calculated as described in the caption of figure 4.2, but with L_2 increased to 56 μH (twice the reference value) and C_2 reduced to 2.5 pF (half the reference value).

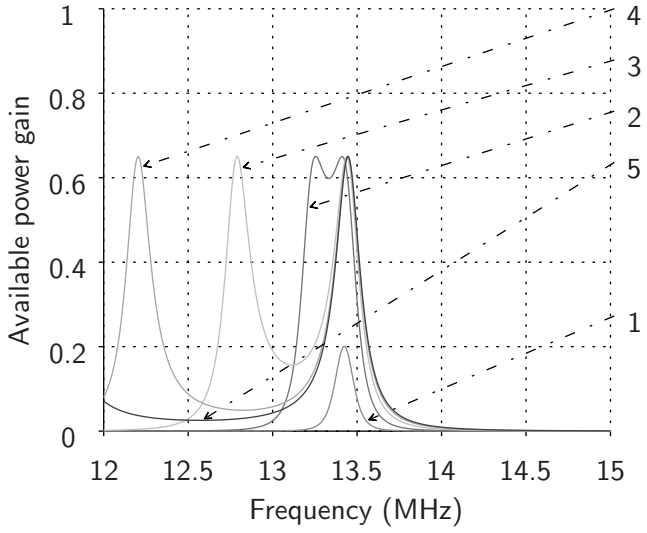

Figure 4.6: Available power gain as a function of frequency for C_3 equal to 0.02 (curve 1), 0.09, 0.27, 0.54 and 0.81 pF (curve 5), calculated as described in the caption of figure 4.2, but with L_1 and L_2 increased to 56 μH (twice the reference values) and C_1 and C_2 reduced to 2.5 pF (half the reference values).

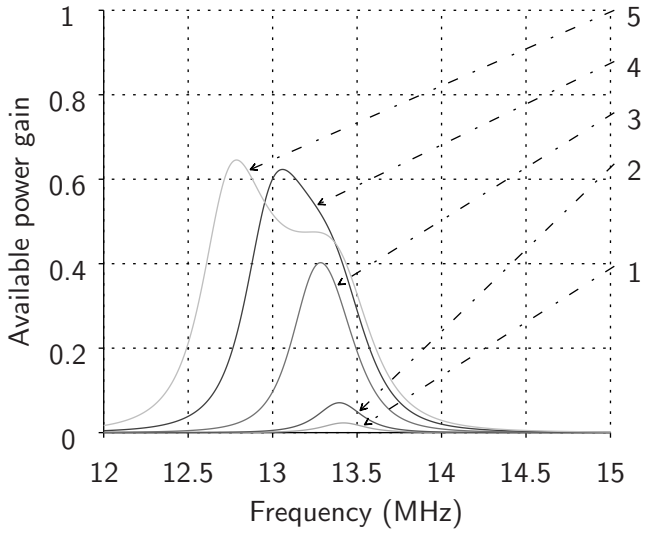

Figure 4.7: Available power gain as a function of frequency for C_3 equal to 0.05 (curve 1), 0.09, 0.27, 0.54 and 0.81 pF (curve 5), calculated as described in the caption of figure 4.2, but with L_2 reduced to 14 μH (half the reference value) and C_2 increased to 10 pF (twice the reference value).

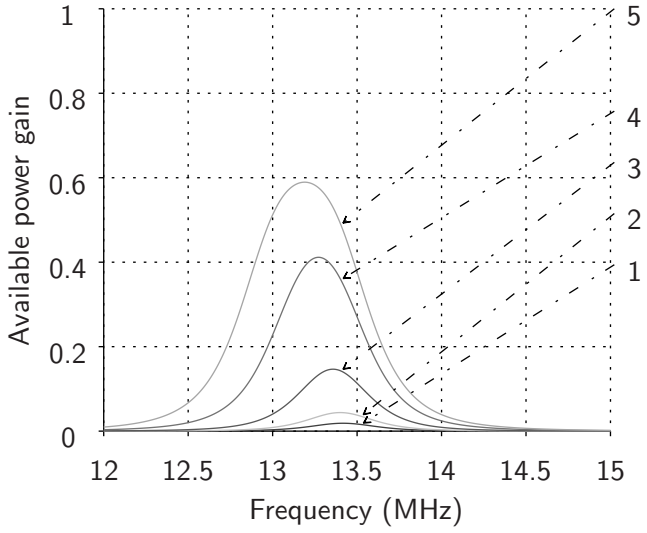

Figure 4.8: Available power gain as a function of frequency for C_3 equal to 0.09 (curve 1), 0.14, 0.27, 0.54 and 0.81 pF (curve 5), calculated as described in the caption of figure 4.2, but with L_1 and L_2 reduced to 14 μH (half the reference values) and C_1 and C_2 increased to 10 pF (twice the reference values).

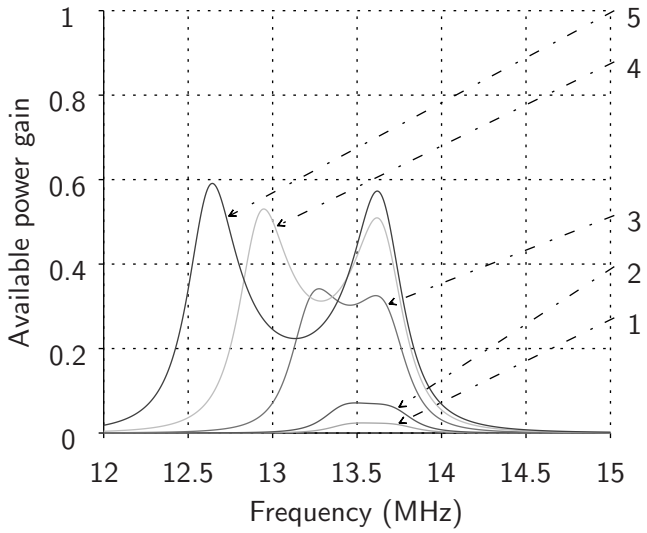

Figure 4.9: Available power gain as a function of frequency for C_3 equal to 0.05 (curve 1), 0.09, 0.27, 0.54 and 0.81 pF (curve 5), calculated as described in the caption of figure 4.2, but with L_2 reduced to 26.6 μH (-5%).

4.2.2 Alternative circuit

Figure 4.10 shows a circuit model that was considered together with the circuit from figure 4.1 during the initial study of resonant electrical coupling. Although comparable results can be obtained with both circuits with similar component values, the circuit from figure 4.1 is more convenient from the point of view of the implementation of a proof of concept, as shown in sections 4.3 and 5.2.

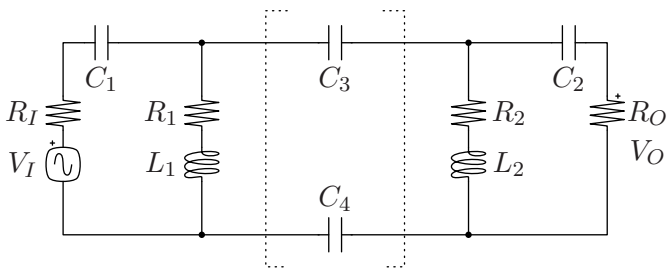

Figure 4.10: Alternative circuit model considered during the initial study of resonant electrical coupling.

4.2.3 Effect of parasitic capacitances

If the two-port network mentioned earlier is replaced by the network shown in figure 4.11 the admittance parameters presented in (4.8), (4.9), (4.10) and (4.11) become

$$Y_{11} = jw(C_3C_4 + C_3C_6 + C_4C_5 + C_5C_6)/D \tag{4.28}$$

$$Y_{12} = jw(C_5C_6 - C_3C_4)/D \tag{4.29}$$

$$Y_{21} = Y_{12} \tag{4.30}$$

$$Y_{22} = jw(C_3C_4 + C_3C_5 + C_4C_6 + C_5C_6)/D, \tag{4.31}$$

in which

$$D = C_3 + C_4 + C_5 + C_6. \tag{4.32}$$

The effect of the capacitances C_5 and C_6 in the response of the model is shown in figure 4.12, considering

$$C_5 = C_3/2 \tag{4.33}$$

$$C_6 = C_5. \tag{4.34}$$

It may be needed to consider these additional unwanted couplings in a practical implementation depending on the physical proximity of C_3 and C_4, and hence this analysis. In general, as C_5 and C_6 increase, the gain degradation becomes much more pronounced. In the worst-case scenario, when the product C_5C_6 is equal to C_3C_4, (4.29) and (4.30) become zero and thus (4.27) and (3.25) also become zero. As a last note, the calculations shown in this sub-section are related with the calculations presented in [55].

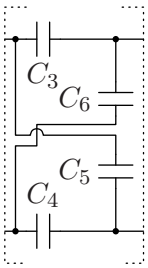

Figure 4.11: Additional capacitances C_5 and C_6 taken into account in the circuit of figure 4.1.

4.3 Proof of concept

An illustration of the proof of concept designed to validate the model from figure 4.1 is presented in figure 4.13. The system consists of two identical devices. One of the devices is used as a power transmitter and the other is used as a receiver. Each device is composed by a coil and two identical

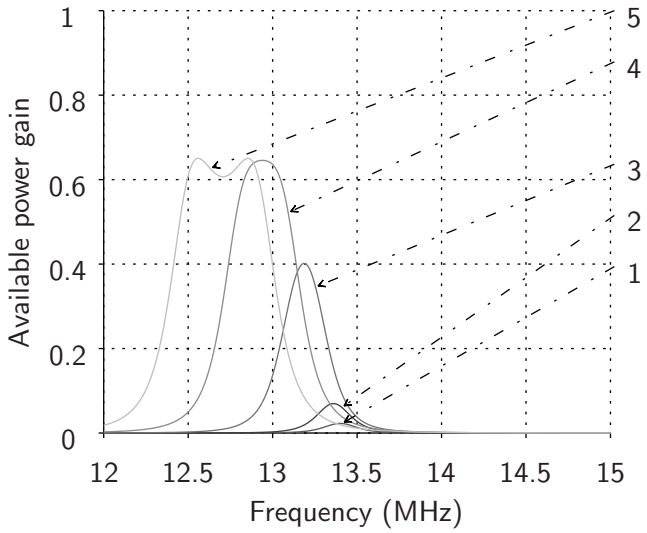

Figure 4.12: Available power gain as a function of frequency for C_3 equal to 0.05 (curve 1), 0.09, 0.27, 0.54 and 0.81 pF (curve 5), calculated as described in the caption of figure 4.2, but with C_5 and C_6 increased from 0 to half of C_3.

conductive plates. A capacitance exists between the two conductive plates in each device, as they are physically close to each other. These are the capacitances that implement C_1 and C_2 from the model. This is convenient because the capacitances are necessarily there and this way they can be used to implement part of the system. This is also the reason why the circuit from figure 4.1 is more convenient than the circuit from figure 4.10 in terms of implementation. The coupling between the transmitter and the receiver is represented by C_3 and C_4. Larger conductive plates help to increase the values of these capacitances and thus the available power gain. In this case, however, it may be more challenging to keep C_1 and C_2 low enough to avoid a behavior similar to the behavior shown in figure 4.8.

Figure 4.13: Graphical illustration of resonant electrical coupling proposed based on the circuit model shown in figure 4.1.

4.4 Possibility of hybrid coupling

In the previous sections, the coupling between L_1 and L_2 has always been considered zero, meaning only electrical coupling. In this part the effect of this coupling is also taken into account. In other words, the left and right parts of the circuit are considered to be coupled electrically through C_3 and C_4 and also magnetically through k_{12}. Figure 4.14 shows the effect of increasing k_{12} from 0 to 0.06 while keeping C_3 fixed at 0.05 pF. As can be seen, the gain increases as k_{12} is increased. In other words, the combination of both coupling techniques effectively results in an improvement. On the other hand, figure 4.15 shows the effect of increasing C_3 from 0 to 0.54 pF while keeping k_{12} fixed at 0.005. As can be seen, the gain increases as C_3 is increased. The existence of asymmetry in the frequency splitting depends on which kind of coupling is the largest contributor. In this last figure the largest contributor is electrical coupling so the splitting is more asymmetrical. In figure 4.14 the largest contributor is magnetic coupling so the splitting is more symmetrical. This hybrid coupling is the subject of [4].

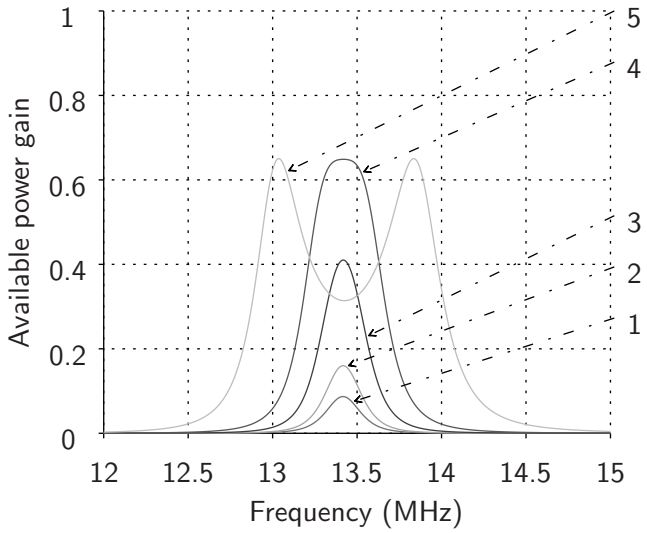

Figure 4.14: Available power gain as a function of frequency for k_{12} equal to 0 (curve 1), 0.002, 0.008, 0.02 and 0.06 (curve 5), calculated as described in the caption of figure 4.2, but with C_3 always equal to 0.05 pF.

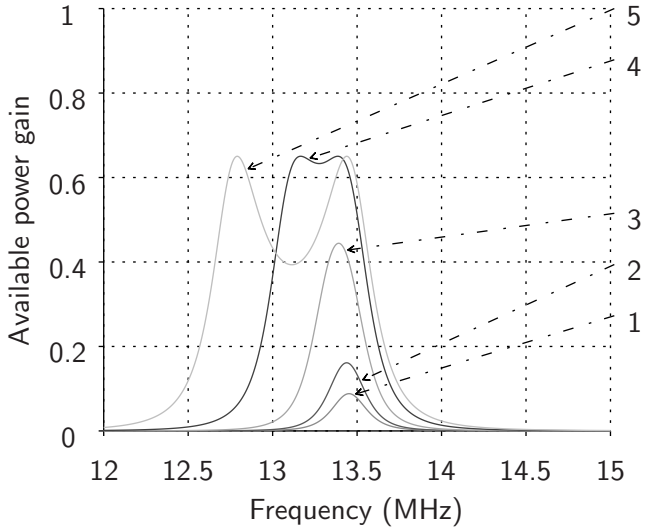

Figure 4.15: Available power gain as a function of frequency for C_3 equal to 0 (curve 1), 0.02, 0.09, 0.27 and 0.54 pF (curve 5), calculated as described in the caption of figure 4.2, but with k_{12} increased from 0 to 0.005.

Chapter 5

Experimental results

5.1 Summary

In the first part of this chapter the implemented prototype based on the illustration of figure 4.13 is described. The scattering parameters of the prototype are then presented. Efficiency measurements using an RF-to-DC converter are then presented. In the last part of the chapter some additional observations made during measurements are described.

5.2 Prototype

A photograph of the proof-of-concept prototype developed based on the illustration from figure 4.13 is shown in figure 5.1. The prototype consists of two mirrored resonators, each one composed by a 16 by 16 cm board made of FR-4 with two large copper zones of equal areas and a coil mounted on the back side. Since the copper zones in each device are implemented in the same piece of FR-4, the distance between them remains constant at all times, which ensures that the values of C_1 and C_2 are stable. One of the most significant challenges in the implementation of resonant electrical coupling is the design of the inductors. In particular, it is very difficult to build an inductor that achieves a high value of inductance at a relatively high frequency, with low resistive losses. In addition, such inductor also has to have a relatively high self resonant frequency, in order to minimize resistive losses. Building high quality inductors is one of the most significant challenges in the design of near-field wireless power systems, as mentioned in [75]. In this prototype both coils have a diameter of 3.6 cm, 40 turns, are both made of 0.8 mm diameter stranded copper wire and were both constructed by hand in order to create an inductance large enough to make the prototype resonate between 12 and 15 MHz. The construction of the coils previously described was made based on available materials and formulas typically used in the estimation of the inductance of solenoids, in particular

$$L = \mu_0 \pi d^2 N^2 / (4l), \tag{5.1}$$

in which μ_0 is the magnetic permability of free space (since no cores are used), d is the diameter of the coil, N is the number of turns and l is the length.

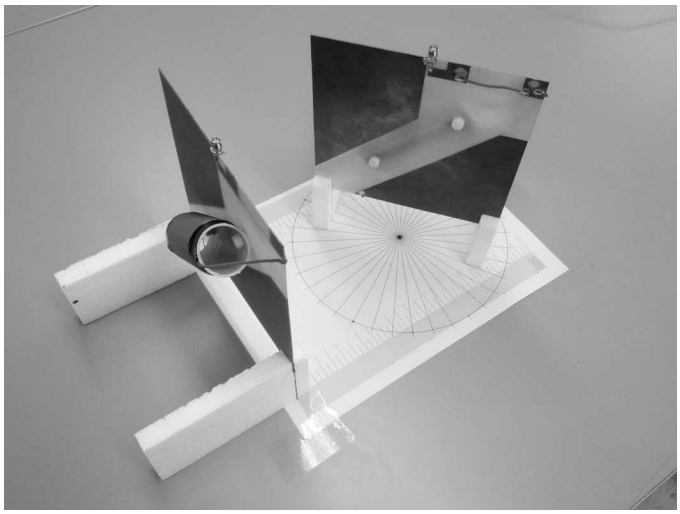

Figure 5.1: Photograph of the prototype used in the experimental validation of the model from figure 4.1.

5.3 Scattering parameters

This section contains the scattering parameters of the previously described prototype measured at distances of 10, 20, 60, 90 and 500 cm. In this test the resonators were placed front to front on top of polystyrene supports approximately 1 m high and connected to an HP 8753D network analyzer, as shown in figure 5.2. As can be seen in the $|S_{21}|$ presented in figure 5.3, a resonant behavior can be effectively observed in practice. For shorter distances, which correspond to higher C_3 values, two distinct resonant frequencies can be observed and the separation between them becomes smaller as the distance is increased, as expected. In addition, the lower resonance moves faster than the upper resonance, although the difference is not as noticeable as seen in figure 4.3, for instance. Some aspects are, however, are clearly not in agreement with the theoretical predictions. For instance, the amplitude of the peaks is not identical. It was observed that the difference between the peaks changes depending on where the experimental setup is mounted, meaning that this difference is most likely due to interference caused by nearby objects, in particular objects made of metal. Additionally, the resonant frequencies do not converge even when the distance is increased up to 500 cm. In fact, $|S_{21}|$ changes very little between 90 and 500 cm, for instance. The reason for this behavior is most likely an additional coupling path established inside the network analyzer which prevents the coupling to decrease from a certain point as the distance is increased. At shorter distances both this additional coupling and the normal coupling contribute to the result.

As the distance is increased, the normal coupling decreases but the additional coupling remains relatively constant, hence the small change from 90 to 500 cm. The peak values of figure 5.3 are listed in tables 5.1 and 5.2.

Figure 5.2: Experimental setup for measuring the scattering parameters of the prototype shown in figure 5.1.

Figure 5.4 shows $\angle S_{21}$. As expected, the zero crossings in this figure occur approximately at the same frequencies where $|S_{21}|$ is maximum. These zero crossings are listed in table 5.3. Figures 5.5 and 5.6 show $|S_{12}|$ and $\angle S_{12}$. As expected, since the two devices in the prototype are identical, there are virtually no differences between $|S_{21}|$ and $|S_{12}|$, and between $\angle S_{21}$ and $\angle S_{12}$.

For the purposes of wireless power transfer, $|S_{21}|$ is the most important result as this parameter is an indicator of power flow from the transmitter to the receiver. For the sake of completeness, $|S_{11}|$, $\angle S_{11}$, $|S_{22}|$ and $\angle S_{22}$ are also presented, in figures 5.7, 5.8, 5.9 and 5.10, respectively. As expected, the minima in these figures match the maxima in $|S_{21}|$.

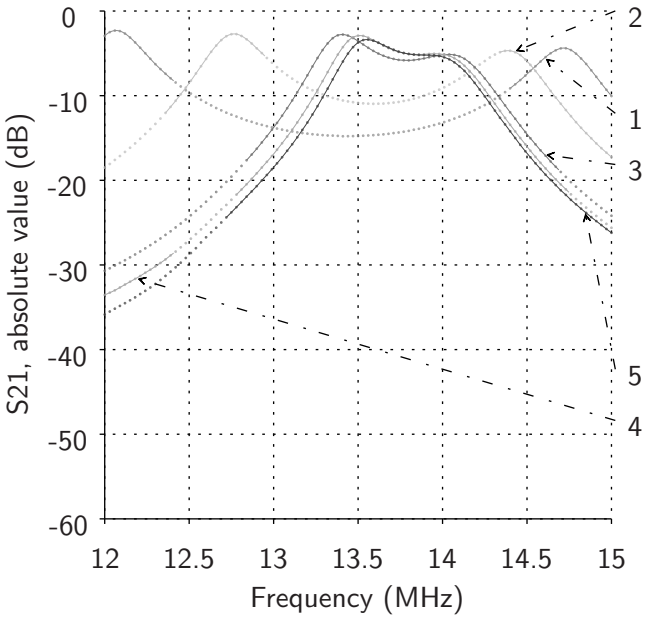

Figure 5.3: Measured $|S_{21}|$ as a function of frequency for distances equal to 10 (curve 1), 20, 60, 90 and 500 cm (curve 5).

Table 5.1: Primary peak $|S_{21}|$ values from figure 5.3 and corresponding frequencies.

Curve	$\|S_{21}\|$ (dB)	Frequency (MHz)
1	-2.31	12.06
2	-2.73	12.78
3	-2.78	13.41
4	-2.91	13.5
5	-3.38	13.56

Table 5.2: Secondary peak $|S_{21}|$ values from figure 5.3 and corresponding frequencies.

Curve	$\|S_{21}\|$ (dB)	Frequency (MHz)
1	-4.4	14.73
2	-4.7	14.4
3	-5.13	14.04
4	-5.05	13.95

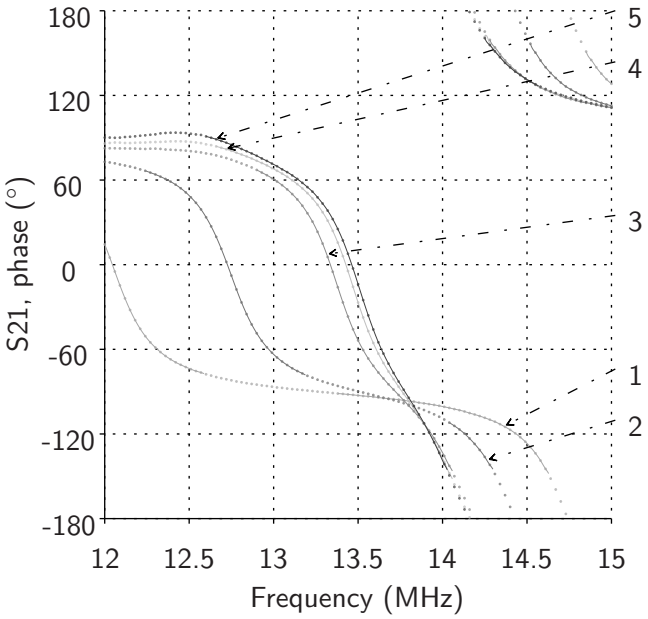

Figure 5.4: Measured $\angle S_{21}$ as a function of frequency for distances equal to 10 (curve 1), 20, 60, 90 and 500 cm (curve 5).

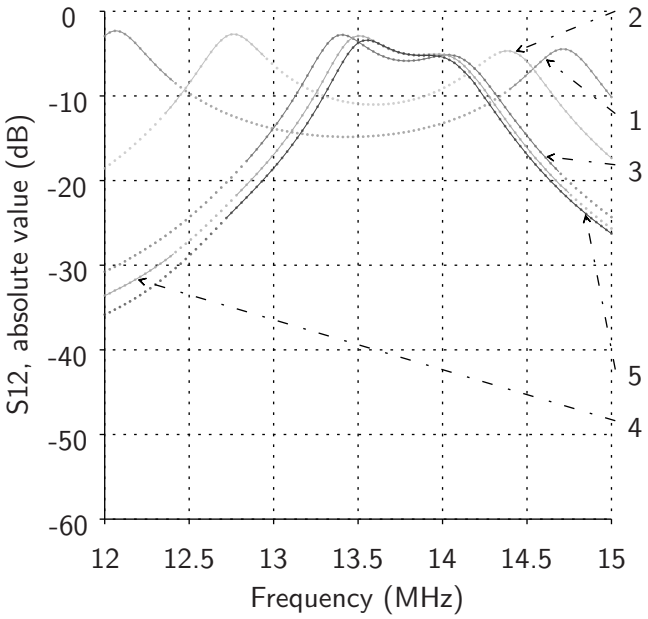

Figure 5.5: Measured $|S_{12}|$ as a function of frequency for distances equal to 10 (curve 1), 20, 60, 90 and 500 cm (curve 5).

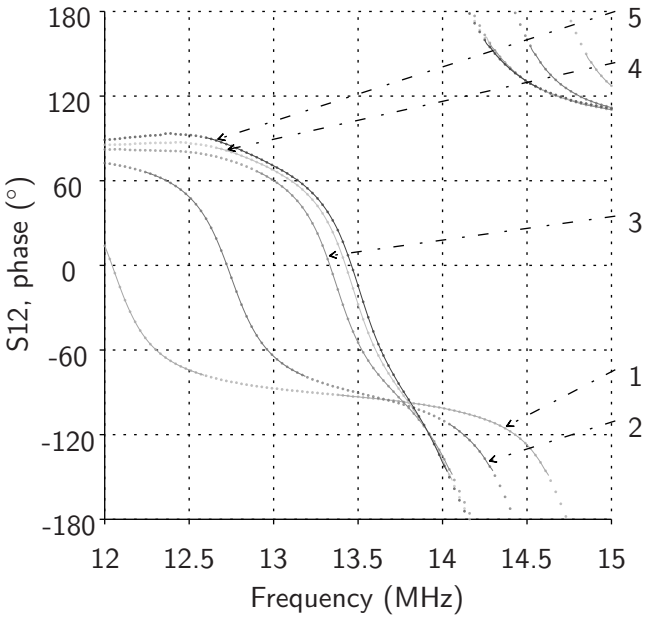

Figure 5.6: Measured $\angle S_{12}$ as a function of frequency for distances equal to 10 (curve 1), 20, 60, 90 and 500 cm (curve 5).

Table 5.3: Values of $\angle S_{21}$ closest to zero from figure 5.4 and corresponding frequencies.

Curve	$\angle S_{21}$ (°)	Frequency (MHz)
1	-4.84	12.06
1	-176.68	14.73
2	2	12.72
2	179.88	14.43
3	-5.04	13.35
3	178.85	14.19
4	-4.49	13.44
4	-179.13	14.16
5	-2.66	13.47
5	179.12	14.16

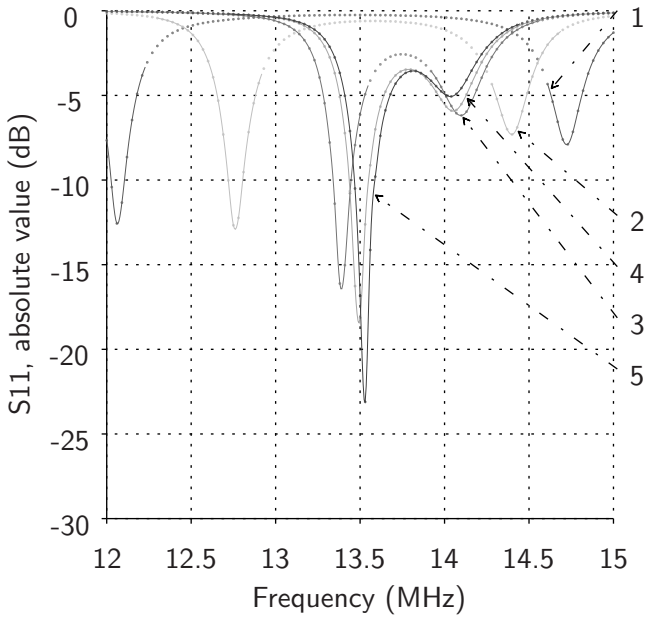

Figure 5.7: Measured $|S_{11}|$ as a function of frequency for distances equal to 10 (curve 1), 20, 60, 90 and 500 cm (curve 5).

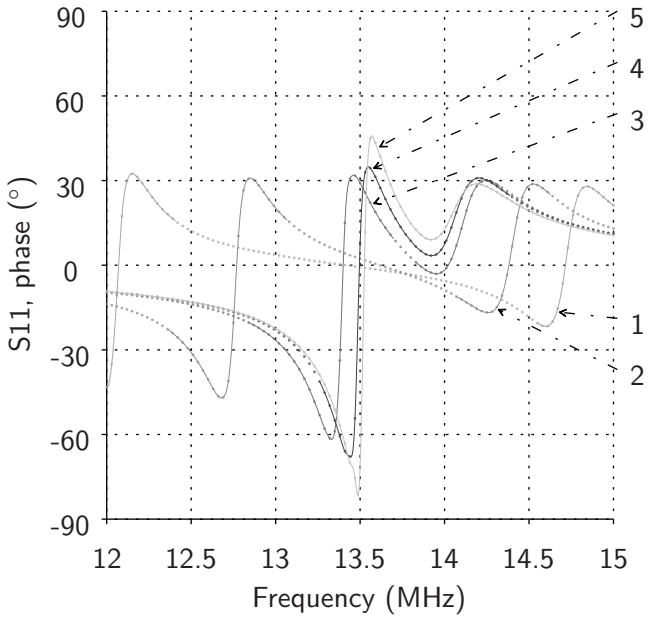

Figure 5.8: Measured $\angle S_{11}$ as a function of frequency for distances equal to 10 (curve 1), 20, 60, 90 and 500 cm (curve 5).

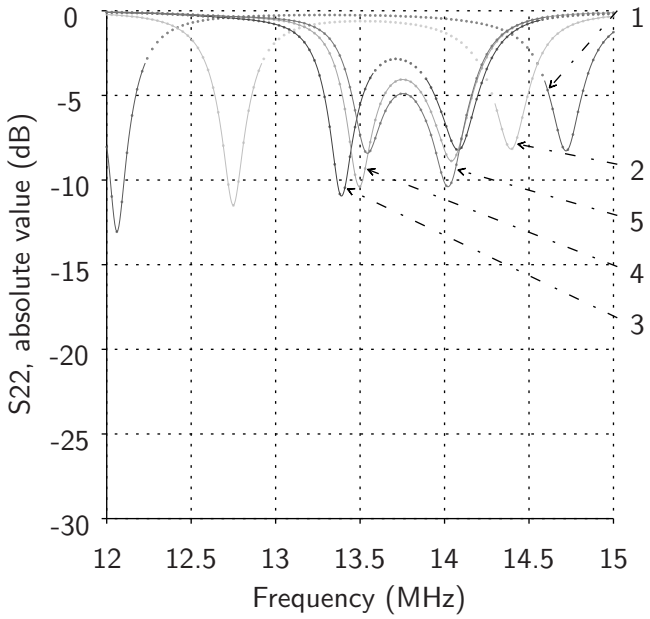

Figure 5.9: Measured $|S_{22}|$ as a function of frequency for distances equal to 10 (curve 1), 20, 60, 90 and 500 cm (curve 5).

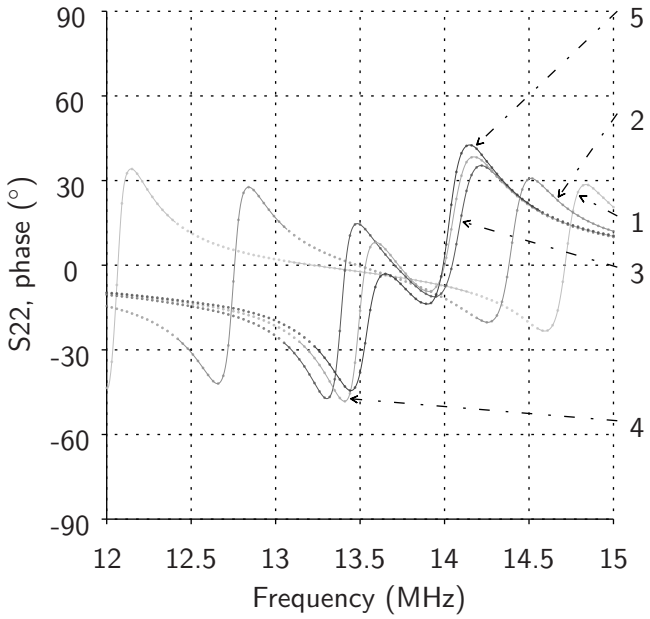

Figure 5.10: Measured $\angle S_{22}$ as a function of frequency for distances equal to 10 (curve 1), 20, 60, 90 and 500 cm (curve 5).

5.4 Use of an RF-to-DC converter

A photograph of the RF-to-DC converter designed to test the prototype can be seen in figure 5.11, on the left. This RF-to-DC converter is based on a Dickson configuration and composed by a 1.8 μH matching inductor (immediately after the connector) then three capacitors, two of 39 pF (center and right on the photograph) and one of 47 pF, three HSMS-282 Schottky diode pairs (series configuration) and then two 47 pF capacitors. At the end of the voltage multiplier is a 6.8 μF capacitor in parallel with an LED. In the right part of the photograph is an identical RF-to-DC converter in which the LED was replaced by a 680 Ω resistor, which is approximately equivalent to the LED when the latter is turned on. A schematic of the circuit is given in figure 5.12. The $|S_{11}|$ of this second RF-to-DC converter as a function of frequency is shown in figure 5.13 for power levels of 2, 4, 6, 8 and 10 dBm. As can be seen, its impedance is reasonably matched to 50 Ω in the considered frequency band.

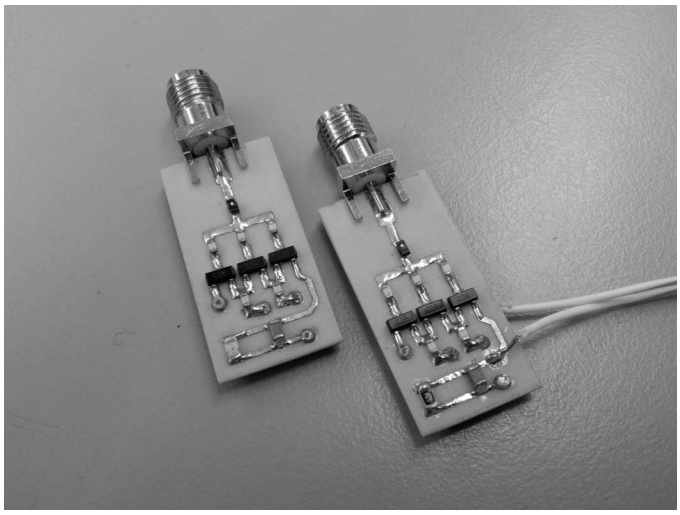

Figure 5.11: Photograph of the two RF-to-DC converters used to test the prototype from figure 5.1.

5.4.1 Distance

The voltage measured at the 680 Ω resistor as a function of frequency for distances of 12, 16, 20, 24 and 30 cm is shown in figure 5.14, considering a transmitted power of 16 dBm and the resonators always front to front, at a fixed distance of 5 cm from the floor. In this test one of the resonators was connected to an HP E4433B signal generator and the other resonator was connected to the RF-to-DC converter, as shown in figure 5.15. A resonant behavior was observed as expected, and in this case the resonances effectively converge when the distance is increased, unlike the case of figure 5.3. Table 5.4 shows the peak voltage and corresponding frequency for

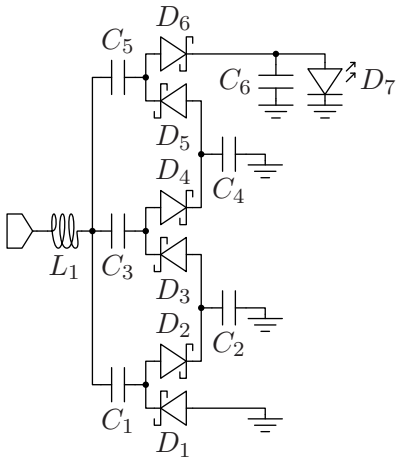

Figure 5.12: Schematic of the RF-to-DC converter with the LED.

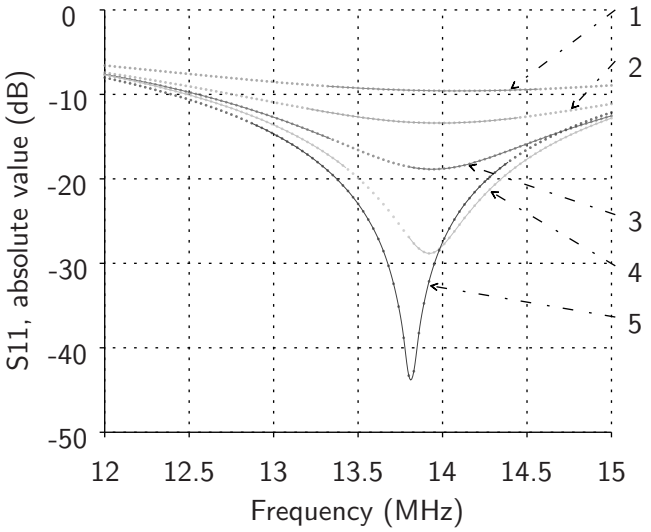

Figure 5.13: Measured $|S_{11}|$ as a function of frequency for power levels equal to 2 (curve 1), 4, 6, 8 and 10 dBm (curve 5).

each one of the curves represented in figure 5.14. An estimate for the available power gain can be obtained by connecting the transmitter and receiver cables directly, thus bypassing the prototype, measuring the power levels needed to generate the same peak voltages at the same frequencies, and then subtracting 16 dBm from those power levels.

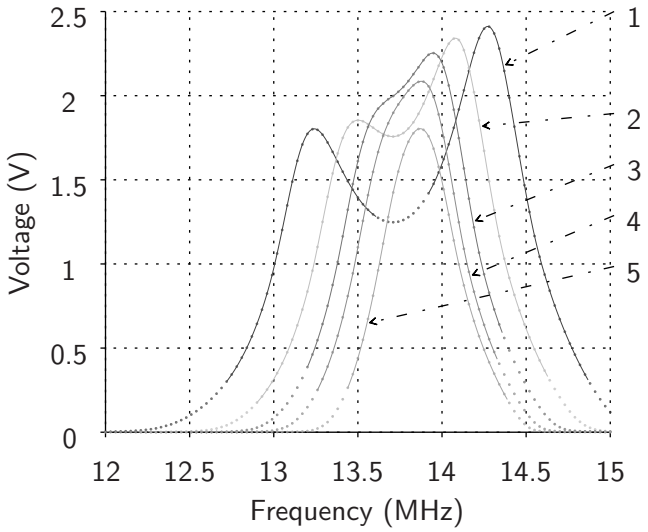

Figure 5.14: Measured voltage as a function of frequency for distances equal to 12 (curve 1), 16, 20, 24 and 30 cm (curve 5), considering a transmitted power of 16 dBm.

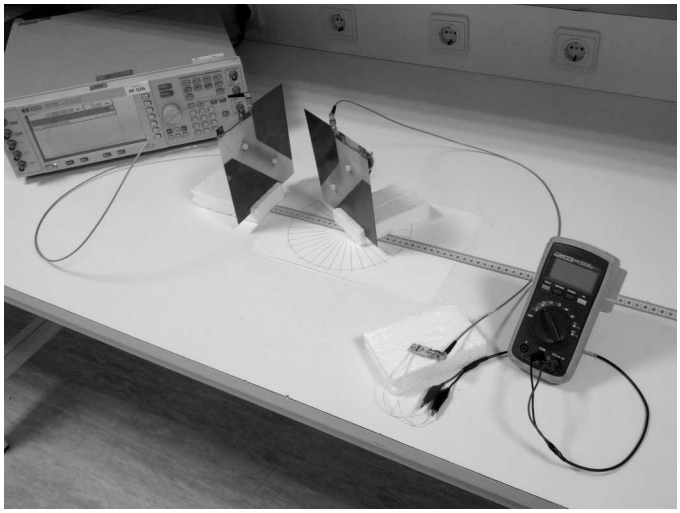

Figure 5.15: Experimental setup for measuring the voltage at the output of the RF-to-DC converter.

Table 5.4: Available power gain calculated for the peak voltages presented in figure 5.14.

Curve	Frequency (MHz)	Voltage (V)	Bypass power (dBm)	Gain
1	14.28	2.41	13.88	0.61
2	14.07	2.4	13.58	0.57
3	13.95	2.25	13.3	0.54
4	13.89	2.08	12.74	0.47
5	13.86	1.8	11.78	0.38

5.4.2 Angle

Angles of -90, -40, 40 and 90° were also considered at 16 cm. As can be seen in figure 5.16, the peak voltage increases for negative angles and decreases for positive angles. This difference is most likely the result of a non-negligible mutual inductance between the coils which can be either constructive or destructive. This result was the main motivation for the analysis of the constructive combination between resonant electrical coupling and resonant magnetic coupling considered in section 4.4. The estimated values of the available power gain for this case, calculated as previously described, can be seen in table 5.5. As a final note, the 40° case is the case represented in figure 5.1.

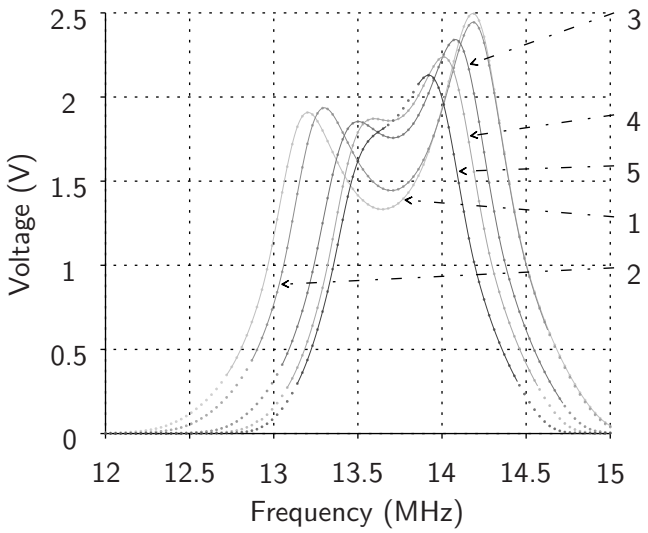

Figure 5.16: Measured voltage as a function of frequency for angles equal to -90 (curve 1), -40, 0 (same as in figure 5.14), 40 and 90° (curve 5), considering a transmitted power of 16 dBm and a distance of 16 cm.

Table 5.5: Available power gain calculated for the peak voltages presented in figure 5.16.

Curve	Frequency (MHz)	Voltage (V)	Bypass power (dBm)	Gain
1	14.19	2.5	14.04	0.64
2	14.19	2.44	13.92	0.62
4	14.01	2.24	13.26	0.53
5	13.92	2.13	12.9	0.49

5.5 Additional observations

It was observed during the experiments made with the RF-to-DC converter that external objects can be used to significantly increase distance. In the case shown in figure 5.17, for instance, placing aluminum foil between the transmitter and the receiver results in the LED being lit at a distance of about 4 times the original distance, which is obviously significant. This behavior, however, is extremely inconsistent.

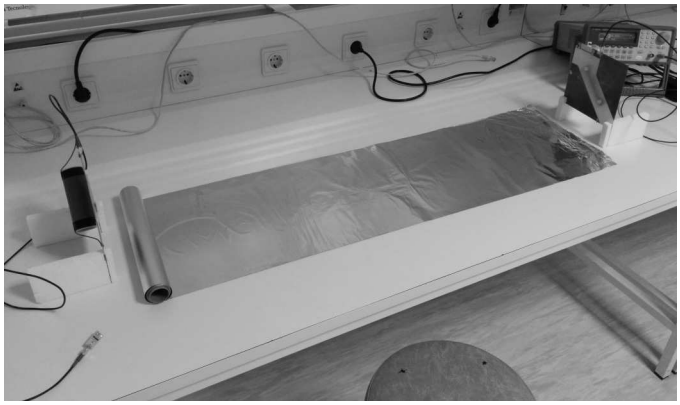

Figure 5.17: Extension of maximum distance based on the insertion of a conductive object between the transmitter and the receiver.

Chapter 6

Conclusions

6.1 Summary

The demonstration of the use of strongly coupled magnetic resonances reported in [13] caused a major impact in the field of wireless power transfer. For the first time, a significant amount of power was transferred across a distance equal to several times the dimensions of the devices involved, with at very reasonable efficiency and, very importantly, using a very simple apparatus. In addition to the technical merit, the demonstration also benefited from excelent timing, as it was made at a time when a convenient and simplified way to charge the multiple types of battery-powered wireless electronic devices in the market was in high demand. For the reasons previously mentioned, the demonstration received a significant attention from the research community, from the industry and from the press, ultimately resulting in the establishment of a new category of wireless power transfer that has been growing ever since. In fact, it is not unreasonable to conclude that the effect was larger than that, as the interest in wireless power in general has increased very significantly in the last few years.

In contrast, the use of resonance in capacitive coupling is in a very early stage of development. However, as described in chapter 4, high efficiencies can be potentially achieved with very low coupling capacitances if the resistive losses are reduced. This is similar to resonant magnetic coupling in the sense that high efficiencies can also be achieved with very low magnetic coupling coefficients if the resistive losses are reduced, as shown in chapter 3. Furthermore, the flexibility in the design of the electrodes mentioned in sub-section 1.3.3 may be very useful in some applications. A wireless transfer of power based on resonant electrical coupling is demonstrated in chapter 5, from a signal generator to an LED with efficiencies of 61% and 38% at distances of 12 cm and 30 cm, respectively, using two devices measuring approximately 16 cm by 16 cm by 3.6 cm. A relatively low variation of efficiency in case of a rotational misalignment, particularly when the receiver is perpendicular to the receiver, can also be observed in the same chapter. This can be seen as an advantage in comparison to the drop in efficiency reported in [30], for the case of

resonant magnetic coupling. However, this is most likely caused by the constructive combination of both electrical and magnetic coupling addressed in section 4.4, rather than resonant electrical coupling alone.

It is important to highlight that the circuit parameters used in the simulations presented in chapters 3 and 4 were selected in order to link specific output variations with specific input variations such as component mismatches or absence of resistive losses. The estimation of circuit parameters from measured data in the case of resonant electrical coupling was not carried out and is thus mentioned here as future work. More future work includes the simulation of the devices described in chapter 5 in a three-dimensional electromagnetic simulator in order to take into account the interaction between the coil and the two electrodes in each device. In addition, it also makes sense to study the insertion of additional objects in simulation, such as in figure 5.17, as these may be used to extend distance. Lastly, it is very important at this point to focus on a specific application, with specific constraints such as dimensions and power levels, in order to effectively prove the usefulness of resonant electrical coupling in practice.

6.2 Concluding remarks

Transferring power from one device to another using a wire will most likely always be more efficient than wireless, and probably less expensive. In addition, a wired connection is far less likely to create interference with other systems. However, the convenience of using wireless power is obvious and significant. Eliminating a power connector is something extremely important, as discussed in subsection 1.3.1. In fact, some future devices may not even have space for a connector. Plenty of examples of the convenience of using wireless power can be found in the literature. Applications of wireless power in a kitchen environment, for instance, are given in [76]. As the spatial freedom increases, so does the number of potential applications of wireless power. This is why spatial freedom is currently so valuable and was also the main reason for the study reported in this document.

Bibliography

[1] Ricardo Dias Fernandes, João Nuno Matos, and Nuno Borges Carvalho. Resonant electrical coupling: Circuit model and first experimental results. *IEEE Transactions on Microwave Theory and Techniques*, 63(9):2983–2990, September 2015.

[2] Ricardo Dias Fernandes, João Nuno Matos, and Nuno Borges Carvalho. Behavior of resonant electrical coupling in terms of range and relative orientation. In *Proceedings of the 2014 IEEE Wireless Power Transfer Conference (WPTC)*, pages 118–121, Jeju, South Korea, May 2014.

[3] Ricardo Dias Fernandes, João Nuno Matos, and Nuno Borges Carvalho. Wireless power transmission based on resonant electrical coupling. In *Proceedings of the 2014 44th European Microwave Conference (EuMC)*, pages 17–20, Rome, Italy, October 2014.

[4] Ricardo Dias Fernandes, João Nuno Matos, and Nuno Borges Carvalho. Constructive combination of resonant magnetic coupling and resonant electrical coupling. In *Proceedings of the 2015 IEEE Wireless Power Transfer Conference (WPTC)*, pages 1–3, Boulder, CO, USA, May 2015.

[5] Ricardo Dias Fernandes, João Nuno Matos, and Nuno Borges Carvalho. Low-power ultra-wide band pulse generator based on a PIN diode. *IET Microwaves, Antennas & Propagation*, 9(11):1230–1232, August 2015.

[6] Alírio Boaventura, Ricardo Dias Fernandes, João Nuno Matos, and Nuno Borges Carvalho. Unconventional RFID systems. In Luca Roselli, editor, *Green RFID Systems*, pages 116–151. Cambridge University Press, Cambridge, October 2014.

[7] Ricardo Dias Fernandes. Design of a battery-free wireless sensor node. Master's thesis, University of Aveiro, Aveiro, Portugal, December 2010.

[8] Ricardo Dias Fernandes, Nuno Borges Carvalho, and João Nuno Matos. Design of a battery-free wireless sensor node. In *Proceedings of the 2011 IEEE EUROCON - International Conference on Computer as a Tool (EUROCON)*, pages 27–29, Lisbon, Portugal, April 2011.

[9] Ricardo Dias Fernandes, Alírio Boaventura, Nuno Borges Carvalho, and João Nuno Matos. Increasing the range of wireless passive sensor nodes using multisines. In *Proceedings of the 2011 IEEE International Conference on RFID-Technologies and Applications (RFID-TA)*, pages 549–553, Barcelona, Spain, September 2011.

[10] Alírio Boaventura, Daniel Belo, Ricardo Dias Fernandes, Ana Collado, Apostolos Georgiadis, and Nuno Borges Carvalho. Boosting the efficiency: Unconventional waveform design for efficient wireless power transfer. *IEEE Microwave Magazine*, 16(3):87–96, April 2015.

[11] Naoki Shinohara. The wireless power transmission: inductive coupling, radio wave, and resonance coupling. *Wiley Interdisciplinary Reviews: Energy and Environment*, 1(3):337–346, November/December 2012.

[12] H. Kamath. Program on technology innovation: Impact of wireless power transfer technology. Technical Report 1020562, Electric Power Research Institute, December 2009.

[13] André Kurs, Aristeidis Karalis, Robert Alexander Moffatt, John D. Joannopoulos, Peter Fisher, and Marin Soljačić. Wireless power transfer via strongly coupled magnetic resonances. *Science*, 317(5834):83–86, July 2007.

[14] Aristeidis Karalis, John D. Joannopoulos, and Marin Soljačić. Efficient wireless non-radiative mid-range energy transfer. *Annals of Physics*, 323(1):34–48, January 2008.

[15] André Kurs. Power transfer through strongly coupled resonances. Master's thesis, Massachusetts Institute of Technology, Cambridge, MA, USA, September 2007.

[16] Morris Kesler. Highly resonant wireless power transfer: Safe, efficient, and over distance. White paper, WiTricity Corporation, 2013.

[17] Mark Estabrook. The convenience of wireless charging: It's just physics. White paper, MediaTek, October 2013.

[18] Jiejian Dai and Daniel C. Ludois. A survey of wireless power transfer and a critical comparison of inductive and capacitive coupling for small gap applications. *IEEE Transactions on Power Electronics*, 30(11):6017–6029, November 2015.

[19] Shinji Goma. Capacitive coupling powers transmission module. *Asia Electronics Industry*, 17(194):20–23, November 2012.

[20] William C. Brown. The history of power transmission by radio waves. *IEEE Transactions on Microwave Theory and Techniques*, 32(9):1230–1242, September 1984.

[21] William C. Brown and E. Eugene Eves. Beamed microwave power transmission and its application to space. *IEEE Transactions on Microwave Theory and Techniques*, 40(6):1239–1250, June 1992.

[22] Peter E. Glaser. Power from the sun: Its future. *Science*, 162(3856):857–861, November 1968.

[23] Susumu Sasaki. It's always sunny in space. *IEEE Spectrum*, 51(5):46–51, May 2014.

[24] Naoki Shinohara. Power without wires. *IEEE Microwave Magazine*, 12(7):S64–S73, December 2011.

[25] Jari-Pascal Curty, Michel Declercq, Catherine Dehollain, and Norbert Joehl. *Design and Optimization of passive UHF RFID Systems*, chapter 2, pages 3–4. Springer, New York, 2007.

[26] Nikola Tesla. Apparatus for transmitting electrical energy. U.S. Patent 1119732, December 1914.

[27] Benjamin L. Cannon, James F. Hoburg, Daniel D. Stancil, and Seth Copen Goldstein. Magnetic resonant coupling as a potential means for wireless power transfer to multiple small receivers. *IEEE Transactions on Power Electronics*, 24(7):1819–1825, July 2009.

[28] André Kurs, Robert Alexander Moffatt, and Marin Soljačić. Simultaneous mid-range power transfer to multiple devices. *Applied Physics Letters*, 96(4):1–3, January 2010.

[29] Robert Alexander Moffatt. Wireless transfer of electric power. Bachelor's thesis, Massachusetts Institute of Technology, Cambridge, MA, USA, June 2009.

[30] Alanson P. Sample, David A. Meyer, and Joshua R. Smith. Analysis, experimental results, and range adaptation of magnetically coupled resonators for wireless power transfer. *IEEE Transactions on Industrial Electronics*, 58(2):544–554, February 2011.

[31] Mehdi Kiani and Maysam Ghovanloo. The circuit theory behind coupled-mode magnetic resonance-based wireless power transmission. *IEEE Transactions on Circuits and Systems I: Regular Papers*, 59(9):2065–2074, September 2012.

[32] Alanson P. Sample, Benjamin H. Waters, Scott T. Wisdom, and Joshua R. Smith. Enabling seamless wireless power delivery in dynamic environments. *Proceedings of the IEEE*, 101(6):1343–1358, June 2013.

[33] Thuc Phi Duong and Jong-Wook Lee. Experimental results of high-efficiency resonant coupling wireless power transfer using a variable coupling method. *IEEE Microwave and Wireless Components Letters*, 21(8):442–444, August 2011.

[34] JinWook Kim, Hyeon-Chang Son, Kwan-Ho Kim, and Young-Jin Park. Efficiency analysis of magnetic resonance wireless power transfer with intermediate resonant coil. *IEEE Antennas and Wireless Propagation Letters*, 10:389–392, May 2011.

[35] Takashi Miyamoto, Shinji Komiyama, Hiroyuki Mita, and Kenichi Fujimaki. Wireless power transfer system with a simple receiver coil. In *Proceedings of the 2011 IEEE MTT-S International Microwave Workshop Series on Innovative Wireless Power Transmission: Technologies, Systems, and Applications (IMWS)*, pages 131–134, Kyoto, Japan, May 2011.

[36] Erin M. Thomas, Jason D. Heebl, Carl Pfeiffer, and Anthony Grbic. A power link study of wireless non-radiative power transfer systems using resonant shielded loops. *IEEE Transactions on Circuits and Systems I: Regular Papers*, 59(9):2125–2136, September 2012.

[37] Brian B. Tierney and Anthony Grbic. Planar shielded-loop resonators. *IEEE Transactions on Antennas and Propagation*, 62(6):3310–3320, June 2014.

[38] Wenxing Zhong, Chi Kwan Lee, and S. Y. Ron Hui. General analysis on the use of tesla's resonators in domino forms for wireless power transfer. *IEEE Transactions on Industrial Electronics*, 60(1):261–270, January 2013.

[39] Bingnan Wang, William Yerazunis, and Koon Hoo Teo. Wireless power transfer: Metamaterials and array of coupled resonators. *Proceedings of the IEEE*, 101(6):1359–1368, June 2013.

[40] Takashi Ohira. Via-wheel power transfer to vehicles in motion. In *Proceedings of the 2013 IEEE Wireless Power Transfer Conference (WPTC)*, pages 242–246, Perugia, Italy, May 2013.

[41] Olutola Jonah, Stavros V. Georgakopoulos, and Manos M. Tentzeris. Orientation insensitive power transfer by magnetic resonance for mobile devices. In *Proceedings of the 2013 IEEE Wireless Power Transfer Conference (WPTC)*, pages 5–8, Perugia, Italy, May 2013.

[42] Wai Man Ng, Cheng Zhang, Deyan Lin, and S. Y. Ron Hui. Two- and three-dimensional omnidirectional wireless power transfer. *IEEE Transactions on Power Electronics*, 29(9):4470–4474, September 2014.

[43] Morris Kesler and Colin McCarthy. Highly resonant wireless power transfer in subsea applications. White paper, WiTricity Corporation, 2013.

[44] Charles W. Van Neste, John E. Hawk, Arindam Phani, Jonathan A. J. Backs, Richard Hull, Tinu Abraham, Samuel J. Glassford, Adam K. Pickering, and Thomas Thundat. Single-contact transmission for the quasi-wireless delivery of power over large surfaces. *Wireless Power Transfer*, 1(2):75–82, September 2014.

[45] Charles W. Van Neste, Richard Hull, Tinu Abraham, John E. Hawk, Arindam Phani, and Thomas Thundat. Wireless single contact power delivery. In *Proceedings of the 2015 IEEE Wireless Power Transfer Conference (WPTC)*, pages 1–4, Boulder, CO, USA, May 2015.

[46] Cheng Yang and Koichi Tsunekawa. Analysis and performance improvement of independent electric coupled resonance WPT system with impedance transformer. In *Proceedings of the 2014 IEEE Wireless Power Transfer Conference (WPTC)*, pages 239–242, Jeju, South Korea, May 2014.

[47] Masahiro Kusunoki, Daiki Obara, and Mitsuru Masuda. Wireless power transfer via electric field resonance coupling. In *Proceedings of the 2014 Asia-Pacific Microwave Conference (APMC)*, pages 1360–1362, Sendai, Japan, November 2014.

[48] Hirokatsu Umegami, Masataka Ishihara, Fumiya Hattori, Mitsuru Masuda, Masayoshi Yamamoto, and Kazuhiro Umetani. Mid-range khz electric resonance coupling wireless power tranfser. In *Proceedings of the 2014 IEEE Energy Conversion Congress and Exposition (ECCE)*, pages 3197–3202, Montréal, QC, Canada, September 2015.

[49] Bart Thoen, Stijn Wielandt, Jeroen De Baere, Jean-Pierre Goemaere, Lieven De Strycker, and Nobby Stevens. Design of an inductively coupled wireless power system for moving receivers. In *Proceedings of the 2014 IEEE Wireless Power Transfer Conference (WPTC)*, pages 48–51, Jeju, South Korea, May 2014.

[50] Bart Thoen and Nobby Stevens. Development of a communication scheme for wireless power applications with moving receivers. *IEEE Transactions on Microwave Theory and Techniques*, 63(3):857–863, March 2015.

[51] Anand Satyamoorthy, Patrick Riehl, Hasnain Akram, Yung-Chih Yen, J. -C. Yang, Brian Juan, Chi-Min Lee, and Fu-Chi Lin. Wireless power receiver for mobile devices supporting inductive and resonant operating modes. In *Proceedings of the 2014 IEEE Wireless Power Transfer Conference (WPTC)*, pages 52–55, Jeju, South Korea, May 2014.

[52] Patrick S. Riehl, Anand Satyamoorthy, Hasnain Akram, Yung-Chih Yen, J. -C. Yang, Brian Juan, Chi-Min Lee, Fu-Chi Lin, Vladimir Muratov, William Plumb, and Philip F. Tustin. Wireless power systems for mobile devices supporting inductive and resonant operating modes. *IEEE Transactions on Microwave Theory and Techniques*, 63(3):780–790, March 2015.

[53] Jinwook Kim, Do-Hyeon Kim, Jeonghee Choi, Kwan-Ho Kim, and Young-Jin Park. Free-positioning wireless charging system for small electronic devices using a bowl-shaped transmitting coil. *IEEE Transactions on Microwave Theory and Techniques*, 63(3):791–800, March 2015.

[54] Jiejian Dai and Daniel C. Ludois. Wireless electric vehicle charging via capacitive power transfer through a conformal bumper. In *Proceedings of the 2015 IEEE Applied Power Electronics Conference and Exposition (APEC)*, pages 3307–3313, Charlotte, NC, USA, March 2015.

[55] Jiejian Dai and Daniel C. Ludois. Biologically inspired coupling pixilation for position independence in capacitive power transfer surfaces. In *Proceedings of the 2015 IEEE Applied Power Electronics Conference and Exposition (APEC)*, pages 3276–3282, Charlotte, NC, USA, March 2015.

[56] Ron-Chi Kuo, Patrick Riehl, Anand Satyamoorthy, William Plumb, Philip Tustin, and Jenshan Lin. A 3D resonant wireless charger for a wearable device and a mobile phone. In *Proceedings of the 2015 IEEE Wireless Power Transfer Conference (WPTC)*, pages 1–3, Boulder, CO, USA, May 2015.

[57] Benjamin H. Waters, Peter R. Fidelman, Jeffrey D. Raines, and Joshua R. Smith. Simultaneously tuning and powering multiple wirelessly powered devices. In *Proceedings of the 2015 IEEE Wireless Power Transfer Conference (WPTC)*, pages 1–4, Boulder, CO, USA, May 2015.

[58] Changbyung Park, Sungwoo Lee, Gyu-Hyeong Cho, and Chun T. Rim. Innovative 5-m-off-distance inductive power transfer systems with optimally shaped dipole coils. *IEEE Transactions on Power Electronics*, 30(2):817–827, February 2015.

[59] Bo H. Choi, Eun S. Lee, Yeong H. Sohn, Gi C. Jang, and Chun T. Rim. Six degrees of freedom mobile inductive power transfer by crossed dipole Tx and Rx coils. *IEEE Transactions on Power Electronics*, pages 1–21, June 2015.

[60] Bo H. Choi, Eun S. Lee, Jin Huh, and Chun T. Rim. Lumped impedance transformers for compact and robust coupled magnetic resonance systems. *IEEE Transactions on Power Electronics*, 30(11):6046–6056, November 2015.

[61] David W. Baarman and Joshua Schwannecke. Understanding wireless power. White paper, Fulton Innovation, December 2009.

[62] John D. Joannopoulos, Aristeidis Karalis, and Marin Soljačić. Wireless non-radiative energy transfer. U.S. Patent 7741734, Massachusetts Institute of Technology, June 2010.

[63] Aristeidis Karalis, André Kurs, Robert Alexander Moffatt, John D. Joannopoulos, Peter H. Fisher, and Marin Soljačić. Wireless energy transfer. U.S. Patent 7825543, Massachusetts Institute of Technology, November 2010.

[64] Joshua R. Smith and Alanson P. Sample. Wireless power transfer apparatus and method thereof. U.S. Patent 2010/0187913, July 2010.

[65] Keiichi Ichikawa and Henri Bondar. Power transfer system. U.S. Patent 2012/0299392, November 2012.

[66] Patrick Camurati and Henri Bondar. Device for transporting energy by partial influence through a dielectric medium. U.S. Patent 2012/0262005, Murata Manufacturing Co., Ltd., and TMMS Co., Ltd., June 2012.

[67] Charging electric cars efficiently inductive. Monthly bulletin, Fraunhofer-Gesellschaft, August 2014.

[68] BMW group is pressing ahead with the development of systems for inductive charging of electric and plug-in hybrid cars. Press release, BMW Group, July 2014.

[69] Wireless power: Patent landscape analysis. Technical report, LexInnova, June 2015.

[70] NXQ1TXA1 evaluation board. Application Note AN11509, NXP, February 2015.

[71] 5W Qi wireless power transmitter reference board. Reference Board Manual P9038-R-EVK, IDT, September 2015.

[72] David W. Baarman. Making wireless truly wireless: The need for a universal wireless power solution. White paper, Fulton Innovation, December 2009.

[73] Niranjan Pathare. A global wireless power standard will open the market, encourage consumers to live without power cords. White Paper SLYY036, Texas Instruments, June 2013.

[74] Michael Joehren, Klaas Brink, Kai Neumann, Rick Dumont, and Mike Bruno. Development of an optimized wireless charging application solution. Technical Report 9397 750 17507, NXP Semiconductors, January 2014.

[75] Jörg Hantschel. Wireless energy transmission - coils as key components. Application note, Würth Elektronik, November 2013.

[76] Cordless kitchen appliances. White paper, Wireless Power Consortium, April 2013.

Appendix A

Contributions

In this appendix are full versions of the papers listed below, in a total of 31 pages.

[1] (8 pages)

[2] (4 pages)

[3] (4 pages)

[4] (3 pages)

[5] (3 pages)

[8] (4 pages)

[9] (5 pages)

Resonant Electrical Coupling: Circuit Model and First Experimental Results

Ricardo Dias Fernandes, *Graduate Student Member, IEEE*, João Nuno Matos, *Member, IEEE*, and Nuno Borges Carvalho, *Fellow, IEEE*

***Abstract*—In this paper, the feasibility of resonant electrical coupling as a wireless power transfer technique is studied. A detailed comparison between this technique and the more popular resonant magnetic coupling based on circuit theory is provided. In this comparison, the strong duality that exists between the two techniques is demonstrated. The analytical results obtained are compared with the results measured with a proof-of-concept prototype.**

***Index Terms*—Resonant capacitive coupling, resonant coupling, resonant electrical coupling, resonant hybrid coupling, resonant magnetic coupling, wireless power transfer.**

I. Introduction

THE RESEARCH on wireless power transfer dates back to the famous experiments carried out by Nikola Tesla at the turn of the 20th Century. His goal was to build a network of towers that would pump large amounts of energy into the atmospheric layers at moderate altitudes. He was convinced that these layers and the planet would behave as good electrical conductors and wanted to prove that it would be possible to use them to transfer energy to anywhere in the planet with very little loss. The accumulated energy would then be collected as needed wirelessly. Tesla managed to secure the necessary funding to begin the construction of the first of these towers in 1901. The Wardenclyffe tower (the name by which this tower became known) was an impressive structure composed by a very large coil wound around a 60-m mast with a 1-m diameter copper ball placed at the top. Also impressive were the 300 kW supplied to the tower at 150 kHz (the resonant frequency of the coil) and the electric potential produced at the sphere, which was in the order of 10^8 V (according to Tesla himself). According to the reports of the journalists of that time, Tesla managed to light up 200 50-W incandescent lamps located 42 km away from the tower (see [1]). Despite the encouraging results, the lack of funding brought the construction to a halt and a few years later, in 1917, the tower was demolished. The principle of operation behind the Wardenclyffe tower relied on concepts still widely used today such as oscillating voltages and currents, magnetic induction, capacitor charging and discharging, and resonators (more details in [2]).

The severe lack of financial resources, which ultimately resulted in the failure of Wardenclyffe, was for the most part due to the significant advancements in the field of wireless communications, in particular long range. As a result, investors shifted from power to communications, and so did research. Wireless power was only brought back later in the 1960s by William C. Brown. Brown conducted several experiments with 2.45-GHz microwave tubes and was the first to coin the term rectenna (which is an antenna especially designed for receiving and rectifying microwaves). One of his main accomplishments took place at the Jet Propulsion Laboratory (JPL), Pasadena, CA, USA, in 1975. He was able to transmit 30 kW from a parabolic antenna with a diameter of 26 m to a 3.4 by 7.2 m rectenna placed 1.6 km away. The maximum efficiency achieved was 82.5% (rectification only), obtained at 2.388 GHz, and the power transmitted by the parabolic antenna was 450 kW. Prior to this demonstration, Brown had already been involved in several other smaller projects related to the same subject. In 1964, he succeeded in transmitting power wirelessly to a tethered helicopter, and four years later to a free-flying version, both at 2.45 GHz. In 1975, he was able to transmit 495 W with a total dc-to-dc efficiency of 54%. Although successful, these experiments (which are described in detail in [3] by Brown himself) were significantly expensive, and in most cases, too large for any practical applications.

In 2007, a team of researchers at the Massachusetts Institute of Technology (MIT), Cambridge, MA, USA, led by Prof. Marin Soljačić proposed a novel and very innovative wireless power technique, which combines the concepts of inductive coupling and magnetic resonance very effectively. Resonant magnetic coupling takes advantage of the fact that the coupling between two coils can be very strong even if the magnetic coupling coefficient is very low (for instance, in the order of 0.01). For this to happen the coils must resonate at the same frequency and also have very high quality Q factors. From this discovery resulted several publications of great scientific ([4], and in particular, [5]) and industrial ([6], [7], and others) importance. Resonant magnetic coupling was first demonstrated using a prototype consisting of two single-turn coils and two helical coils. In this prototype, the copper wires used to build the coils had a cross-sectional diameter of 6 mm (a rather large value in order to minimize losses, and thus increase Q). The outer diameter of the helical coils was 60 cm (not very small, but not unreasonable). Using this prototype, the researchers were able to light up a 60-W incandescent light bulb placed at a distance

Manuscript received March 06, 2015; revised June 18, 2015; accepted July 07, 2015. Date of publication August 03, 2015; date of current version September 01, 2015. This work was supported by the Fundação para a Ciência e a Tecnologia (FCT) under Grant SFRH/BD/69392/2010 and Project EXCL/EEI-TEL/0067/2012 (CREaTION), and by COST Action IC1301 (WiPE). This paper is an expanded version from the IEEE MTT-S Wireless Power Transfer Conference, Jeju, Korea, May 8–9, 2014.

The authors are with the Instituto de Telecomunicações, Universidade de Aveiro, 3810-193 Aveiro, Portugal (e-mail: rdf@ua.pt; matos@ua.pt; nbcarvalho@ua.pt).

Digital Object Identifier 10.1109/TMTT.2015.2458323

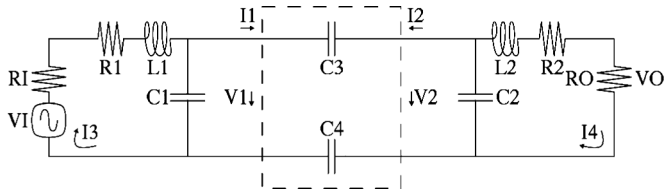

Fig. 1. Circuit model used in the analytical analysis of resonant electrical coupling.

of 2 m. More importantly, they managed to do so with a transfer efficiency of 40%. A very interesting result, especially given the fact that it was obtained with such a simple apparatus. Unsurprisingly, the attention given to this demonstration by the media was quite remarkable. One of the key features of resonant magnetic coupling is the balanced tradeoff between efficiency, range, simplicity (cost), size, and power transfer capability.

In this paper, which is an extension of [8], the feasibility of resonant electrical coupling as a wireless power transfer technique is studied. In this version, a more detailed analytical analysis of resonant electrical coupling is provided. Moreover, a comparison with resonant magnetic coupling, which demonstrates the strong duality between the two techniques, is included. Novel experimental results based on the use of an RF-to-dc converter are also included. This paper also extends the results reported in [9] and [10], especially in terms of theoretical analysis and measurements. No other publications related to the use of resonant electrical coupling for wireless power transfer were found.

II. Model of Resonant Electrical Coupling

Here, the relevance of resonant electrical coupling for wireless power transfer will be analyzed based on the circuit model presented in Fig. 1. The purpose of the analysis is to link specific parameter variations to specific output variations. In the model, the power source is represented by the voltage source V_I plus the resistance R_I and the load is represented by R_O. No magnetic coupling is considered between the inductances L_1 and L_2, which means that the source and the load are assumed to be only coupled capacitively through C_3 and C_4. The remaining capacitances C_1 and C_2 are included in the model to resonate with L_1 and L_2, respectively. Lastly, the losses in L_1 and L_2 are taken into account in R_1 and R_2. An analytical analysis of resonant magnetic coupling is given in the Appendix for comparison purposes, in particular to demonstrate the strong duality that exists between the two techniques. If C_3 and C_4 are considered as an admittance two-port network (highlighted in the figure via the dashed line), it is possible to write

$$Y_{11} = jwC_3C_4/(C_3 + C_4) \tag{1}$$
$$Y_{12} = -Y_{11} \tag{2}$$
$$Y_{21} = -Y_{11} \tag{3}$$
$$Y_{22} = Y_{11} \tag{4}$$

and for the complete model,

$$(R_I + R_1 + jwL_1)I_3 + V_1 - V_I = 0 \tag{5}$$
$$I_1 - I_3 + jwC_1V_1 = 0 \tag{6}$$
$$I_2 + I_4 + jwC_2V_2 = 0 \tag{7}$$
$$(R_2 + jwL_2)I_4 - V_2 + V_O = 0 \tag{8}$$
$$R_OI_4 - V_O = 0 \tag{9}$$
$$I_1 - Y_{11}V_1 - Y_{12}V_2 = 0 \tag{10}$$
$$I_2 - Y_{21}V_1 - Y_{22}V_2 = 0. \tag{11}$$

The voltage gain V_O/V_I can be calculated from the previous set of equations and written as

$$V_O/V_I = R_OY_{21}/(Y_{12}Y_{21}Z_1Z_2 - [1 + K_1Z_1][1 + K_2Z_2]) \tag{12}$$

in which

$$K_1 = Y_{11} + jwC_1 \tag{13}$$
$$K_2 = Y_{22} + jwC_2 \tag{14}$$

and

$$Z_1 = R_I + R_1 + jwL_1 \tag{15}$$
$$Z_2 = R_O + R_2 + jwL_2. \tag{16}$$

Since the power delivered to R_O is

$$P_O = |V_O|^2/(2R_O) \tag{17}$$

and the power source is able to supply at most (considering a matched load) a power of

$$P_A = |V_I|^2/(8R_I) \tag{18}$$

the available power gain can be written as a function of the voltage gain presented in (12) using

$$P_O/P_A = 4R_I|V_O/V_I|^2/R_O. \tag{19}$$

The response of the model as a function of frequency for C_3 equal to 0.02, 0.06, 0.3, 0.4, and 0.9 pF considering the parameters listed in Table I is shown in Fig. 2. These parameters were selected based on the parameters used for resonant magnetic coupling (in order to ensure a fair comparison), which, in turn, were based on [11]. Also, C_4 is assumed to always have the same value as C_3. This assumption is not unreasonable since a variation in the physical distance between the power source and the load is likely to affect C_3 and C_4 in the same way. In the figure, it can be seen that if C_3 is very small (which corresponds to a larger separation between the plates), only a very small fraction of the power available in the source reaches the load, as expected. In fact, if C_3 tends to zero then (1)–(4) all tend to zero, and as a consequence, (12) and thus (19) tend to zero as well. As C_3 is increased, the resonant behavior becomes evident. If C_3 is increased beyond approximately 0.3 pF, the peak gain no longer improves and instead the resonance splits into two. An important conclusion that can be drawn from this figure is that significant gains can be obtained with relatively small C_3 values. It is this aspect that best distinguishes this technique from plain capacitive coupling. Before the splitting occurs, the resonant frequency f_r can be estimated using

$$f_r = 1/(2\pi\sqrt{L_iC_i}) \tag{20}$$

TABLE I
REFERENCE PARAMETERS USED IN THE ANALYSIS OF THE CIRCUIT MODEL FROM FIG. 1

Parameter	Value
R_I, R_O	50 Ω
R_1, R_2	12 Ω
L_1, L_2	28 μH
C_1, C_2	5 pF

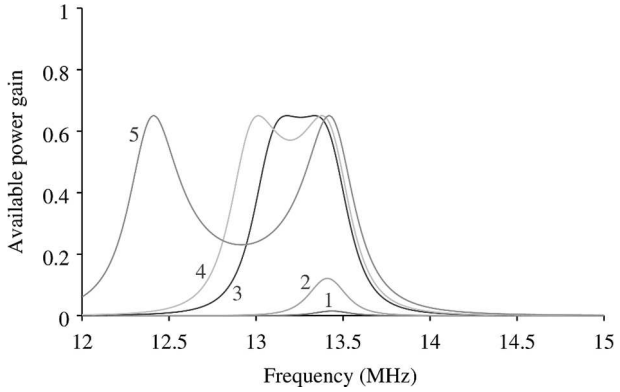

Fig. 2. Available power gain as a function of frequency for C_3 equal to 0.02 (curve 1), 0.06, 0.3, 0.4, and 0.9 pF (curve 5).

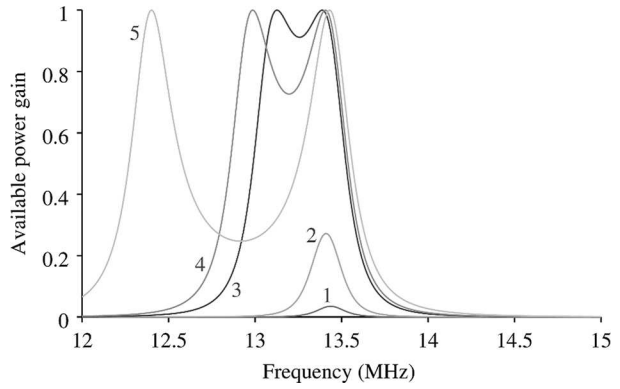

Fig. 3. Available power gain as a function of frequency for C_3 equal to 0.02 (curve 1), 0.06, 0.3, 0.4, and 0.9 pF (curve 5) with R_1 and R_2 reduced to zero.

with i equal to 1 or 2. The behavior shown in Fig. 2 is in general similar to the behavior shown in Fig. 18 for resonant magnetic coupling. The most noticeable difference is clearly the more asymmetrical frequency splitting. The difference in peak gain is not important since obtaining an equal gain in both cases is simply a matter of slightly adjusting the resistive elements. The strong dependency between the peak gain and the resistive elements is illustrated in Fig. 3. As a result of reducing R_1 and R_2 to zero, the peak gain increases to the maximum possible value. This is clearly the ideal case in which all the power available at the source is delivered to the load. In resonant magnetic coupling, the change in behavior is identical if R_1, R_2, R_3, and R_4 are reduced to zero, as can be seen in Figs. 18 and 19. In general, the peak gain tends to 1 as the resistive elements tend to zero (higher Q's) and vice versa. For the same L_iC_i product in (20), the response of the model can change substantially. As an example, in Fig. 4, L_1 and L_2 are doubled and C_1 and C_2 are reduced to half. Compared to Fig. 2, the gain increases considerably faster, and as expected, the peak value remains the same. In this case, however, the resonances are narrower and an inductance with twice the value (significantly more difficult to

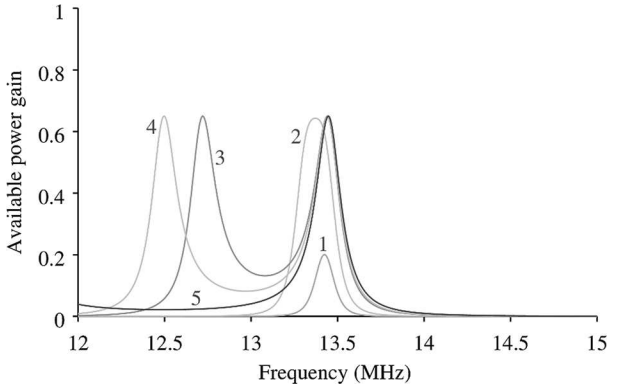

Fig. 4. Available power gain as a function of frequency for C_3 equal to 0.02 (curve 1), 0.06, 0.3, 0.4, and 0.9 pF (curve 5) with L_1 and L_2 increased to 56 μH and C_1 and C_2 reduced to 2.5 pF.

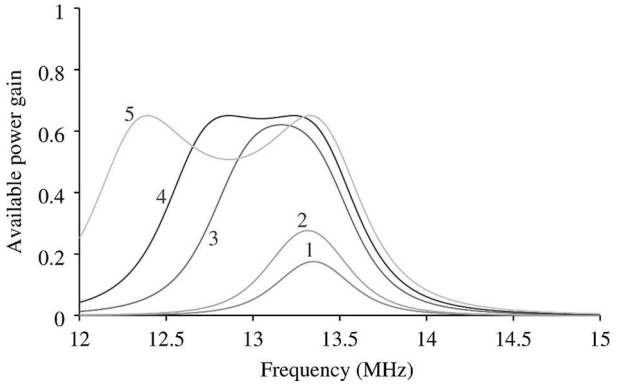

Fig. 5. Available power gain as a function of frequency for C_3 equal to 0.3 (curve 1), 0.4, 0.9, 1.3, and 2 F (curve 5) with C_1 and C_2 increased to 10 pF and L_1 and L_2 reduced to 14 μH.

implement) is required. If instead C_1 and C_2 are doubled and L_1 and L_2 are reduced to half, the behavior is the opposite, as illustrated in Fig. 5. In this case, the gain increases at a slower rate and the resonances are wider. Additionally, the peak value is only reached when C_3 is in the order of 1.3 pF. In this figure, the curves corresponding to C_3 equal to 0.02 and 0.06 pF were not considered because the gain at these lower values is negligible. Lastly, the response of the model after a reduction of 10% in L_2 (without reducing L_1 by the same amount) is illustrated in Fig. 6. The mismatch causes the two parts of the model to resonate at different frequencies, which ultimately leads to a substantial gain degradation. As can be seen in the figure, the peak value is still not reached even when C_3 is increased to 2 pF. Furthermore, for the first time, two distinct resonances are always present, even at the lower C_3 values. Once again, the curves corresponding to C_3 equal to 0.02 and 0.06 pF were not considered due to the negligible gain. As can be seen in Fig. 20, in resonant magnetic coupling the gain degradation caused by an equivalent mismatch is very similar.

If the two-port network mentioned earlier is replaced by the network shown in Fig. 7, the admittance parameters presented in (1)–(4) become

$$Y_{11} = jw(C_3C_4 + C_3C_6 + C_4C_5 + C_5C_6)/D \quad (21)$$

$$Y_{12} = jw(C_5C_6 - C_3C_4)/D \quad (22)$$

$$Y_{21} = Y_{12} \quad (23)$$

$$Y_{22} = jw(C_3C_4 + C_3C_5 + C_4C_6 + C_5C_6)/D \quad (24)$$

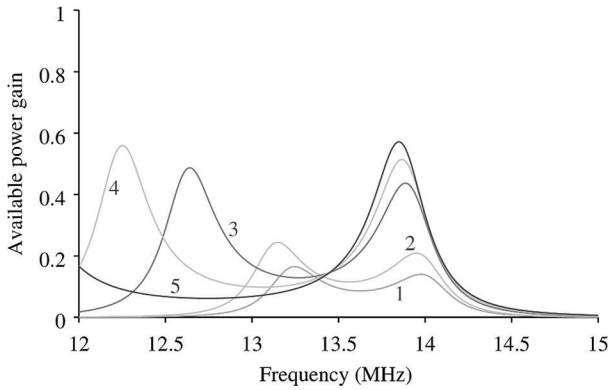

Fig. 6. Available power gain as a function of frequency for C_3 equal to 0.3 (curve 1), 0.4, 0.9, 1.3, and 2 pF (curve 5) with L_2 reduced to 25.2 μH (-10%).

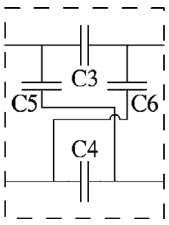

Fig. 7. Additional capacitances C_5 and C_6 considered in the circuit model of Fig. 1.

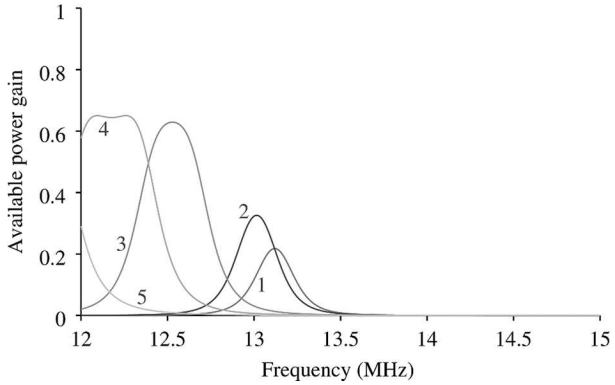

Fig. 8. Available power gain as a function of frequency for C_3 equal to 0.3 (curve 1), 0.4, 0.9, 1.3, and 2 pF (curve 5) with C_5 and C_6 set to 70% of C_3.

in which

$$D = C_3 + C_4 + C_5 + C_6. \tag{25}$$

The effect of the capacitances C_5 and C_6 in the response of the model is shown in Fig. 8, considering

$$C_5 = 0.7C_3 \tag{26}$$

$$C_6 = C_5. \tag{27}$$

Once again, the curves corresponding to C_3 equal to 0.02 and 0.06 pF were not considered due to negligible gain. It may be needed to consider these additional unwanted couplings in a practical implementation depending on the physical proximity of C_3 and C_4, and hence, this analysis. In this case, the peak value is only reached when C_3 is in the order of 2 pF. In general, as C_5 and C_6 increase, the gain degradation becomes much more pronounced. In the worst case scenario, when the product C_5C_6 is equal to C_3C_4, (22) and (23) become 0, and thus, (12) and (19) also become 0.

III. Experimental Results

A photograph of the proof-of-concept prototype developed to validate the model from Fig. 1 is shown in Fig. 9. The prototype consists of two identical (mirrored) resonators, each one composed by a 16 by 16 cm board made of FR-4 with two large copper zones of equal areas and a coil mounted on the back side. Assuming the resonator on the left as the transmitter, the copper zone marked with the letter A in the photograph implements the left half of C_3, B implements the left half of C_4, and E implements L_1. As for C_1, the value of this capacitance depends on the distance between A and B. On the receiver side, C implements the right half of C_3, D implements the right half of C_4, and F (not visible) implements L_2. Similarly to C_1, the value of C_2 depends on the distance between C and D. It is important to notice that since the distances between A and B and between C and D are kept constant by the FR-4, a significant mismatch between C_1 and C_2 is less likely to occur. Moreover, using smaller copper zones results in a smaller size, but also lower values of C_3 and C_4 for the same distance, which, in turn, result in a lower available power gain. If the copper zones are larger, the effect is the opposite. In this case, however, it may be more challenging to keep C_1 and C_2 low enough to avoid the behavior previously illustrated in Fig. 5. In this prototype, both coils have a diameter of 3.6 cm, 40 turns, are both made of 0.8-mm diameter stranded copper wire, and were both constructed by hand in order to create an inductance large enough to make the prototype resonate between 12 and 15 MHz.

A. Scattering Parameters

The $|S_{21}|$ of the prototype as a function of frequency for the distances of 10, 20, 60, 90, and 500 cm is given in Fig. 10. In this test, the resonators were placed front to front on top of polystyrene supports approximately 1 m high and connected directly to an HP 8753D network analyzer. One of the most important conclusions that can be drawn from this figure is that a resonant behavior can be effectively observed in practice. For shorter distances (which correspond to higher C_3 values), two distinct resonant frequencies can be observed, and as the distance is increased, the separation becomes smaller, as expected. In addition, the lower resonance moves faster than the upper resonance, even though the difference is not as extreme as in Fig. 2. Some aspects, however, are clearly not in agreement with the theoretical predictions. For instance, the amplitude of the peaks is not identical. Also, the resonant frequencies do not converge even when the distance is increased up to 500 cm, and as a matter of fact, $|S_{21}|$ changes very little between 90 and 500 cm. Although these aspects were not expected, they were observed consistently across several measurements and also confirmed with a second network analyzer, an Agilent E8361C. As for the remaining parameters, no significant differences were found between $|S_{21}|$ and $|S_{12}|$ as expected, and $|S_{11}|$ and $|S_{22}|$ can be seen in Figs. 11 and 12, respectively. Although not identical,

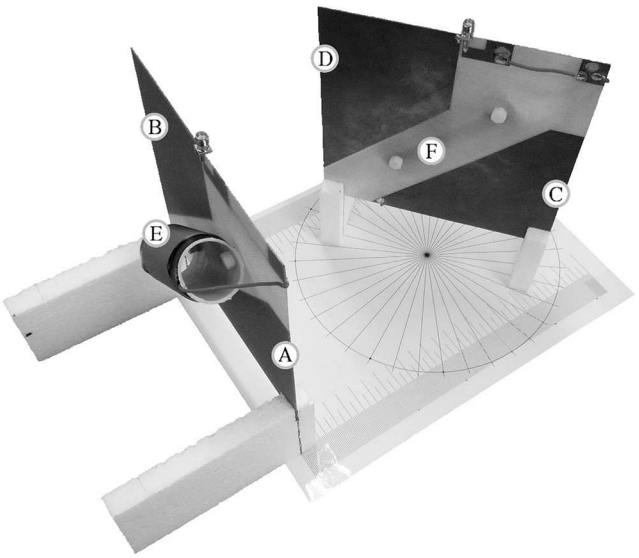

Fig. 9. Photograph of the prototype used in the experimental validation of the model from Fig. 1.

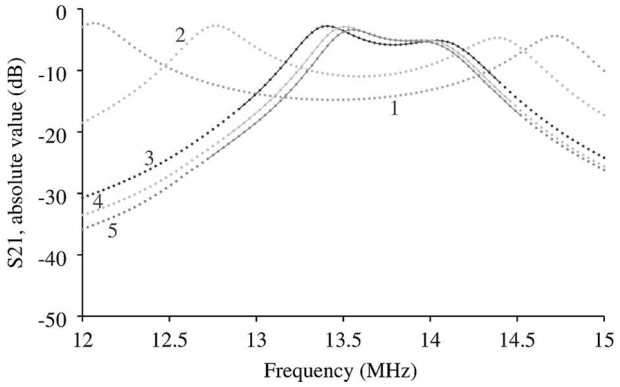

Fig. 10. Measured $|S_{21}|$ as a function of frequency for distances equal to 10 (curve 1), 20, 60, 90, and 500 cm (curve 5). Some of the experimental points are connected by lines.

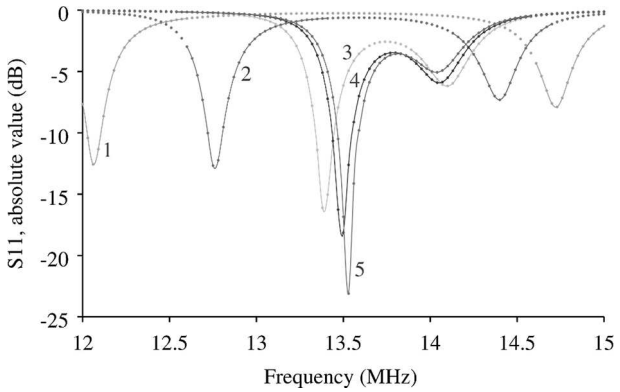

Fig. 11. Measured $|S_{11}|$ as a function of frequency for distances equal to 10 (curve 1), 20, 60, 90, and 500 cm (curve 5). Some of the experimental points are connected by lines.

these two parameters are both minimum at the same frequencies that maximize $|S_{21}|$. The peak $|S_{21}|$ values from Fig. 10 and corresponding frequencies are given in Table II.

B. RF-to-DC Converter

A photograph of the RF-to-dc converter designed to further test the prototype can be seen in Fig. 13, on the left. This

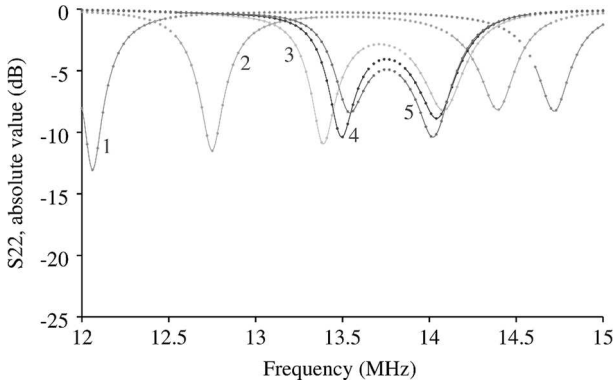

Fig. 12. Measured $|S_{22}|$ as a function of frequency for distances equal to 10 (curve 1), 20, 60, 90, and 500 cm (curve 5). Some of the experimental points are connected by lines.

TABLE II
MAXIMUM $|S_{21}|$ VALUES FROM FIG. 10 AND CORRESPONDING FREQUENCIES

Curve	Frequency (MHz)	$\lvert S_{21}\rvert$ (dB)
1	12.06	-2.31
2	12.78	-2.73
3	13.41	-2.78
4	13.5	-2.91
5	13.56	-3.38

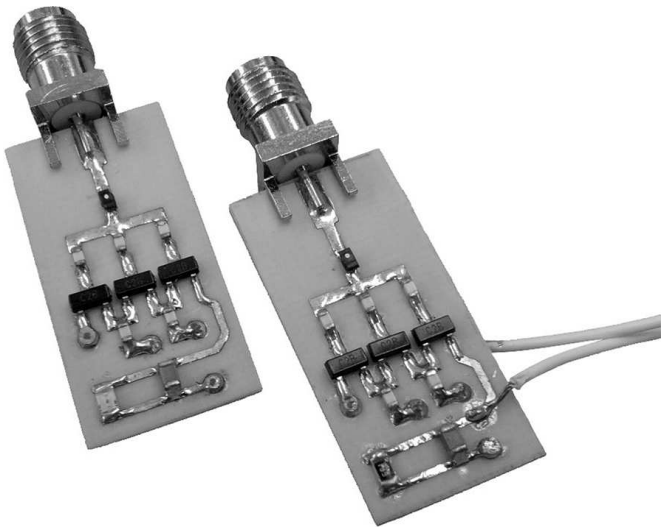

Fig. 13. Photograph of the two RF-to-dc converters used to test the prototype from Fig. 9.

RF-to-dc converter is based on a Dickson configuration and is composed by a 1.8-μH matching inductor (immediately after the connector), then three capacitors, two of 39 pF (center and right on the photograph) and one of 47 pF, three HSMS-282 Schottky diode pairs (series configuration), and then two 47-pF capacitors. At the end of the voltage multiplier is a 6.8-μF capacitor in parallel with an LED. On the right part of the photograph is an identical RF-to-dc converter in which the LED was replaced by a 680-Ω resistor (which is approximately equivalent to the LED when the latter is turned on). $|S_{11}|$ of this second RF-to-dc converter as a function of frequency is shown in Fig. 14 for power levels of 2, 4, 6, 8, and 10 dBm. As can be seen, its impedance is reasonably matched to 50 Ω

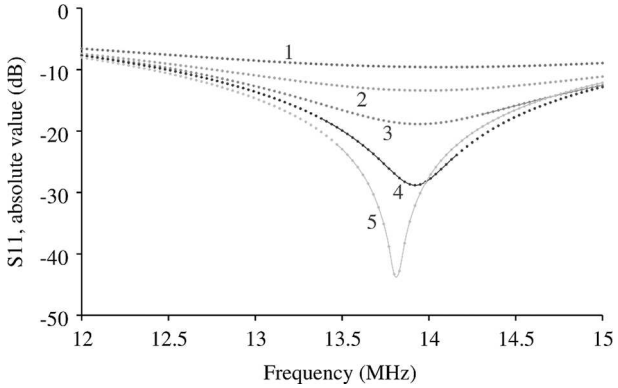

Fig. 14. Measured $|S_{11}|$ as a function of frequency for power levels equal to 2 (curve 1), 4, 6, 8, and 10 dBm (curve 5). Some of the experimental points are connected by lines.

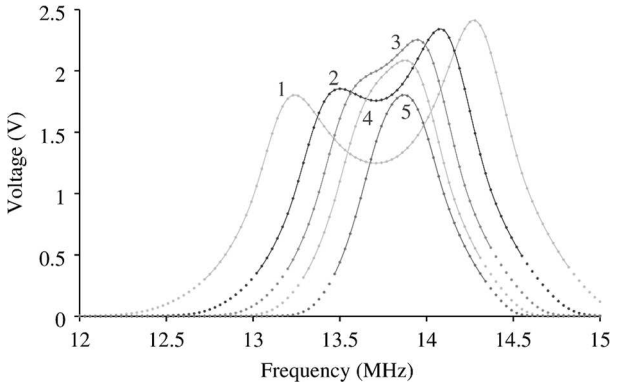

Fig. 15. Measured voltage as a function of frequency for distances equal to 12 (curve 1), 16, 20, 24, and 30 cm (curve 5) considering a transmitted power of 16 dBm. Some of the experimental points are connected by lines.

in the considered frequency band. The voltage measured at the 680-Ω resistor as a function of frequency for distances of 12, 16, 20, 24, and 30 cm is shown in Fig. 15, considering a transmitted power of 16 dBm and the resonators always front to front, at a fixed distance of 5 cm from the floor. In this test, one of the resonators was connected to an Agilent E4433B signal generator and the other resonator was connected to the RF-to-dc converter. A resonant behavior was observed as expected, and in this case, the resonances effectively converge when the distance is increased. This means that the results shown in Fig. 10, especially curve 5, are most likely caused by an additional coupling path established inside the network analyzers. Table III shows the peak voltage and corresponding frequency for each one of the curves represented in Fig. 15. An estimate for the available power gain can be obtained by connecting the transmitter and receiver cables directly (thus bypassing the prototype), measuring the power levels needed to generate the same peak voltages at the same frequencies and then subtracting 16 dBm from those power levels. This information is also included in Table III. Angles of -90, -40, 40, and 90° were also considered at 16 cm. As can be seen in Fig. 16, the peak voltage increases for negative angles and decreases for positive angles. This difference is most likely the result of a non-negligible mutual inductance between the coils, which can be either constructive or destructive. More information on this last subject can be found in [12]. The estimated values for the available power gain in this case can

TABLE III
AVAILABLE POWER GAIN CALCULATED FOR THE PEAK VOLTAGES PRESENTED IN FIG. 15

Curve	Frequency (MHz)	Voltage (V)	Bypass power (dBm)	Gain
1	14.28	2.41	13.88	0.61
2	14.07	2.4	13.58	0.57
3	13.95	2.25	13.3	0.54
4	13.89	2.08	12.74	0.47
5	13.86	1.8	11.78	0.38

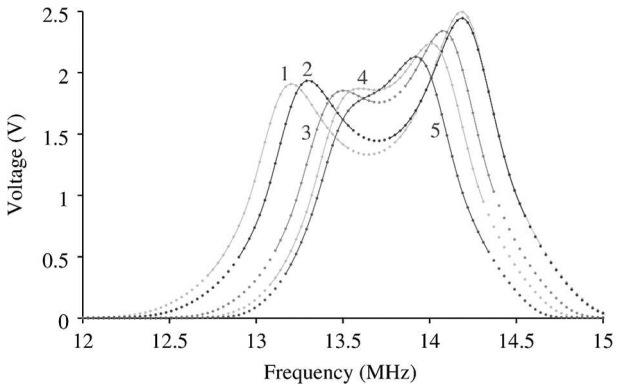

Fig. 16. Measured voltage as a function of frequency for angles equal to -90 (curve 1), -40, 0, 40, and 90° (curve 5) considering a transmitted power of 16 dBm. Some of the experimental points are connected by lines.

TABLE IV
AVAILABLE POWER GAIN CALCULATED FOR THE PEAK VOLTAGES PRESENTED IN FIG. 16

Curve	Frequency (MHz)	Voltage (V)	Bypass power (dBm)	Gain
1	14.19	2.5	14.04	0.64
2	14.19	2.44	13.92	0.62
4	14.01	2.24	13.26	0.53
5	13.92	2.13	12.9	0.49

be seen in Table IV. As a final note, the 40° case is the case represented in Fig. 9.

IV. CONCLUSION

Resonant magnetic coupling is currently one of the most popular techniques in the field of wireless power transfer. One of the major reasons for this popularity is the balanced tradeoff between efficiency, range, simplicity (cost), size, and power transfer capability that can be achieved with this technique. Resonant electrical coupling is not as popular as resonant magnetic coupling at this point, but the potential of this technique is significant. As a matter of fact, from a theoretical point of view, resonant electrical coupling and resonant magnetic coupling are quite similar. One of the main objectives in this paper was to highlight the strong duality that exists between these two techniques (in general, and also in specific conditions, such as component mismatches or no resistive losses). The second main objective in this paper was to demonstrate that a resonant behavior can be effectively observed in practice. Future work will focus on a better characterization of resonant electrical coupling and also on the possibility of constructively combining the two types of coupling in order to create a hybrid coupling with improved performance.

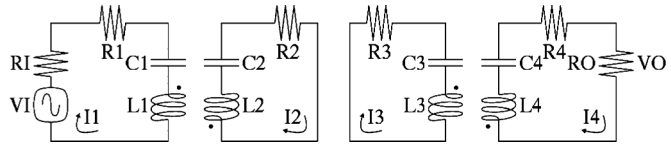

Fig. 17. Circuit model most commonly used in the analytical analysis of resonant magnetic coupling.

TABLE V
REFERENCE PARAMETERS USED IN THE ANALYSIS OF THE CIRCUIT MODEL FROM FIG. 17

Parameter	Value
R_I, R_O	50 Ω
R_1, R_4	2 Ω
R_2, R_3	10 Ω
L_1, L_4	1 μH
L_2, L_3	28 μH
C_1, C_4	140 pF
C_2, C_3	5 pF
k_{12}, k_{34}	0.1

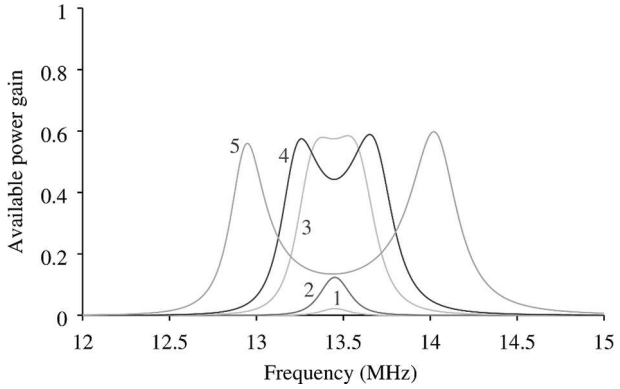

Fig. 18. Available power gain as a function of frequency for k_{23} equal to 0.002 (curve 1), 0.005, 0.023, 0.035, and 0.08 (curve 5).

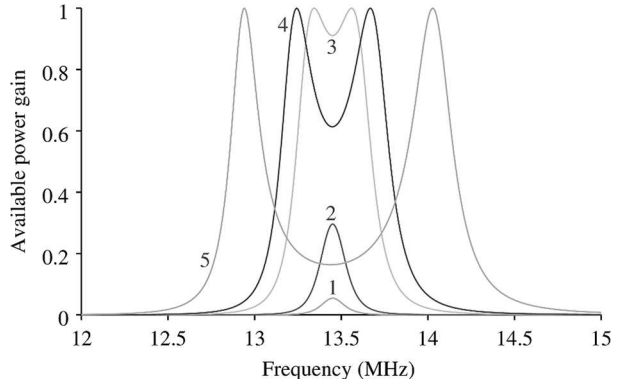

Fig. 19. Available power gain as a function of frequency for k_{23} equal to 0.002 (curve 1), 0.005, 0.023, 0.035, and 0.08 (curve 5) with R_1, R_2, R_3, and R_4 reduced to zero.

APPENDIX

Currently the circuit model shown in Fig. 17 is the model most widely used to describe the behavior of resonant magnetic coupling (see, for instance, [11], [13], or [14]). In this model, L_1 is considered to be coupled to L_2, L_2 is considered to be coupled to L_3, L_3 is considered to be coupled to L_4, and the power is transferred from the source represented by V_I plus R_I to the load represented by R_O. Using M to represent mutual inductance, it is possible to write

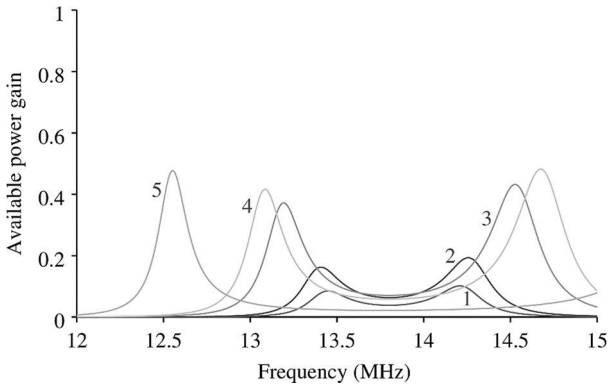

Fig. 20. Available power gain as a function of frequency for k_{23} equal to 0.023 (curve 1), 0.035, 0.08, 0.1, and 0.2 (curve 5) with L_3 reduced to 25.2 μH (-10%).

$$(R_I + R_1 + jwL_1 - j/[wC_1])I_1 + jwM_{12}I_2 - V_I = 0 \tag{28}$$

$$jwM_{12}I_1 + (R_2 + jwL_2 - j/[wC_2])I_2 + jwM_{23}I_3 = 0 \tag{29}$$

$$jwM_{23}I_2 + (R_3 + jwL_3 - j/[wC_3])I_3 + jwM_{34}I_4 = 0 \tag{30}$$

$$jwM_{34}I_3 + (R_4 + jwL_4 - j/[wC_4])I_4 + V_O = 0 \tag{31}$$

$$R_O I_4 - V_O = 0. \tag{32}$$

The voltage gain V_O/V_I can be calculated from the previous set of equations and written as

$$V_O/V_I = -jw^3 R_O k_{12} k_{23} k_{34} L_2 L_3 \sqrt{L_1 L_4}/ (K_1 K_2 + w^2 k_{23}^2 L_2 L_3 Z_1 Z_4) \tag{33}$$

in which

$$K_1 = Z_1 Z_2 + w^2 k_{12}^2 L_1 L_2 \tag{34}$$

$$K_2 = Z_3 Z_4 + w^2 k_{34}^2 L_3 L_4 \tag{35}$$

and

$$Z_1 = R_I + R_1 + jwL_1 - j/(wC_1) \tag{36}$$

$$Z_2 = R_2 + jwL_2 - j/(wC_2) \tag{37}$$

$$Z_3 = R_3 + jwL_3 - j/(wC_3) \tag{38}$$

$$Z_4 = R_O + R_4 + jwL_4 - j/(wC_4) \tag{39}$$

and also

$$k_{12} = M_{12}/\sqrt{L_1 L_2} \tag{40}$$

$$k_{23} = M_{23}/\sqrt{L_2 L_3} \tag{41}$$

$$k_{34} = M_{34}/\sqrt{L_3 L_4}. \tag{42}$$

The response of this model as a function of frequency for k_{23} equal to 0.002, 0.005, 0.023, 0.035, and 0.08 considering the parameters listed in Table V is illustrated in Fig. 18. In this case, (19) remains valid and (20) can also still be used with i equal to 1, 2, 3, or 4 to estimate the resonant frequency before

the splitting occurs. As can be seen in the figure, significant gains can be obtained with relatively small k_{23} values. It is this aspect that best distinguishes this technique from plain inductive coupling. In Fig. 19, the effect of reducing R_1, R_2, R_3, and R_4 to zero is shown. In Fig. 20, the effect of reducing L_3 by 10% (without also reducing L_2) is shown.

REFERENCES

[1] J.-P. Curty, M. Declercq, C. Dehollain, and N. Joehl, *Design and Optimization of Passive UHF RFID Systems*. New York, NY, USA: Springer, 2007, ch. 2, pp. 3–4.

[2] N. Tesla, "Apparatus for transmitting electrical energy," U.S. Patent 1 119 732, Dec. 1, 1914.

[3] W. C. Brown, "The history of power transmission by radio waves," *IEEE Trans. Microw. Theory Techn.*, vol. MTT-32, no. 9, pp. 1230–1242, Sep. 1984.

[4] A. Kurs, "Power transfer through strongly coupled resonances," Master's thesis, Dept. Phys., Massachusetts Inst. Technol., Cambridge, MA, USA, 2007 [Online]. Available: http://dspace.mit.edu/handle/1721.1/45429

[5] A. Kurs, A. Karalis, R. Moffatt, J. D. Joannopoulos, P. Fisher, and M. Soljačić, "Wireless power transfer via strongly coupled magnetic resonances," *Science*, vol. 317, no. 5834, pp. 83–86, Jul. 2007.

[6] J. D. Joannopoulos, A. Karalis, and M. Soljačić, "Wireless non-radiative energy transfer," U.S. Patent 7 741 734, Jun. 22, 2010.

[7] A. Karalis, A. Kurs, R. Moffatt, J. D. Joannopoulos, P. H. Fisher, and M. Soljačić, "Wireless energy transfer," U.S. Patent 7 825 543, Nov. 2, 2010.

[8] R. Fernandes, J. Matos, and N. Carvalho, "Behavior of resonant electrical coupling in terms of range and relative orientation," in *Proc. Wireless Power Transfer Conf.*, Jeju, Korea, May 2014, pp. 118–121.

[9] K. Ichikawa and H. Bondar, "Power transfer system," U.S. Patent 20 120 299 392, Nov. 29, 2012.

[10] C. Yang and K. Tsunekawa, "Analysis and performance improvement of independent electric coupled resonance WPT system with impedance transformer," in *Proc. Wireless Power Transfer Conf.*, Jeju, Korea, May 2014, pp. 239–242.

[11] A. P. Sample, D. A. Meyer, and J. R. Smith, "Analysis, experimental results, and range adaptation of magnetically coupled resonators for wireless power transfer," *IEEE Trans. Ind. Electron.*, vol. 58, no. 2, pp. 544–554, Feb. 2011.

[12] R. Fernandes, J. Matos, and N. Carvalho, "Constructive combination of resonant magnetic coupling and resonant electrical coupling," in *Proc. Wireless Power Transfer Conf.*, Boulder, CO, USA, May 2015, pp. 1–3.

[13] J. R. Smith and A. P. Sample, "Wireless power transfer apparatus and method thereof," U.S. Patent 20 100 187 913, Jul. 29, 2010.

[14] A. P. Sample, B. H. Waters, S. T. Wisdom, and J. R. Smith, "Enabling seamless wireless power delivery in dynamic environments," *Proc. IEEE*, vol. 101, no. 6, pp. 1343–1358, Jun. 2013.

Ricardo Dias Fernandes (S'10–GSM'12) was born in Aveiro, Portugal, on May 17, 1987. He received the M.S. degree in electronics and telecommunications engineering from the Universidade de Aveiro, Aveiro, Portugal, in 2010, and is currently working toward the Ph.D. degree in electrical engineering at the Universidade de Aveiro.

In 2011 he joined the Radio Systems Group, Instituto de Telecomunicações, Aveiro, Portugal, as a Researcher. His main research interests include wireless power transmission, energy harvesting, and wireless sensors.

Mr. Fernandes has been a reviewer for the IEEE TRANSACTIONS ON MICROWAVE THEORY AND TECHNIQUES since 2012. He was the recipient of two merit scholarships awarded by the Universidade de Aveiro in 2007 and 2008, the First Prize of the Fraunhofer Portugal Challenge 2011, the Best Paper Award of the IEEE Wireless Power Transfer Conference 2014, the Best Poster Award of the Research Day 2014 Poster Session promoted by the Universidade de Aveiro, and the Second Prize of the Wireless Energy Harvesting Design Competition of the IEEE Microwave Theory and Techniques Society (IEEE MTT-S) International Microwave Symposium (IMS) 2015.

João Nuno Matos (M'11) was born in Oliveira de Azeméis, Portugal, in 1959. He received the Diploma degree in electronics and telecommunications engineering from the Universidade de Aveiro, Aveiro, Portugal, in 1982, the Master's degree in electrical sciences from the Universidade de Coimbra, Coimbra, Portugal, in 1989, and the Doctoral degree in electrical engineering from the Universidade de Aveiro, Aveiro, Portugal, in 1995.

He is currently an Associated Professor with the Universidade de Aveiro, and a Senior Researcher with the Instituto de Telecomunicações. He has authored or coauthored approximately 100 journal and international conference papers. He worked twice within industry, from 1982 to 1983, with Portugal Telecom Innovation, Aveiro, Portugal, and in 1990, with Ensa Electronic, Madrid, Spain. With the Instituto de Telecomunicações he has participated or has led different projects in RF/microwave (MW) circuits, system design, and system integration. His research interests are in the area of radio communications. His current topics of interest are wireless power transfer, vehicular communications, and smart antennas.

Dr. Matos is a member of several conference and journal scientific committees, as well as professional organizations.

Nuno Borges Carvalho (S'97–M'00–SM'05–F'15) was born in Luanda, Angola, in 1972. He received the Diploma and Doctoral degrees in electronics and telecommunications engineering from the Universidade de Aveiro, Aveiro, Portugal, in 1995 and 2000, respectively.

He is currently a Full Professor and a Senior Research Scientist with the Instituto de Telecomunicações, Universidade de Aveiro. He coauthored *Intermodulation in Microwave and Wireless Circuits* (Artech House, 2003), *Microwave and Wireless Measurement Techniques* (Cambridge Univ. Press, 2013), and *White Space Communication Technologies* (Cambridge Univ. Press, 2014). He has been a reviewer and author of over 200 papers in magazines and conferences. He co-holds four patents. His main research interests include software-defined radio front-ends, wireless power transmission, nonlinear distortion analysis in microwave/wireless circuits and systems, and measurement of nonlinear phenomena. He has recently been involved in the design of dedicated radios and systems for newly emerging wireless technologies.

Dr. Borges Carvalho was the co-chair of the IEEE MTT-20 Technical Committee and the past-chair of the IEEE Portuguese Section. He is also the chair of the URSI-Portugal Metrology Group. He is an associate editor of the IEEE TRANSACTIONS ON MICROWAVE THEORY AND TECHNIQUES, *IEEE Microwave Magazine*, and the *Cambridge Wireless Power Transfer Journal*. He was the recipient of the 1995 Universidade de Aveiro and the Portuguese Engineering Association Prize for the best 1995 student at the Universidade de Aveiro, the 1998 Student Paper Competition (Third Place) of the IEEE Microwave Theory and Techniques Society (IEEE MTT-S) International Microwave Symposium (IMS), and the 2000 IEE Measurement Prize.

Behavior of resonant electrical coupling in terms of range and relative orientation

Ricardo Dias Fernandes, João Nuno Matos, Nuno Borges Carvalho
Instituto de Telecomunicações
Departamento de Electrónica, Telecomunicações e Informática, Universidade de Aveiro
Aveiro, Portugal

***Abstract*—The subjects addressed in this document fall under the topic of wireless power transmission (WPT). Power is transferred using a novel coupling technique based on electrical coupling and resonance across a distance of 5 meters with 40% efficiency. The experimental results obtained so far suggest that the efficiency of the proposed system remains stable when the relative orientation between the transmitter and the receiver is altered. The prototypes used in the experiments measure 16 by 16 cm by 3.7 cm at most. The ratio between the range of the system and the maximum dimension of each prototype is therefore around 30.**

***Index Terms*—Resonant electrical coupling; resonant capacitive coupling; resonant coupling.**

I. Introduction

The very first implementation of a device designed for wireless power transmission (WPT) was initiated in 1901. It consisted of a very large coil wound around a mast of about 60 m in height. At the top of mast was a massive 1 m diameter copper ball. This device, which became known as the Wardenclyffe tower, was envisioned by Nikola Tesla a few years before. Tesla's goal was to build a network of these towers so that energy could be collected wirelessly all over the globe. According to the journalists of that time, Tesla managed to light up 200 50 W incandescent lamps located 42 km away from the tower, using 300 kW and a frequency of 150 kHz[1]. Despite these encouraging results, the lack of funding brought the project to a halt and a few years later the tower was demolished. The theory of operation behind the system proposed by Tesla makes use of concepts such as oscillating voltages and currents, capacitor charging and discharging, resonators and magnetic induction[2].

Several important discoveries in the field of wireless communications were made in the years that followed Tesla's experiments. As a result, the development of wireless technologies focused on communications rather than power transmission. It was only during the 1960s that the topic of WPT was brought back by W. C. Brown. He carried out many kinds of WPT experiments with 2.45 GHz microwave tubes and was the first to coin the term rectenna, which he used to describe an antenna specifically designed for receiving and rectifying microwaves. One of his major accomplishments took place in 1975 at the Jet Propulsion Laboratory, California, and consisted in the transmission of 30 kW from a 26 m diameter parabolic antenna to a 3.4 by 7.2 m rectenna placed 1.6 km away. A rectifying efficiency of 82.5% was achieved at 2.388 GHz using a transmitted power of 450 kW[3]. Brown's experiments became well known mainly because of the large power levels and distances involved. However, the equipment required for the demonstrations was very large and particularly expensive, and thus not suitable for any realizable practical applications. Moreover, most high efficiency microwave WPT systems (including the previous one) tend to make use of highly directive antenna configurations. This approach results in a higher efficiency if the alignment between transmitter and receiver is perfect, but a lower efficiency otherwise. The need for aligment is one of the most important issues in a WPT system. For example, in laser-based systems a very precise alignment (and clear line of sight) between the transmitter and the receiver is needed at all times. This requirement, together a costly equipment, a high complexity and the risk of serious accidents (permanent eye injuries for instance) help explain why laser systems are generally discarded in the WPT literature. The role of lasers in WPT may however change substantially in the future, particularly if progress is made in the photovoltaic receivers in terms of the optical to electrical conversion efficiency.

More recently, in 2007, a team of researchers at the Massachusetts Institute of Technology (MIT) made a substantial contribution to the state of the art of WPT. They proposed a system composed of 4 copper coils (largest diameter of 60 cm, wire cross sectional radius of 3 mm). Using this configuration they were able to light up a 60 W incandescent light bulb placed 2 m away with an efficiency of 40%. The attention drawn by the demonstration was remarkable. The system seemed to be already close to a commercial product, much closer than other WPT systems proposed before, especially given the apparently simple apparatus. This technique takes advantage of the strong magnetic coupling formed between coils with very high Qs (quality factors) at resonance[4], [5]. The first coil, a single turn loop, is connected to a power source and the second coil, a multi turn coil, is placed near the first loop on the same axis. A capacitor is added to the loop in order to make it resonant at the frequency at which the multi turn coil self-resonates. The receiver is defined in a similar fashion, except that the loop is in this case connected to the load of the system. Each one of the loops is magnetically coupled to the nearest multi turn coil because of the close proximity. In addition, the multi turn coils are also magnetically coupled to each other because their very high Qs counteract the effect of distance. Thus, it becomes possible to transfer power from the source to the load. It should be noted that even though

the efficiency is maximized only when all coils share the same axis, the loss of efficiency due to misalignment is not substantial unless the transmitter and the receiver are placed nearly perpendicular to each other, as shown in [6]. The resonant magnetic coupling (RMC) remains very popular in the literature because of its balanced set of features.

Even though the number of RMC-based implementations reported in the literature is quite large, WPT systems based on electrical coupling are rare and often limited in one or more key attributes such as range, for instance[7]. In this work a novel WPT system based on resonant electrical coupling (REC) is proposed and analyzed, both theoretically and experimentally.

II. Proposed system

Figures 1 and 2 represent the conceptual diagram and the circuit model of the proposed WPT system, respectively.

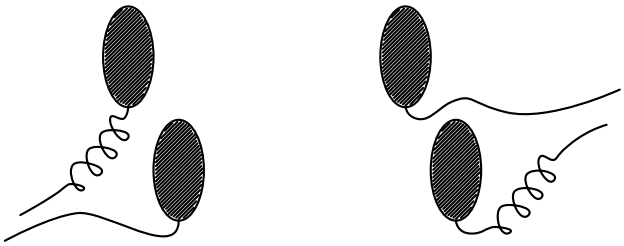

Fig. 1. Conceptual diagram of the proposed system.

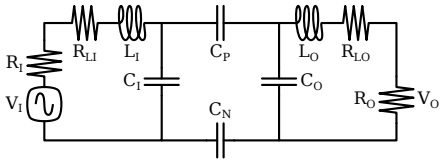

Fig. 2. Circuit model of the proposed system.

In the simplest configuration the system is composed by 4 conductive plates and 2 inductors, as shown in the previous diagram. The electrical coupling between the conductive plates is represented in the circuit model with C_I, C_O, C_P and C_N. The inductors are represented by L_I plus R_{LI} and L_O plus R_{LO}. The power source connected to the system is represented by V_I and R_I and the load by R_O. Regarding this circuit, it can be written that

$$-V_I + I_1(R_I + R_{LI} + jwL_I) + \frac{1}{jwC_I}(I_1 - I_2) = 0 \quad (1)$$

$$\frac{1}{jwC_I}(I_2 - I_1) + \frac{1}{jwC_O}(I_2 - I_3) + I_2\left(\frac{1}{jwC_P} + \frac{1}{jwC_N}\right) = 0 \quad (2)$$

$$\frac{1}{jwC_O}(I_3 - I_2) + I_3(R_O + R_{LO} + jwL_O) = 0 \quad (3)$$

$$V_O - R_O I_3 = 0, \quad (4)$$

in which I_1, I_2 and I_3 are the mesh currents (defined clockwise in this case). Given the previous equations, the ratio between V_O and V_I can be written as

$$\frac{V_O}{V_I} = \frac{R_O}{Z_I Z_O}\left[- jwC_X + \frac{1}{jwC_X}\left(jwC_X + jwC_I + \frac{1}{Z_I}\right)\left(jwC_X + jwC_O + \frac{1}{Z_O}\right)\right]^{-1}, \quad (5)$$

with $Z_{(I,O)} = R_{(I,O)} + R_{L(I,O)} + jwL_{(I,O)}$ and C_X defined as the series combination of C_P and C_N.

In a first approximation, C_P and C_N can be estimated based on the equation of a parallel plate capacitor

$$C_{(P,N)} = \epsilon_0 A_{(P,N)}/d, \quad (6)$$

in which the areas of the conductive plates shown in figure 1 are used to calculate $A_{(P,N)}$.

The available power at the input of the system and V_I can be related by $P_A = |V_I|^2/(8R_I)$ and the power delivered to the load is, in average, $P_O = |V_O|^2/(2R_O)$. Therefore, the available power gain of this circuit is

$$G_A = \frac{4R_I}{R_O}\left|\frac{V_O}{V_I}\right|^2. \quad (7)$$

Figure 3 illustrates the behavior of G_A (calculated as indicated in the previous equations) for the parameters listed in table I.

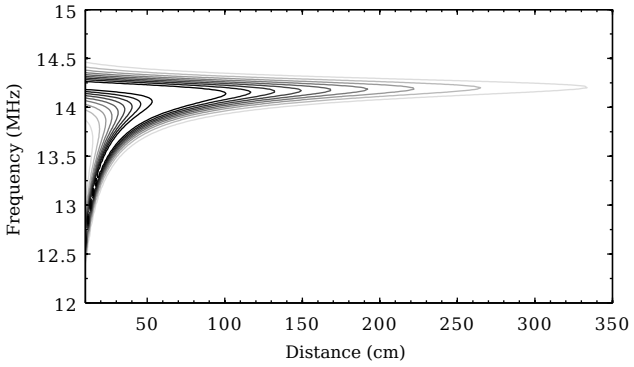

Fig. 3. Simulated available power gain. The darker contour lines represent values closer to unity.

TABLE I
EXAMPLE PARAMETERS USED IN THE GENERATION OF FIGURE 3, EXTRACTED FROM [6].

Parameter	Value
R_I, R_O	50 Ω
L_I, L_O	50 μH
R_{LI}, R_{LO}	30 Ω
C_I, C_O	2.5 pF
A_N, A_P	76 cm^2

It can be seen in figure 3 that for shorter distances there are 2 distinct frequencies which maximize G_A. The gap

between these frequencies decreases gradually as the distance is increased. Once a single frequency is reached it remains stable for higher distances. On the other hand, the maximum G_A remains stable before the frequencies converge but begins to drop after that. The behavior highlighted in the previous figure is only observable if the devices are tuned to resonate at the same frequency, that is, only if

$$L_I C_I = L_O C_O. \tag{8}$$

III. Preliminary results

The results reported in this section were obtained with the prototype shown in figure 4. This particular realization of the concept illustrated in figure 1 is composed by a 16 by 16 cm FR-4 board with 2 large copper areas and a helical coil built using 0.8 mm diameter stranded copper wire with 40 turns and a diamater of 3.6 cm. As seen in the figure, the coil is located on the back side of the FR-4 board.

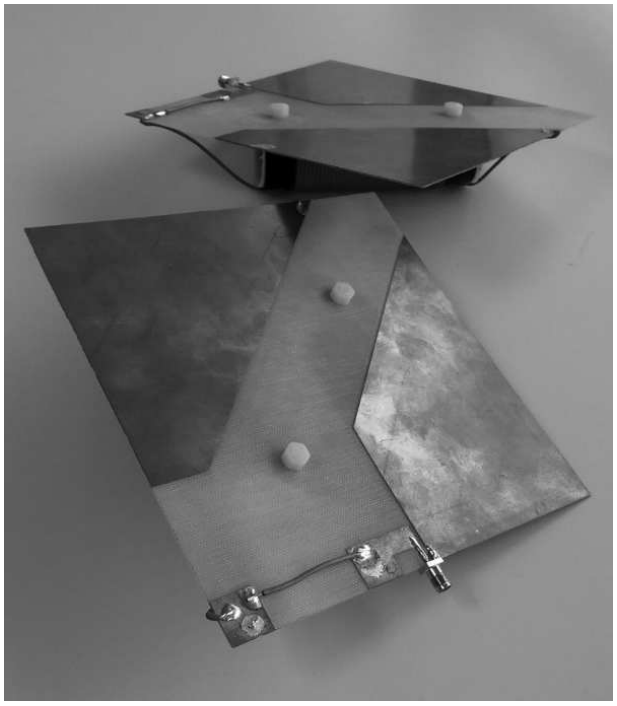

Fig. 4. Photograph of the prototype used in the measurements.

Figure 5 shows the measured voltage gain of the proposed system as a function of distance. The values presented in the figure were obtained with an HP 8753D network analyzer. The prototypes of figure 4 were first mounted on top of supports made of polystyrene with the objective of keeping the devices always about 1 m above the floor. During this test the prototypes were placed facing each other. In figure 5, each point corresponds to the maximum $|S_{21}|$ measured at a given distance. Figure 6 shows the frequencies at which these peak gain values were observed.

These figures show that the maximum $|S_{21}|$ values remain close to -4 dB for distances of 40 cm and above. Below this threshold a drop of 7 dB at most is observed. This pattern is

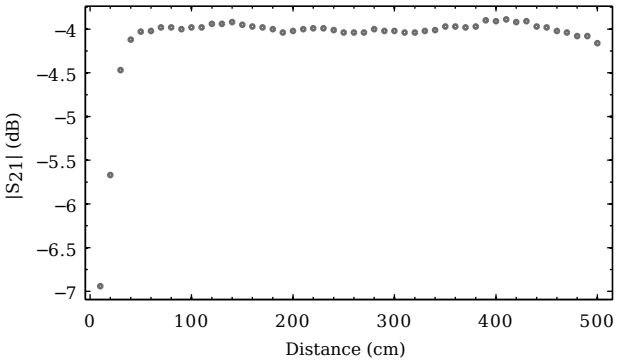

Fig. 5. Measured maximum $|S_{21}|$ of the proposed system for various distances.

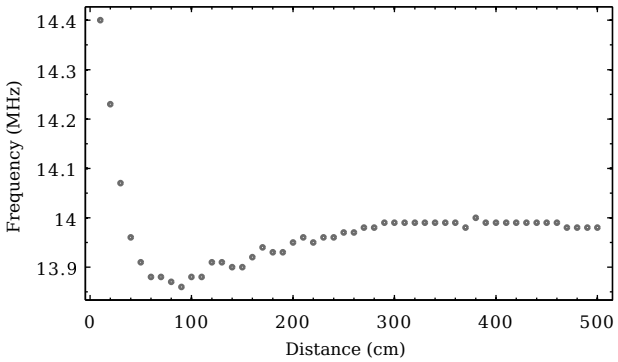

Fig. 6. Measured frequencies of maximum $|S_{21}|$.

also found in the frequency domain as the frequencies with the highest $|S_{21}|$ tend to vary less as the distance is increased. A value of -4 dB in $|S_{21}|$ results in a G_A of 0.4 using

$$G_A \approx |S_{21}|^2. \tag{9}$$

Once at a distance of 5 meters the receiver was rotated in small increments and the $|S_{21}|$ was read for each angle. During this test the operating frequency of the system was not changed. The corresponding results are shown in figure 7.

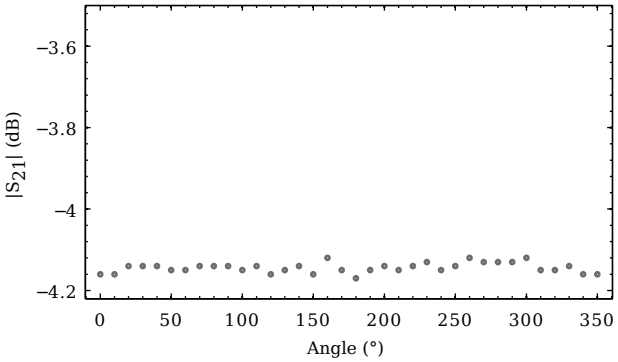

Fig. 7. Measured maximum $|S_{21}|$ of the proposed system for various relative orientations.

Based on these results, it seems that the $|S_{21}|$ remains approximately constant across all angles, including when the transmitter and the receiver are perpendicular to each other.

IV. Conclusions and ongoing work

The novel WPT system reported in this document was designed investigate the feasibility of resonant electrical coupling. The results presented suggest that an interesting balance between power, efficiency, distance and robustness to changes in relative orientation can be achieved. A circuit model was proposed for the system, however so far it only predicts part of the results observed in practice. The model is currently under research. Future work will focus primarily on the increase of the power efficiency.

Acknowledgment

The authors would like to thank the support provided by the portuguese Foundation for Science and Technology (through the grant SFRH/BD/69392/2010) and COST action IC1301.

References

[1] J.-P. Curty, M. Declercq, C. Dehollain, and N. Joehl, *Design and Optimization of passive UHF RFID Systems*. New York: Springer, 2006.

[2] N. Tesla, "Apparatus for transmitting electrical energy," Patent US1119732 A, December 1914.

[3] W. C. Brown, "The history of power transmission by radio waves," *Microwave Theory and Techniques, IEEE Transactions on*, vol. 32, no. 9, pp. 1230–1242, 1984.

[4] A. Kurs, "Power transfer through strongly coupled resonances," Master's thesis, Massachusetts Institute of Technology, 2007.

[5] A. Kurs, A. Karalis, R. Moffatt, J. D. Joannopoulos, P. Fisher, and M. Soljaoić, "Wireless power transfer via strongly coupled magnetic resonances," *Science*, vol. 317, no. 5834, pp. 83–86, July 2007.

[6] A. Sample, D. Meyer, and J. Smith, "Analysis, experimental results, and range adaptation of magnetically coupled resonators for wireless power transfer," *Industrial Electronics, IEEE Transactions on*, vol. 58, no. 2, pp. 544–554, 2011.

[7] P. Camurati and H. Bondar, "Device for transporting energy by partial influence through a dielectric medium," Murata Manufacturing Co., Ltd., and TMMS Co., Ltd., Patent US 2012/0262005 A1, October 2012.

Wireless Power Transmission Based on Resonant Electrical Coupling

Ricardo Dias Fernandes, João Nuno Matos, Nuno Borges Carvalho
Instituto de Telecomunicações
Departamento de Electrónica, Telecomunicações e Informática, Universidade de Aveiro
Aveiro, Portugal

***Abstract*—A novel technique for wirelessly transferring power over non-negligible distances is proposed and discussed in this document. In this technique the transfer of power is based on electrical coupling and resonance. In contrast, other systems proposed in the literature in the same class tend to make use of magnetic coupling. With prototypes measuring 16 by 16 cm by 3.7 cm at most it was possible to achieve a power efficiency of approximately 40% at a distance of 5 meters. These preliminary results indicate that resonant electrical coupling can be used for wireless power transmission (WPT) purposes.**

***Index Terms*—Resonant electrical coupling; resonant capacitive coupling; resonant coupling.**

I. Introduction

Several different ways to transfer energy without using any kind of wired connection exist. The very first attempt to build a system designed with wireless power transfer (WPT) in mind was made in 1899 by Nicola Tesla. He coordinated the construction of the Wardenclyffe tower, from where he believed he would be able to wirelessly distribute energy. His goal was to create a large number of these towers so that wireless energy could be collected all over the globe (a grand objective, even by today's standards). However, Tesla was forced to abandon the idea due to funding shortages before the first tower was finished. The apparatus used in the original Wardenclyffe experiment consisted of a large coil wound around a mast of about 60 m in height. At the highest point of the mast was a large copper ball. The theory of operation behind the system proposed by Tesla makes use of concepts such as oscillating currents and voltages (at about 150 kHz), capacitor charging and discharging, resonators and magnetic induction[1].

In the years that followed Tesla's experiments the research efforts devoted to WPT were reduced drastically because the development of wireless technologies focused more on communications. In fact, the discoveries made at the time in the field of wireless communications were decisive for the loss of interest in Tesla's results and WPT in general as they drew much more attention. It was only during the 1960s that the topic of WPT was brought back by W. C. Brown. Brown carried out several WPT demonstrations based on microwave technology. One of his major accomplishments took place in 1975. It consisted in the transmission of 30 kW from a 26 m diameter parabolic antenna to a 3.4 by 7.2 m rectenna placed 1.6 km away. Brown transmitted 450 kW in order to achieve the results mentioned. The obtained rectifying efficiency was 82.5% at a frequency of 2.388 GHz[2]. Brown's experiments became well known mainly because of the very large power levels and distances involved. However, the equipment required for the demonstrations was expensive and large, and therefore not suitable for any realizable practical applications. This system as well as other high efficiency microwave systems proposed in the literature tend to make use of highly directive antenna configurations. This approach results in a higher efficiency if the alignment between transmitter and receiver is perfect, but a lower efficiency otherwise. The need for aligment is one of the most important issues in a WPT system. For example, in laser-based WPT systems a very precise alignment is needed at all times. This requirement, together a costly equipment, clear line of sight, a high complexity and the risk of serious accidents (permanent eye injuries, for instance) help explain why laser systems are generally discarded. The role of lasers in WPT may however change substantially in the future, in particular if progress is made in the photovoltaic receivers in terms of the optical to electrical conversion efficiency.

Some years ago, in 2007, researchers at the Massachusetts Institute of Technology (MIT) made a significant contribution to the state of the art of WPT. They announced a system consisting of 4 coils (largest diameter of 60 cm) with which they were able to light up a 60 W incandescent light bulb located 2 m away with an efficiency of 40%. The attention drawn by the demonstration was quite remarkable. In addition to the obvious quality of the results, the system seemed to be already close to a commercial product, substantially closer than other WPT systems proposed before. In this technique the efficiency of the transfer relies on the strong magnetic coupling formed between coils with very high Qs (quality factors) at resonance[3], [4]. The first coil, a single turn loop, is connected to a power source. The second coil, a multi turn coil, is placed near the first loop on the same axis. A capacitor is added to the first loop to make it resonant precisely at the frequency at which the multi turn coil self-resonates. The receiver is defined identically, except that the loop is connected to the load. The loops are coupled to the multi turn coils magnetically. In addition, the coils are also magnetically coupled to each other because the high Qs counteract the effect of distance. Hence, it becomes possible to transfer power from the source to the load. It should be noted that while the efficiency of the power transfer is maximum when all the coils are placed on the same axis, the loss of efficiency due to misalignment is not critical until the transmitter and the receiver are nearly perpendicular[5].

In this work, the feasibility of resonant electrical coupling for WPT purposes is investigated. A prototype based on this

type of coupling is proposed and analyzed.

II. Proposed system

Comparisons between WPT systems can be based on several different aspects depending on the application. However, efficiency and range are often considered the most important factors. Robustness against changes in relative orientation is usually desirable. A small, inexpensive and easy to build apparatus is usually desirable as well. It is sometimes important to evaluate if a system can be scaled for different power levels. One of the strong points of resonant magnetic coupling (RMC) is that compromise achieved is unique and particularly useful. The strong presence of this technique in the literature is mostly due to this fact. In contrast, systems based on electrical coupling are very difficult to find. In addition, the few WPT systems proposed that make use of this coupling technique tend to lack some key attributes, such as range[6].

The proposed WPT system is based on electrical coupling and consists of 2 identical devices as shown in figure 1.

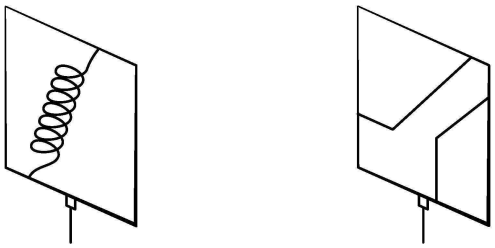

Fig. 1. Diagram of the proposed system.

Each one of the devices is composed by an FR-4 board measuring 16 by 16 cm with 2 large conductive areas (copper) on the front side and a helical coil attached to the back side. The latter consists of 40 turns of 0.8 mm diameter stranded copper wire and has a diameter of approximately 3.6 cm.

A. Circuit model

The circuit model developed for the previously introduced system is presented in figure 2.

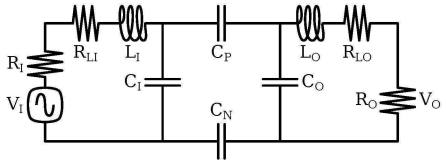

Fig. 2. Circuit model developed for the proposed system.

In this model, the parameters V_I and R_I represent the power source connected to the transmitter. Each helical coil is represented by an inductor, L_I or L_O, in series with a parasitic resistance, R_{LI} or R_{LO}. The capacitors included in the model represent the coupling between the conductive areas mentioned earlier: C_I and C_O refer to intra-device coupling, while C_P and C_N refer to the inter-device coupling. The load of the system is modeled by the resistor R_O. The ratio between V_O and V_I for this model can be written as

$$\frac{V_O}{V_I} = \frac{R_O}{Z_I Z_O}\left[-jwC_X + \frac{1}{jwC_X}\left(jwC_X + jwC_I + \frac{1}{Z_I}\right)\left(jwC_X + jwC_O + \frac{1}{Z_O}\right)\right]^{-1}, \quad (1)$$

with $Z_I = R_I + R_{LI} + jwL_I$, $Z_O = R_O + R_{LO} + jwL_O$ and C_X defined as the series combination of C_P and C_N.

In a first approximation, C_P and C_N can be estimated based on the equation of a parallel plate capacitor

$$C_P = \epsilon_0 A_P / d \quad (2)$$

$$C_N = \epsilon_0 A_N / d \quad (3)$$

in which the conductive areas are used to calculate A_P and A_N, ϵ_0 is the permittivity of vacuum and d is the distance between devices.

From circuit theory, the available power at the input of the system can be calculated from V_I by $P_A = |V_I|^2/(8R_I)$. Moreover, the power delivered to the load is, in average, $P_O = |V_O|^2/(2R_O)$. Given these equations the available power gain of the system can be written as

$$G_A = \frac{4R_I}{R_O}\left|\frac{V_O}{V_I}\right|^2. \quad (4)$$

Figure 3 illustrates the behavior of G_A for the parameters listed in table I.

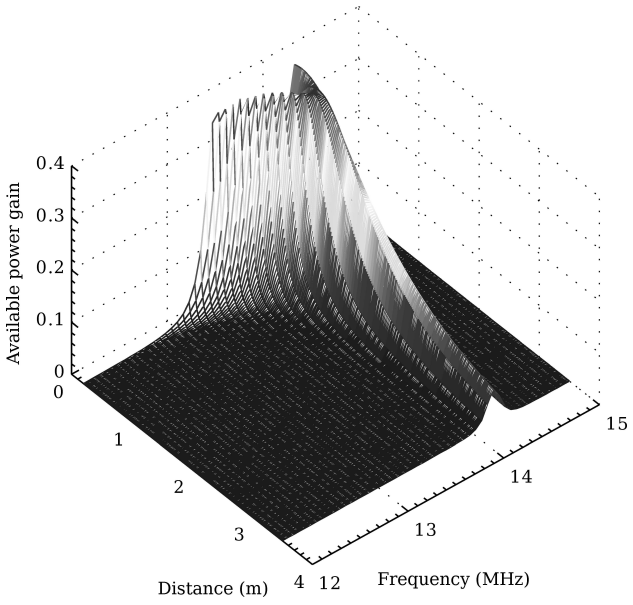

Fig. 3. Simulated available power gain (G_A) as a function of distance and frequency.

TABLE I
PARAMETERS USED IN THE GENERATION OF FIGURE 3.

Parameter	Value
R_I, R_O	50 Ω
L_I, L_O	50 μH
R_{LI}, R_{LO}	30 Ω
C_I, C_O	2.5 pF
A_N, A_P	76 cm^2

It can be clearly seen that for shorter distances there are 2 different frequencies that maximize G_A. The gap between them decreases gradually as the distance is increased and eventually disappears. When the distance is increased past the point where the frequencies converge the value of G_A begins to drop. It is interesting to note that this behavior is similar to the behavior of RMC (which can be seen for instance in [5]), even though the coupling technique is entirely different. This result is only achievable if both devices are tuned to resonate at the exact same frequency, that is, only if

$$\frac{1}{2\pi\sqrt{L_I C_I}} = \frac{1}{2\pi\sqrt{L_O C_O}} \Leftrightarrow L_I C_I = L_O C_O. \quad (5)$$

III. PRELIMINARY RESULTS

Figure 4 shows the measured voltage gain (amplitude only) of the proposed system as a function of distance. The values presented in the figure were obtained with an HP 8753D network analyzer. In this experiment the devices under test were oriented as illustrated in figure 1 and placed on top of supports made of polystyrene with the purpose of maintaining a constant distance of 1 m to the floor at all times. Each point in the graphic corresponds to the maximum $|S_{21}|$ measured at a given distance. Figure 5 shows the frequencies at which these maximum values were found. A photograph of the prototypes used in these tests can be seen in figure 6.

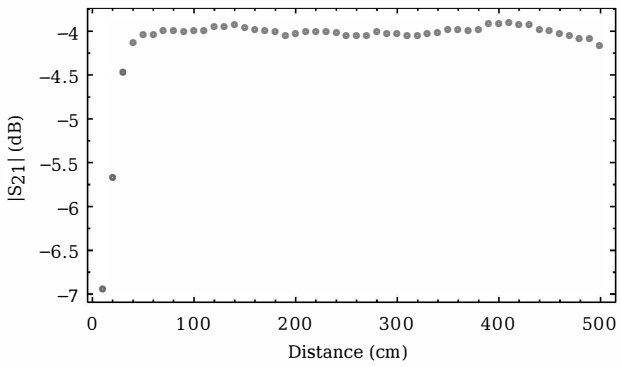

Fig. 4. Maximum $|S_{21}|$ of the proposed system, measured.

From the previous results it can be seen that the maximum $|S_{21}|$ values remain close to -4 dB for distances of 40 cm and above. Below this threshold a drop of 7 dB is observed when the devices are placed very close to one another. The cause of this drop is not yet known but it may be related to the establishment of additional electrical couplings not taken into account by the current model or a magnetic coupling between the inductors. In terms of frequency, the highest $|S_{21}|$ tend to vary more below the 40 cm threshold, possibly due to the aforementioned reasons. For higher distances the values tend to stabilize. It should be noted that the values in table I (except for R_I and R_O) were estimated from the geometrical properties of the prototypes. It should be also noted that a value of -4 dB in $|S_{21}|$ results in a G_A of 0.4 using

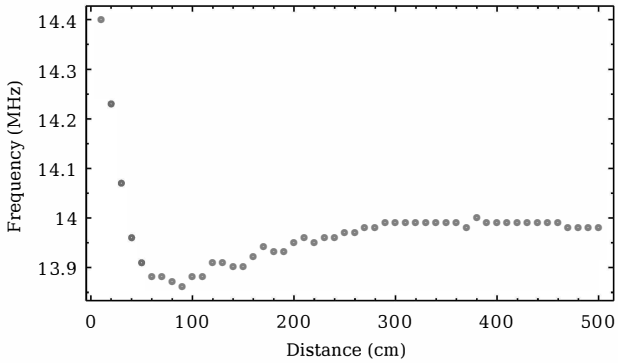

Fig. 5. Frequencies of maximum $|S_{21}|$, measured.

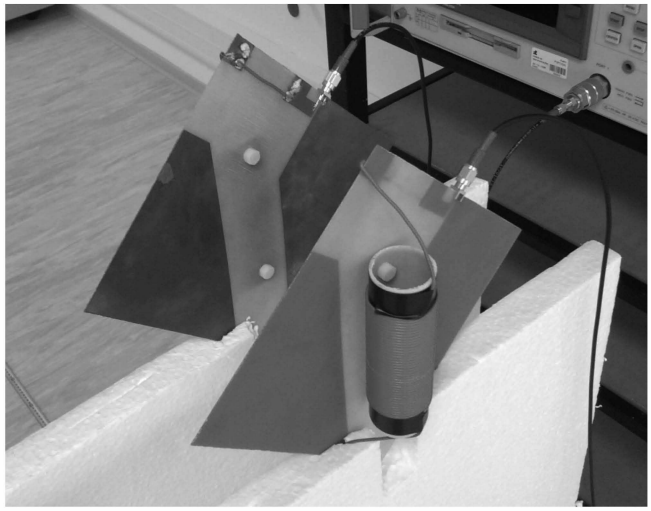

Fig. 6. Photograph of the prototype used in the measurements.

$$G_A \approx |S_{21}|^2. \quad (6)$$

IV. CONCLUSIONS AND ONGOING WORK

The novel system reported in this document was designed to assess the feasibility of resonant electrical coupling. The theoretical results obtained suggest that an interesting balance between power efficiency and distance can be achieved. So far only a partial match between the model and the experimental results was achieved. Future work will therefore focus on the improvement of the model with the purpose of increasing the maximum power efficiency.

ACKNOWLEDGMENT

The authors would like to thank the support provided by the portuguese Foundation for Science and Technology (through the grant SFRH/BD/69392/2010) and COST action IC1301.

REFERENCES

[1] N. Tesla, "Apparatus for transmitting electrical energy," Patent US1119732 A, December 1914.

[2] W. C. Brown, "The history of power transmission by radio waves," *Microwave Theory and Techniques, IEEE Transactions on*, vol. 32, no. 9, pp. 1230–1242, 1984.

[3] A. Kurs, "Power transfer through strongly coupled resonances," Master's thesis, Massachusetts Institute of Technology, 2007.

[4] A. Kurs, A. Karalis, R. Moffatt, J. D. Joannopoulos, P. Fisher, and M. Soljaoić, "Wireless power transfer via strongly coupled magnetic resonances," *Science*, vol. 317, no. 5834, pp. 83–86, July 2007.

[5] A. Sample, D. Meyer, and J. Smith, "Analysis, experimental results, and range adaptation of magnetically coupled resonators for wireless power transfer," *Industrial Electronics, IEEE Transactions on*, vol. 58, no. 2, pp. 544–554, 2011.

[6] P. Camurati and H. Bondar, "Device for transporting energy by partial influence through a dielectric medium," Murata Manufacturing Co., Ltd., and TMMS Co., Ltd., Patent US 2012/0262005 A1, October 2012.

Constructive combination of resonant magnetic coupling and resonant electrical coupling

Ricardo Dias Fernandes, João Nuno Matos and Nuno Borges Carvalho
Instituto de Telecomunicações
Departamento de Electrónica, Telecomunicações e Informática, Universidade de Aveiro
Aveiro, Portugal

***Abstract*—In this paper the possibility of combining resonant magnetic coupling and resonant electrical coupling is proposed and discussed. Equivalent circuit models are used to demonstrate that efficiency can be improved quite significantly using a hybrid approach. A comparison between resonant magnetic coupling only, resonant electrical coupling only and several hybrid combinations is provided.**

***Index Terms*—Wireless power transfer, resonant electrical coupling, resonant hybrid coupling, resonant magnetic coupling.**

I. Introduction

In 2007 a group of researchers at the Massachusetts Institute of Technology (MIT) proposed a novel and very innovative wireless power technology by combining the concepts of inductive coupling and magnetic resonance very effectively. Resonant magnetic coupling takes advantage of the fact that the coupling between two coils can be very strong even if the magnetic coupling coefficient is very low (something in the order of 0.01, for instance). For this to happen the coils must resonate at the same frequency and must have very high Qs (quality factors). Several publications of great scientific importance resulted from this discovery, in particular [1], which has over 1000 citations to date. Resonant magnetic coupling was first demonstrated using a prototype consisting of two single-turn coils and two helical coils. In this prototype the copper wires used to build the coils had a cross-sectional diameter of 6 mm (a rather large value in order to minimize losses, and thus increase Q). The outer diameter of the helical coils was 60 cm (not exactly small but also not unreasonable). Using this prototype the researchers were able to light up a 60 W incandescent light bulb placed 2 meters away. Even more importantly, they managed to do so with a transfer efficiency of 40%. A very surprising result, especially given the fact that it was obtained with such a simple apparatus. One of the key features of resonant magnetic coupling is the balanced trade-off between efficiency, range, simplicity (cost), size and power transfer capability.

In this paper the combination of resonant magnetic coupling and resonant electrical coupling in the same system is proposed and studied. A circuit model is used to demonstrate that efficiency can be significantly increased if the two coupling methods are used simultaneously. This is the main contribution in this paper. Resonant electrical coupling has been recently proposed in [2] and [3]. In this technique the goal is to transfer power efficiently between capacitively coupled conductive plates, rather than between coils. In the next section the equivalent circuit model of resonant magnetic coupling will be considered. The results presented in this part will be used later in the paper for comparison purposes. The combination of resonant magnetic coupling and resonant electrical coupling will then be presented.

978-1-4673-7447-7/15/$31.00

II. Resonant magnetic coupling

Figure 1 shows the circuit model currently most commonly used in the literature to represent resonant magnetic coupling (see [4] for more information on this model). Starting from the equations obtained with Kirchhoff's voltage law and additionally taking into consideration that the magnetic coupling coefficient between two inductors i and j can be calculated from the mutual inductance using

$$k_{ij} = M_{ij}/\sqrt{L_i L_j}, \tag{1}$$

the voltage gain V_O/V_I can be written as

$$V_O/V_I = -jw^3 R_O k_{12} k_{23} k_{34} L_2 L_3 \sqrt{L_1 L_4}/(K_1 K_2 + w^2 k_{23}^2 L_2 L_3 Z_1 Z_4), \tag{2}$$

with K_1 and K_2 given by

$$K_1 = Z_1 Z_2 + w^2 k_{12}^2 L_1 L_2 \tag{3}$$

$$K_2 = Z_3 Z_4 + w^2 k_{34}^2 L_3 L_4, \tag{4}$$

and Z_1, Z_2, Z_3 and Z_4 given by

$$Z_1 = R_I + R_1 + jwL_1 - j/(wC_1) \tag{5}$$

$$Z_2 = R_2 + jwL_2 - j/(wC_2) \tag{6}$$

$$Z_3 = R_3 + jwL_3 - j/(wC_3) \tag{7}$$

$$Z_4 = R_O + R_4 + jwL_4 - j/(wC_4). \tag{8}$$

The available power gain P_O/P_A of the circuit can be written as a function of (2) using

$$P_O/P_A = 4R_I |V_O/V_I|^2 / R_O. \tag{9}$$

Figure 2 illustrates the response of the model as a function of frequency for k_{23} values between 0.002 and 0.06. The values of the other parameters, which were selected based on [4], are listed in table I. If the magnetic coupling coefficient

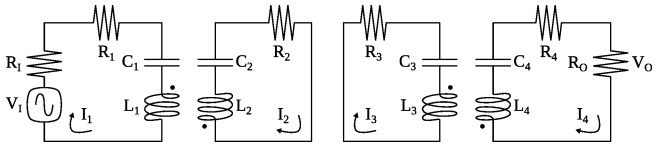

Fig. 1. Circuit model most commonly used to represent resonant magnetic coupling.

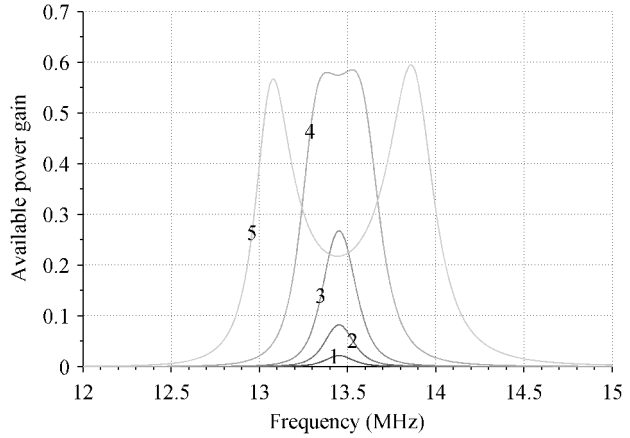

Fig. 2. Resonant magnetic coupling with k_{23} equal to 0.002 (line 1), 0.004, 0.008, 0.023 and 0.06 (line 5).

between L_2 and L_3 is very small (which corresponds to a larger distance between the coils) only a very small fraction of the power available in the source reaches the load. As k_{23} is increased the resonance becomes much more evident. If k_{23} is increased beyond approximately 0.023 (line 4) the gain no longer increases. Instead, the resonant frequency splits into two. The peak gain depends heavily on the values chosen for the resistive elements in the circuit. The peak gain tends to 1 as the resistive elements tend to 0 (higher Qs). Significant gains obtained with very small magnetic coupling coefficients is what best distinguishes this technique from plain inductive coupling.

III. Resonant hybrid coupling

Figure 3 shows the circuit model that will be considered in this part of the paper. In this circuit the left and right sides are coupled magnetically (L_1 and L_2) and electrically (C_3 and C_4). Also, C_3 and C_4 will be treated as an admittance two-port network (as indicated by the dashed line). For this circuit the voltage gain V_O/V_I can be calculated as

$$V_O/V_I = R_O(jwk_{12}\sqrt{L_1L_2}K_3 + Y_{21})/(jwk_{12}\sqrt{L_1L_2}[Y_{12}+Y_{21}] - w^2k_{12}^2L_1L_2K_3 + Y_{12}Y_{21}Z_1Z_2 - [1+K_1Z_1][1+K_2Z_2]), \quad (10)$$

with K_1, K_2 and K_3 given by

$$K_1 = Y_{11} + jwC_1 \quad (11)$$

$$K_2 = Y_{22} + jwC_2 \quad (12)$$

$$K_3 = K_1K_2 - Y_{12}Y_{21}, \quad (13)$$

TABLE I
Parameters used in the analysis of the circuit model presented in figure 1.

Parameter	Value
R_I, R_O	50 Ω
R_1, R_4	2 Ω
R_2, R_3	10 Ω
L_1, L_4	1 μH
L_2, L_3	28 μH
C_1, C_4	140 pF
C_2, C_3	5 pF
k_{12}, k_{34}	0.1

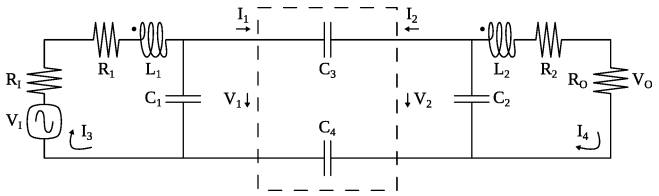

Fig. 3. Circuit model considered in this study of hybrid resonant coupling.

Z_1 and Z_2 given by

$$Z_1 = R_I + R_1 + jwL_1 \quad (14)$$

$$Z_2 = R_O + R_2 + jwL_2, \quad (15)$$

and Y_{11}, Y_{12}, Y_{21} and Y_{22} given by

$$Y_{11} = jwC_3C_4/(C_3+C_4) \quad (16)$$

$$Y_{12} = -Y_{11} \quad (17)$$

$$Y_{21} = -Y_{11} \quad (18)$$

$$Y_{22} = Y_{11}. \quad (19)$$

In this case the expression for the available power gain indicated in (9) continues to be valid.

Figure 4 illustrates the response of the model as a function of frequency for C_3 values between 0.02 and 0.9 pF. In this figure only the electrical coupling is considered (k_{12} is considered zero). Also, C_4 is assumed to always have the same value as C_3. The behavior observed in this figure is in general similar to the behavior observed in figure 2. The most noticeable difference is the asymmetrical frequency splitting. Significant gains obtained with relatively small C_3 values (which correspond to potentially higher distances) is what best distinguishes this technique from plain capacitive coupling. The remaining circuit parameters used in this case can be found in table II. This purely electrical resonant coupling is the subject addressed in [2] and [3].

Figure 5 shows the effect of increasing k_{12} from 0 to 0.075 while keeping C_3 fixed at 0.04 pF. As can be seen, the gain increases as k_{12} is increased. For instance, when k_{12} is increased from 0 to 0.004 the gain goes from 0.05 to 0.2. The most significant conclusion to be drawn from the figure is that the combination of both coupling techniques effectively results in an improvement. Since the resistive elements in the circuit were not altered the peak gain remains unchanged from figure 4.

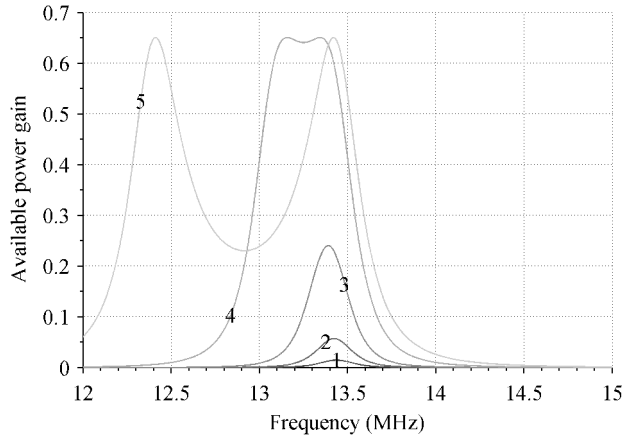

Fig. 4. Resonant electrical coupling with C_3 (in pF) equal to 0.02 (line 1), 0.04, 0.09, 0.31 and 0.9 (line 5).

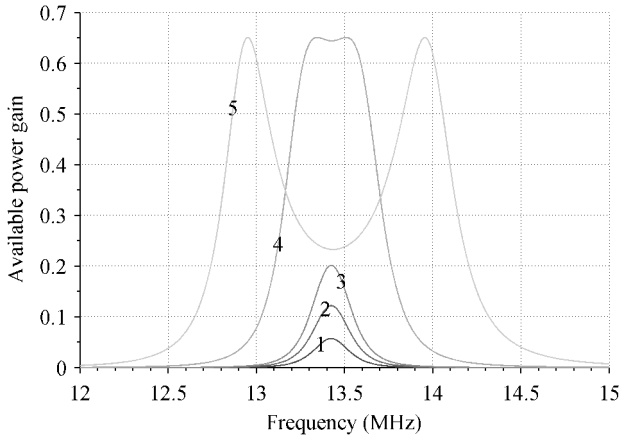

Fig. 5. Resonant hybrid coupling with C_3 equal to 0.04 pF and k_{12} equal to 0 (line 1), 0.002, 0.004, 0.025 and 0.075 (line 5).

TABLE II
PARAMETERS USED IN THE ANALYSIS OF THE CIRCUIT MODEL PRESENTED IN FIGURE 3.

Parameter	Value
R_I, R_O	50 Ω
R_1, R_2	12 Ω
L_1, L_2	28 μH
C_1, C_2	5 pF

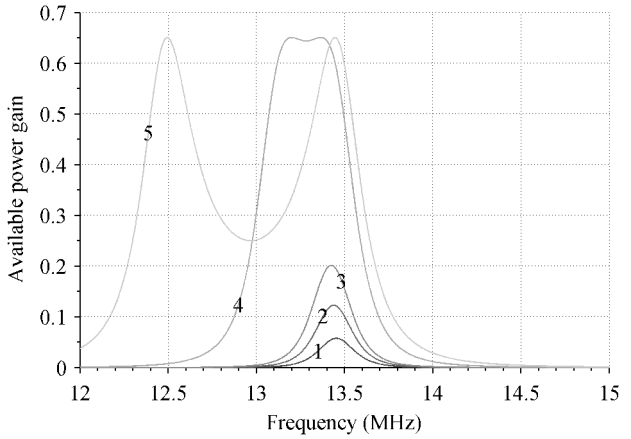

Fig. 6. Resonant hybrid coupling with k_{12} equal to 0.004 and C_3 (in pF) equal to 0 (line 1), 0.02, 0.04, 0.26 and 0.8 (line 5).

Finally, figure 6 shows the effect of increasing C_3 from 0 to 0.8 pF while keeping k_{12} fixed at 0.004. As can be seen, the gain increases as C_3 is increased. line 1 represents the case in which only magnetic coupling is taken into account (Y_{11}, Y_{12}, Y_{21} and Y_{22} are all considered zero). The existence of asymmetry in the frequency splitting depends on which kind of coupling is the largest contributor. In this figure the largest contributor is electrical coupling so the splitting is asymmetrical. In figure 5 the largest contributor is magnetic coupling so the splitting is more symmetrical.

IV. Conclusions and ongoing work

The most relevant conclusion to be drawn from this paper is that resonant magnetic coupling and resonant electrical coupling can be constructively combined. This conclusion is based on circuit theory. The simultaneous use of both coupling techniques leads to a noticeable improvement in terms of efficiency. As far as the authors know this is the first time a hybrid wireless power system is proposed. The authors are currently working on a prototype designed to demonstrate the analytical results presented in this paper.

Acknowledgment

The authors gratefully acknowledge the financial support provided by the FCT (Fundação para a Ciência e a Tecnologia) under the projects SFRH/BD/69392/2010 and PEst-OE/EEI/LA0008/2013 and by the COST action IC1301.

References

[1] A. Kurs, A. Karalis, R. Moffatt, J. D. Joannopoulos, P. Fisher, and M. Soljačić, "Wireless power transfer via strongly coupled magnetic resonances," *Science*, vol. 317, no. 5834, pp. 83–86, July 2007.

[2] R. D. Fernandes, J. N. Matos, and N. B. Carvalho, "Behavior of resonant electrical coupling in terms of range and relative orientation," in *Wireless Power Transfer Conference (WPTC), 2014 IEEE*, May 2014, pp. 118–121.

[3] C. Yang and K. Tsunekawa, "Analysis and performance improvement of independent electric coupled resonance wpt system with impedance transformer," in *Wireless Power Transfer Conference (WPTC), 2014 IEEE*, May 2014, pp. 239–242.

[4] A. P. Sample, D. A. Meyer, and J. R. Smith, "Analysis, experimental results, and range adaptation of magnetically coupled resonators for wireless power transfer," *Industrial Electronics, IEEE Transactions on*, vol. 58, no. 2, pp. 544–554, February 2011.

IET Microwaves, Antennas & Propagation

Research Article

Low-power ultra-wide band pulse generator based on a PIN diode

ISSN 1751-8725
Received on 13th August 2014
Revised on 3rd March 2015
Accepted on 26th March 2015
doi: 10.1049/iet-map.2014.0491
www.ietdl.org

Ricardo Dias Fernandes ✉, *João Nuno Matos*, *Nuno Borges Carvalho*

Departamento de Electrónica, Telecomunicações e Informática, Instituto de Telecomunicações, Universidade de Aveiro, 3810-193, Aveiro, Portugal
✉ *E-mail: rdf@ua.pt*

Abstract: Radio-frequency identification (RFID) tags (passive kind) are typically not designed to include ultra-wide band (UWB) pulse generators, but may be in the future. The reason is that the very short pulses produced by the RFID tags could be used to estimate their positions with errors of solely a few centimetres using time difference of arrival techniques. Currently, the method most commonly used to estimate tag positions relies on received signal strengths (less accurate). An UWB pulse generator based on a PIN diode is presented in this study. This pulse generator was designed to produce a positive unipolar pulse for each high-to-low transition (1.8 V to 0) it receives at its input. This trigger signal is generated by a microntroller-based battery-free RFID tag. The end result is a pulse with an amplitude of ~300 mV and a duration of slightly <2 ns measured using a 50 Ω load.

1 Introduction

Future passive radio-frequency identification (RFID) systems will probably be capable of not only identifying objects, but also estimating with good precision where they are. Localisation seems to be a natural step in the evolution of this technology. The challenge is to add this feature while keeping the tags simple and, even more importantly, battery-free. As mentioned in [1], ultra-wide band (UWB) is currently considered a possible solution, because it has a few characteristics that are very interesting. These characteristics are mentioned in the following subsection. Then, an example of a very low-power RFID tag with localisation capabilities is presented. Even though in this example the tag is powered by a battery (and thus not battery-free), it shows that combining RFID and UWB can yield positive results. The last part of Section 1 is dedicated to UWB pulse generation methods. A brief description of the methods most frequently found in the literature is given. The proposed PIN diode-based UWB pulse generator is presented in Section 2. The passive RFID tag used to test it is also briefly described in Section 2. The experimental results are presented in Section 3.

1.1 Advantages of integrating UWB in passive RFID

RFID communications are always reader-initiated. The process starts with the reader radiating a high power unmodulated wave to the tags to wirelessly power them. The tags switch back and forth between a low reflection state (where they absorb most of the incident power) and a high reflection state (which they use, together with the first one, to create modulated backscatter). Reader to tag communication is usually also possible using ASK since ASK receivers are typically low power and simple enough to be integrated in RFID tags. Nonetheless, RFID communications are generally uplink-dominated since tags operate mainly as transmitters (see [2]). Integrating UWB technology in RFID does not necessarily mean adding an UWB receiver plus transmitter block to each RFID tag. In fact, the receiver is usually left out because of its relatively large power consumption (as pointed out in [3]). In contrast, UWB transmitters are low power and thus compatible with passive RFID tags. UWB transmitters generate very short pulses which can be used to estimate the positions of the tags more accurately than using backscatter. In addition, backscatter requires the existence of an incoming unmodulated wave to work while UWB does not. Other UWB-related features worth mentioning are the possibility of achieving high throughput, resistance to multipath and coexistence with narrowband signals (small interference caused, very good immunity).

1.2 Example of a low-power RFID tag with UWB

In [4], a UWB-based RFID system is presented. The tags in this example are not passive (they are powered by CR2032 batteries), but some of the experimental data reported are important even for systems with battery-free tags. They are transmitting-only and thus not able to receive any data. Each tag consists simply of a pulse generator, a microcontroller unit (MCU) and a battery. The MCU is used to trigger the pulse generator. The UWB pulse generated has a peak-to-peak voltage of ~2.8 V on a 50 Ω load (which gives ~15.5 dBm) and a duration of 1.5 ns. The pulses move away from the RFID tag and towards several fixed UWB receivers placed at different, well-known locations. The position of the tag can be estimated by making use of the differences between the pulse arrival times reported by each one of the receivers. This technique is very popular and is known as time difference of arrival (TDOA). In terms of accuracy (which is one of the most relevant features in any localisation system), the value reported is 10 cm, measured in a 6×6 m room, and using a total of four UWB receivers. In this case, the receivers are non-coherent and have a sensitivity of approximately −71 dBm.

1.3 Techniques used in the generation of UWB pulses

To be considered UWB a signal must have a bandwidth of at least 500 MHz absolute at −10 dB or 0.2 fractional (which is given by the ratio between the absolute bandwidth and the centre frequency). This UWB definition was initially proposed by the Federal Communications Commission (FCC), and is currently the most frequently found in the literature. In terms of regulations, for the United States the FCC established the core UWB frequency band as being from 3.1 to 10.6 GHz. Within this band, the transmitted power spectral density (PSD) limit is higher, fixed and equal to −41.3 dBm/MHz. In the time domain, there are essentially no restrictions to be taken into account. In Europe,

there are also no restrictions on the pulse shapes, but the maximum PSD is equal to −41.3 dBm/MHz only from 6 to 8.5 GHz. Outside the previous band, it is always −65 dBm/MHz or lower. Additional details about regulations can be found in [5].

In general, UWB pulse generators are based on high-speed logic gates, transistors driven in the avalanche region, or one of several types of diodes, which can be an avalanche, tunnel or step recovery (SRDs). Pulse generators made with logic gates usually only need two of these (the NOT plus AND is a popular example). The circuit is designed to force a race condition at the output gate, causing a short glitch. Creating UWB pulses using this method are, however, not straightforward. The reason is that generating shorter pulses requires faster logic, and the faster logic families tend to consume more power. If there is little energy available (such as in an RFID tag) the problem becomes quite obvious. A comparison between several types of pulse generators, including logic-based, is presented in [6]. Transistors driven in the avalanche region can be used to generate extremely short pulses but usually require high supply voltages, as mentioned in [7]. For instance, the pulse generator described in [6] uses a supply voltage of 300 V. High voltages are also often linked to avalanche diodes. In fact, the latter is normally only used to generate high-power pulses (necessary for applications like long-range radar). Tunnel diodes are very suitable to be used in extremely short (sub-nanoseconds) pulse generators. This is true because of their small transition time (the smallest of all the diode types mentioned). The disadvantage of this kind of diodes is their relatively low-output voltage (see [7]). Another point worth noting is that tunnel diodes are not easy to obtain (because of the low-volume manufacturing). Lastly, SRDs are not as good as tunnel diodes in terms of transition times, but are not affected by the output voltage problem. SRDs are commonly found in the literature related to UWB pulse generation, more than any other kind of diode. These diodes are currently seen as very promising devices for low-power UWB applications, yet (like tunnel diodes) they are not easy to obtain. Some authors even call it a 'dying art'. A table with the most relevant parameters of SRDs can be found in [7]. While not as good as SRDs in terms of UWB pulse generation, PIN diodes have the advantage of being cheap and very easy to obtain. It was mainly because of these aspects that a PIN diode was selected. PIN diodes are not generally linked to pulse generators. In fact, no PIN diode-based UWB pulse generators were found in the literature (low power or not).

2 Proposed UWB pulse generator

The proposed short pulse generator and the RFID tag used to test it are described in this section.

2.1 Schematic and circuit layout

The pulse generator consists of a PIN diode (BA592), a 1 nF capacitor, an 820 Ω resistor and a 3.9 nH inductor. The layout and schematic are both shown in Fig. 1. The board represented in the figure is made of RO4003C (a high-frequency, low-loss material, in this case 0.813 mm thick). In the layout, the top pin is the pin connected to the resistor, the middle pin is the ground and the bottom pin is connected to the capacitor. It is important to note that the top and bottom pins were not short-circuited directly on the board for testing purposes but represent a single input.

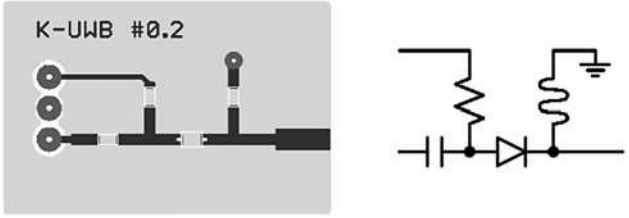

Fig. 1 *Physical layout of the proposed UWB pulse generator and corresponding schematic*

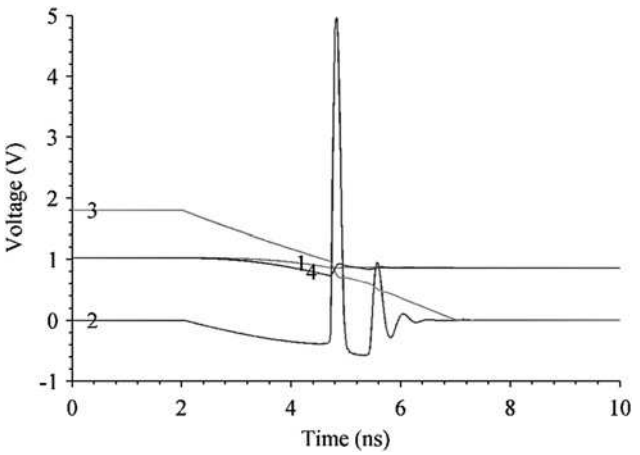

Fig. 2 *Simulated response of the UWB pulse generator to a 1.8 V to 0 transition*

Curve 1 is the voltage in the capacitor, curve 2 is the output voltage (or voltage in the inductor), curve 3 is the input voltage and curve 4 is the voltage in the resistor

Figs. 2 and 3 illustrate the behaviour of the pulse generator in terms of voltage and current, respectively, in response to a 1.8 V to 0 transition. If the input voltage is set to 0 V the pulse generator is turned off and the consumed power is virtually 0. On the other hand, if the input voltage is 1.8 V a current flows through the resistor, diode and inductor. No current flows through the load since the latter is in parallel with the inductor which at DC behaves as a short circuit. In this state, both the capacitor and the diode (internal capacitance) accumulate charges. The amount of current that flows through the diode is set by the resistor. As the input voltage is decreased again to 0 part of this input variation is transferred to the output due to the fact that the voltages at the terminals of the capacitor and the diode cannot change instantaneously. As a consequence of the output voltage variation a current starts to flow through the inductor, diode and capacitor since this is for a brief moment a path of almost no resistance. During this part, the diode continuously loses charges. Once the discharge is complete it changes from almost a short circuit to almost an open circuit in a very short time (the transition time). The current flowing through the inductor cannot stop instantaneously, and is thus forced to go to the load. As a consequence, the output voltage increases. This increase in output

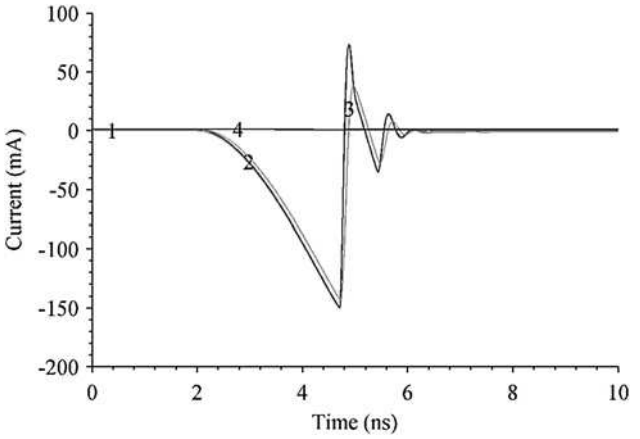

Fig. 3 *Simulated response of the UWB pulse generator to a 1.8 V to 0 transition*

Curve 1 is the current in the capacitor, curve 2 is the current in the diode, curve 3 is the current in the inductor and curve 4 is the current in the resistor

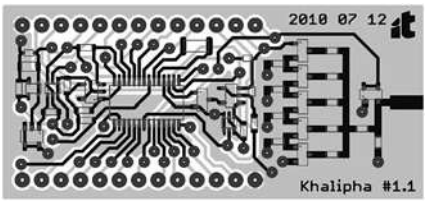

Fig. 4 *Layout of the passive RFID tag (shown on a 1:1 scale) used to test the pulse generator, taken from [8]*

voltage, generates an opposite current in the inductor and helps to quickly bring the output voltage back to 0. The result of the entire process is a positive unipolar pulse. Smaller capacitor values result in the capacitor discharging before the diode, leading to a smaller pulse. Higher capacitor values are possible, but bring no significant improvements. In the case of the resistor, lower values lead to an excessive bias current and higher values may result in a current too low to properly bias the diode. As for the inductor, lower values result in narrower pulses but with some ringing and higher values lead to wider pulses, mainly because of a slower return to 0. In addition, a higher inductor is most likely to have a higher parasitic resistance. The simulation considered in this subsection was done in ADS (transient analysis, using the 2011.05 version). The PIN diode was modelled based on the diode parameters and package parasitics made available by Infineon (the manufacturer).

2.2 Passive RFID tag

The pulse generator was originally designed to be connected to the RFID tag shown in Fig. 4 (see [8]). This tag converts RF energy at 866.6 MHz to DC using a multi-level charge pump and a low-dropout voltage regulator of 1.8 V (hence the 1.8 V used in the previous simulation). In terms of processing capabilities, it includes a 16-bit flash MCU from the MSP430 series, model F2132. The I/O pin from this tag that was used as the input for the pulse generator was modelled in simulation as a step generator with a negative slope of 1.8 V per 5 ns followed by a series resistance of 0.9 Ω.

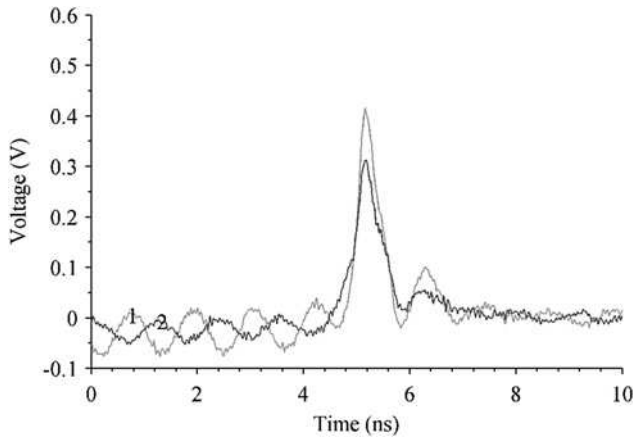

Fig. 5 *Pulse generated by the proposed UWB pulse generator, in response to a high-to-low transition (1.8 V to 0) produced by the RFID tag*

Curve 1 corresponds to a distance of 1 m and curve 2 corresponds to a distance of 2.6 m

3 Experimental results

Fig. 5 shows the response of the UWB pulse generator to a 1.8 V to 0 transition produced by the RFID tag. In this test, the pulse generator was connected to the tag and the tag was programmed to trigger pulses at a rate of 1 per second. A dipole antenna (the same antenna used in [8]) was attached to the tag to harvest energy from a 2 W_{erp} pure 866.6 MHz source placed nearby, in direct line of sight. Both the power source and the tag were always kept at a distance of ∼1 m to the floor and at least 1 m to all other obstacles. The output of the pulse generator was measured with a Tektronix MSO71604C oscilloscope. The pulses represented in the figure were measured at the distances of 1 and 2.6 m from the power source. It was found that the tag is able to consistently generate pulses at up to 2.6 m. At some higher distances it was also possible to detect pulses but not consistently, most likely because of multipath (as the measurements were carried out indoors). Although the shape of the pulses obtained in practice is generally similar to the pulses obtained in simulation there are differences in terms of duration and amplitude (especially amplitude). This result was not unexpected since the currents shown in Fig. 3 are limited in practice by the energy available in the tag and the maximum rate at which the tag is able to deliver that energy to the pulse generator. As a last note, the oscillations visible in the figure are the result of some of the signal from the power source being picked up by the pulse generator.

4 Conclusions and future work

One of the most important conclusions from this work is that it is possible to build a low-power UWB pulse generator very inexpensively, using only a PIN diode and a few passive components. As demonstrated, the proposed pulse generator can be used in conjunction with passive RFID tags because of its reduced power consumption. Future work will focus on improving the pulse in terms of amplitude and duration and also trying to generate more complex pulse shapes, such as monocycles and doublets, without compromising power consumption.

5 Acknowledgments

This work was fully supported by the FCT, the Portuguese Foundation for Science and Technology, in particular by the doctoral grant SFRH/BD/69392/2010.

6 References

1 Dardari, D., D'Errico, R., Roblin, C., Sibille, A., Win, M.: 'Ultrawide bandwidth rfid: the next generation?', *Proc. IEEE*, 2010, **98**, (9), pp. 1570–1582
2 Ryckaert, J., Desset, C., Fort, A., *et al.*: 'Ultra-wide-band transmitter for low-power wireless body area networks: design and evaluation', *IEEE Trans. Circuits Syst. I, Regul. Pap.*, 2005, **52**, (12), pp. 2515–2525
3 Turcu, C. (Ed.): 'Development and implementation of RFID technology' (I-Tech Education and Publishing, Vienna, Austria, 2009)
4 Zhou, Y., Law, C.L., Xia, J.: 'Ultra low-power rfid tag with precision localization using ir-uwb'. IEEE MTT-S Int. Microwave Symp. Digest (MTT), 2011, June 2011, pp. 1–4
5 Nikookar, H., Prasad, R.: 'Introduction to ultra wideband for wireless communications' (Springer Publishing Company, Incorporated, 2008, 1st edn.)
6 De Angelis, A., Dionigi, M., Giglietti, R., Carbone, P.: 'Experimental comparison of low-cost sub-nanosecond pulse generators', *IEEE Trans. Instrum. Meas.*, 2011, **60**, (1), pp. 310–318
7 Wei, Y.Y.: 'Ultra wideband signal generation', *Microw. J.*, 2005, **48**, (9), pp. 172–184
8 Fernandes, R., Carvalho, N., Matos, J.: 'Design of a battery-free wireless sensor node'. IEEE EUROCON – Int. Conf. on Computer as a Tool (EUROCON), 2011, April 2011, pp. 1–4

Design of a Battery-free Wireless Sensor Node

Ricardo Dias Fernandes, Nuno Borges Carvalho, João N. Matos
Departamento de Electrónica, Telecomunicações e Informática,
Instituto de Telecomunicações,
Universidade de Aveiro

***Abstract*—In this paper, a battery-free wireless sensor designed to harvest energy from electromagnetic waves at 866.6MHz and its detachable antenna system are described, with an emphasis on high frequency front-end design. In addition to having no local power source, the proposed sensor node is programmable, since it integrates a general-purpose microcontroller. Other features of the device are a standard 50Ω port and an interface for debugging and expansion, with of a total of 26 pins. In practice, the proposed system is capable of carrying out communication and processing tasks at up to a distance of 4.1 meters away from a transmitter antenna operating within the limits imposed by local regulatory entities, with respect to radiated power. Uplink communication is achieved using modulated backscattering. The proposed antenna system consists of a printed dipole-based antenna, with an overall efficiency in the order of 96%.**

I. Introduction

Wireless sensor networks (WSNs) often consist of a number of small-sized sensors scattered over an area in which a certain physical phenomenon is to be sensed or measured. Wireless sensors currently include controllers optimized for low-power operation that support various operating modes, and with the ability to jump from a deep sleep state to a fully active mode both quickly and seamlessly. Moreover, most of these devices have various power switches that cut the power to peripheral hardware modules, in case their controller determines those to be unnecessary at a given moment of time. But of course, this delicate management of energy is only achievable if a suitable set of software routines are loaded onto them. These routines, usually referred to as energy-aware software routines, basically instruct the controller to minimize its power consumption as much as possible, while still ensuring a minimum wireless awareness, so that incoming transmissions can be received and responded to (in case that is necessary). When combined with energy-efficient communication devices, these advancements in hardware and software design effectively reduce the power consumption requirements of sensor nodes, not only allowing them to operate autonomously for significant periods of time that can actually stretch up to a few years, but also creating a major opportunity for the use of energy harvesting systems, especially since the primary challenge in WSN deployment is still the limited network lifetime due to finite capacity power sources, that is, batteries (in [1], many design questions that relate to WSNs are identified and discussed, not only in terms of hardware, but also in terms of networking protocols and software algorithms).

The conventional communication model of WSNs assumes the deployment of low-power multifunctional wireless sensor nodes operating on the limited power capacity of disposable batteries. Although this model works decently in small WSNs comprised of a small number of wireless nodes, it does not scale very well, and as a matter of fact, it is easy to understand that the potential maintenance cost of replacing batteries for a few hundreds of nodes quickly becomes a continuous and cost-prohibitive undertaking. Considering for instance no more than a couple hundred wireless sensor nodes, each one capable of unattended operation for roughly one year before its power source collapses, the maintenance costs immediately begin to escalate because of the (unavoidable) need to replace batteries every few days, on average. Battery replacements occurring at such a fast pace can easily represent an unsustainable cost for many applications.

Maintaing battery-operated sensor nodes in hard-to-service locations creates yet another significant challenge. In this not so unrealistic scenario, maintenance operations become much more difficult to accomplish and hence more expensive, thus adding a substantial cost to the already high cost of replacing batteries. In fact, this problem can even limit where the sensors are placed (in case they are not deployed randomly, because that would introduce further issues), potentially reducing the effectiveness of the overall deployment. Moreover, for WSNs to achieve a true ubiquitous deployment, the size of the nodes has to decrease dramatically. Small batteries and appropriate form factors indeed help minimize the size of a sensor node, but generally contain less energy than other (more traditional) larger batteries and thus have shorter life spans.

In short, the need shared by most wireless sensor nodes for longer lifetimes and smaller sizes does not match particularly well with the power density of current battery technology, and even though substantial improvements have indeed ocurred in other hardware modules, those have not yet ocurred in battery technology, and no significant changes are antecipated for now (in [2], energy harvesting is seen as a promising new approach precisely because batteries are currently not progressing at the same rate that other hardware components are).

Electromagnetic energy harvesting, frequently also referred to as Radio Frequency (RF) energy harvesting, allows sensors to be used in inaccessible or hazardous areas, or in locations where battery replacements are impractical. With the capacity to power multiple devices from a single RF power source, this solution allows WSNs to scale by supplying maintenance-free power for hundreds or thousands of sensor nodes. Moreover, other alternative energy sources such as solar, piezoelectric or thermal share the limitation of being reliant on ambient energy

sources that are generally beyond control. Since in a solution based on RF harvesting power can be replenished as desired (either continuously or not), no such issues arise.

A. Wireless Passive Sensor Networks (WPSNs)

Unlike conventional wireless sensor nodes, wireless passive sensor nodes are fed remotely by an external RF power source and remain functioning as long as energy is delivered in. By definition, passive sensor nodes have no batteries (or any other disposable part) and use modulated backscatter to send data to sink devices, which can be the same devices that supply power to them or not. Moreover, there may be various power sources operating in a single network (advantages and disadvantages of different powering topologies and many other subjects related to this paradigm are discussed in [3]). If no RF power sources are active at a given moment of time, the energy accumulated in the passive sensor nodes eventually depletes, at which time they cease to function. Once a sufficient amount of energy is accumulated as a result of energy harvesting, the nodes start to function once again.

In hardware, a passive sensor node deviates from a typical sensor node on the power unit and on the transceiver, but other than those, there are no significant differences. Passive sensor nodes have energy harvesters instead of traditional batteries, and backscatter modulators instead of active transmitters. The new functional blocks are widely used in the design of passive Radio Frequency Identification (RFID) tags.

B. RFID Sensor Networks (RSNs)

A typical RFID system is composed of one or more readers and many tags which, by definition, are attached to the objects they are meant to identify. A reader radiates power to tags in its wireless range and also communicates with them in order to collect information about objects, normally in the form of an alphanumeric identification code. In order to make the tags cheap enough to be mass-produced, these systems shift nearly all complexity towards the side of the readers. Moreover, and since there are no batteries involved, passive tags can be made reliable, paper-thin and often physically flexible. The absence of a battery is also the primary reason for which these tags do not have active transmitters built into them. By itself, the energy harvester would not be able to adequately compensate the significant power consumption of this device (compared to other components within the tag). Instead, passive tags use backscatter modulators, which allow them to transmit data at little power expense (additional information related with other types of tags, coupling methods, and other subjects concerning the basics of RFID can be found in [4]).

The antenna of a tag is usually designed to match its input impedance, in order to maximize the power transfer between the two, however, when the tag wants to transmit information to the reader, it deliberately modifies the load impedance seen by its antenna, thus making the latter re-radiate a portion of the incoming power back. By switching between these two states according to a data stream, an amplitude-modulated response can be generated. It is this controlled reflection of waves that is called modulated backscatter (modulations in amplitude are the most widely used in passive tags, phase modulations are also realizable, as explained in [5]).

While traditional passive tags find uses in a vast number of applications (where low price outweighs functionality), a new class of sensor-enhanced passive tags is emerging. These tags are able to report back to RFID readers not only their (static) identification numbers, but also the dynamic data collected by their sensors (in [6], the research challenges associated with these networks are discussed).

II. System overview

The developed sensor node, whose layout is shown (using a 1:1 scale) in figure 1, is made of a RO4003C high frequency laminate having a thickness of 0.813mm and layers of copper on both sides. Solely commercial off-the-shelf hardware parts were utilized in the design of the device. More information is available in [7].

Like many other wireless sensor nodes, the proposed device was designed to operate inside an Industrial Scientific Medical (ISM) band, in this particular case, the band that ranges from 865 to 867.6MHz. From within this band, only a small portion of spectrum ranging from 865.6 to 867.6MHz was of interest because of its higher radiated power limit of 2W$_{\text{erp}}$ (maximum radiated power levels for distinct frequency bands and distinct countries can be found in [4]).

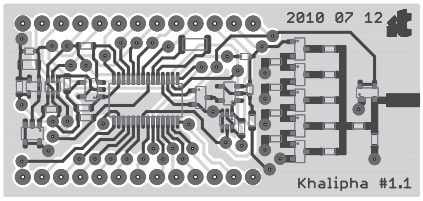

Fig. 1. Physical layout of the proposed sensor node (shown on a 1:1 scale), in which dark-colored lines refer to the top copper layer, lighter areas and lines refer to the bottom layer, circular shapes represent vias, and other drawings (also drawn with lighter colors) identify component outlines. At the right side of the figure is a wider line segment, designed to accomodate an edge-mount 50Ω SMA connector, and at the top and bottom sides, the vias were designed to be soldered to standard 2.54mm (0.1 inch) pitch pin headers.

In addition to having a wireless power supply, the proposed sensor node integrates a general-purpose, fully programmable 16-bit flash microcontroller, a MSP430F2132. This device is well suited to meet the stringent power requirements imposed by the lack of an onboard power source on the node, since it has various operating modes, a minimum current consumption of only 0.1μA, and does not take long to switch from a sleep state to an fully active mode. Other important features include an operating frequency of up to 6MHz with a supply voltage of 1.8V, a total of 8KB of built-in flash memory, and also a very flexible clock system (more information on the MSP430 platform can be found in [8], [9] and [10]).

As can be viewed in the layout, various signals from within the sensor node were connected to either one or another of the rows of larger vias (containing 13 pins each), in order to allow the microcontroller to be programmed as desired, to simplify

hardware debugging, and also to provide a support for testing new hardware.

A. Functional blocks

The block diagram of the proposed wireless sensor node is shown in figure 2. In the sensor node, when a signal is captured by the antenna block, it goes through the impedance matching block, then entering the energy harvester. In conjunction with the voltage regulator, the energy harvester rectifies the received energy into a regulated voltage to power the sensor. Connected directly to the output of the power harvester, the demodulator extracts a data stream from the incoming carrier wave (in case the latter is modulated). The extracted baseband waveform is then read and interpreted by the microcontroller. Uplink data is sent via the backscatter modulator, which was implemented with a single transistor acting as a binary switch (the transistor itself is clearly visible at the right side of the layout).

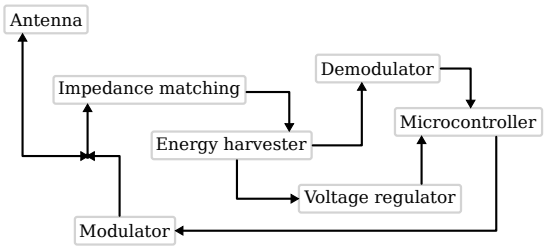

Fig. 2. Block diagram of the proposed wireless sensor node (in which the arrow tips indicate in which directions power, data, or both, depending on the context, are permitted to flow).

Additional functional modules that were integrated into the sensor node include:

- a voltage protection module based on a Transient Voltage Suppressor (TVS) diode, meant to protect sensitive parts from voltage spikes;
- an energy storage module, consisting on a single 6.8μF capacitor;
- a supply voltage supervisor, to guarantee that the sensor node enters active mode only when a suitable voltage is accumulated at the storage capacitor;
- and a memory module based on an Electrically Erasable Programmable Read-Only Memory (EEPROM) memory chip (since the flash built into the MSP430F2132 cannot be written to at a supply voltage of 1.8V) of 1KB.

It is important to mention that some of the circuits utilized in the proposed sensor node were based on those of the Intel Wireless Identification and Sensing Platform (WISP), which is a notable example of a sensor-enhanced RFID tag (additional information regarding the most recent WISP platforms can be found in [11]).

B. High frequency front-end

The simulation model that is shown in figure 3 was created to mimic the behavior of the sensor node in terms of energy harvesting. The model was designed in the Advanced Design System (ADS) simulator, using blocks available in databases related to microstrip lines and lumped components, except for the diodes, which were modeled based upon the information contained in [12], related to the diodes themselves, and [13], related to their packaged versions.

The diode chain is a multi-stage voltage multiplier, known as the Dickson charge pump.

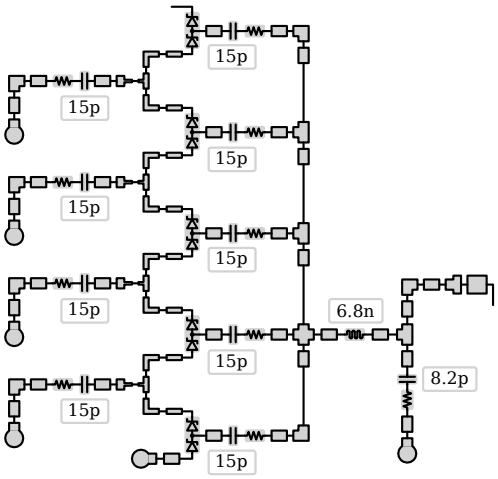

Fig. 3. Simulation model representing the front-end of the proposed sensor node, in which parasitic resistances are either added in the form of resistors (0.2Ω in case of the capacitors), or included directly into the components to which they refer to (4.11Ω in case of the inductor).

The load that was connected to the output of the simulation model was essentially comprised of the storage capacitor and an ideal current source, whose value was set according to the estimated maximum current consumption of the sensor at the mode of operation that minimizes the consumed power, in this case 5μA.

C. Antenna

The proposed antenna, shown in figure 4 (on a 1:2 scale), is a printed antenna, based on the traditional half-wave dipole, and made of a 0.8mm thick layer of FR4.

Both the antenna itself and an edge-mount SMA connector were modeled using the High Frequency Structure Simulator (HFSS) and the resulting three-dimensional model was tuned for maximum efficiency. In order to do this, several degrees of freedom were explored, which included varying the length and width of the arms of the dipole, creating copper areas at its tips and modifying those at its center, sliding one arm over the other, adding parasitic copper shapes, and so forth.

Fig. 4. Physical layout of the proposed antenna (on a 1:2 scale), in which the large rectangular area corresponds to a substrate board and the copper shapes represent a pair of radiating structures, printed on opposite sides of the board.

In addition to its eficiency in the order of 96% (achieved in simulation, and not the result of an actual measurement), the antenna was verified to be affected by the size of the substrate in which it is built on, but not by dielectric constant variations

or significant loss tangents (which were the reasons why FR4 could be used without causing any major efficiency loss).

III. Experimental results

Figure 5 presents the voltage harvested by the sensor node under different input power conditions. In this test, the device was attached to a signal generator setup to output a sinusoid at 866.6MHz. The output power was then slowly varied first from -12 to 2dBm, and then from 2 back to -12dBm, staying for a few seconds at each measurement point and then taking the average voltage harvested in that time window. During this test, the sensor was prevented to switch to active mode.

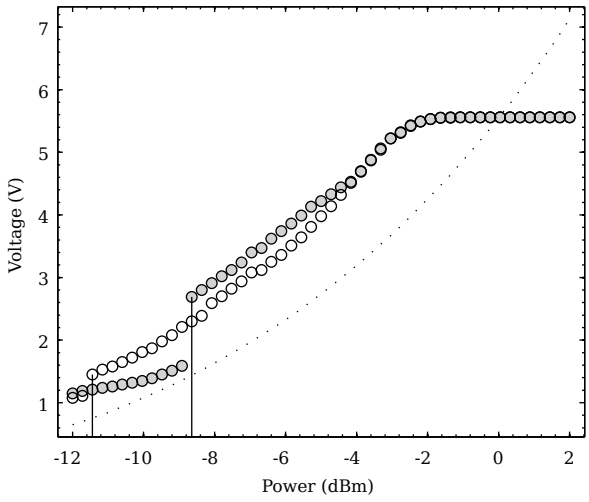

Fig. 5. Voltage measured at the storage capacitor within the sensor node in function of increasing and decreasing input power levels (plotted with filled and empty circles, respectively), in comparison to the predicted results, and considering a sinousoidal waveform at 866.6MHz. Solid lines were plotted to highlight points located at -11.44 and -8.64dBm.

The figure demonstrates that the results obtained in practice follow the predicted results, and with higher values, which is not unreasonable, since a worst-case scenario was assumed in the design of the sensor node. Also, there is a clear hysteresis behavior in the harvested voltage, meaning that for a certain number of power levels the node can either be turned on or turned off, depending on its power history. Also in the figure, the minimum power that the sensor node requires to turn on and the power below which it is no longer able to sustain its sleep mode are both highlighted. Finally, at higher power levels (more or less above -2dBm), the effect of the transient voltage suppression diode is clearly visible. It is important to note that the predicted curve shows no clipping only because that diode was not included into the simulation model.

With its antenna attached, the sensor node was tested with a circularly polarized antenna having a gain of 5.5dBil (taken from a commercial RFID reader) and setup to radiate a $2W_{erp}$ sinusoid at 866.6MHz, and was found to sustain operation at up to 4.1 meters away, still below the 5.4 meters yielded by the Friis formula, but a reasonable result (calculations were carried out considering the developed antenna to have the gain of a traditional half-wave dipole and the received power to be equal to the turn on threshold measured for the node).

IV. Conclusion

It is almost ironic that the same hardware component which enabled (and that in many cases still enables) sensor nodes to operate wirelessly is now hindering their natural evolution towards smaller sizes and longer lifetimes. That is the reason why a new class of sensor nodes that contain no batteries and harvest their energy from electromagnetic waves is emerging, and it is to this class that the wireless sensor node discussed in this paper belongs.

In its current state, the developed wireless sensor node can already be used for experimenting with new software and new hardware through the interfaces it provides, but the device is still very underexplored. Future improvements may lead to an extended range, a smaller size, and more functionality.

References

[1] I. Akyildiz, W. Su, Y. Sankarasubramaniam, and E. Cayirci, "A survey on sensor networks," *Communications Magazine, IEEE*, vol. 40, no. 8, pp. 102 – 114, aug 2002.

[2] R. Want, K. Farkas, and C. Narayanaswami, "Guest editors' introduction: Energy harvesting and conservation," *Pervasive Computing, IEEE*, vol. 4, no. 1, pp. 14 – 17, jan. 2005.

[3] O. Akan, M. Isik, and B. Baykal, "Wireless passive sensor networks," *Communications Magazine, IEEE*, vol. 47, no. 8, pp. 92 –99, august 2009.

[4] V. Chawla and D. S. Ha, "An overview of passive rfid," *Communications Magazine, IEEE*, vol. 45, no. 9, pp. 11 –17, september 2007.

[5] J.-P. Curty, M. Declercq, C. Dehollain, and N. Joehl, *Design and Optimization of passive UHF RFID Systems*. New York: Springer, 2006.

[6] A. S. Michael Buettner, Ben Greenstein and J. R. Smith, "Revisiting smart dust with rfid sensor networks," in *Seventh ACM Workshop on Hot Topics in Networks (HotNets-VII)*, October 2008.

[7] R. D. Fernandes, "Design of a battery-free wireless sensor node," Master's thesis, Universidade de Aveiro, 2010.

[8] *MSP430F21x2 Mixed Signal Microcontroller*, Rev. g ed., Texas Instruments, December 2009.

[9] *MSP430x2xx Family User's Guide*, Texas Instruments, 2008.

[10] J. H. Davies, *MSP430 Microcontroller Basics*. Newton, MA, USA: Newnes, 2008.

[11] D. Yeager, P. Powledge, R. Prasad, D. Wetherall, and J. Smith, "Wirelessly-charged uhf tags for sensor data collection," apr. 2008, pp. 320 –327.

[12] *HSMS-2850 Series - Surface Mount Zero Bias Schottky Detector Diodes*, Agilent Technologies, 1999.

[13] *Application Note 1124 - Linear Models for Diode Surface Mount Packages*, Hewlett-Packard, 1997.

Increasing the Range of Wireless Passive Sensor Nodes using Multisines

Ricardo Dias Fernandes, Alírio S. Boaventura, Nuno Borges Carvalho, João N. Matos
Departamento de Electrónica, Telecomunicações e Informática,
Instituto de Telecomunicações,
Universidade de Aveiro

***Abstract*—Wireless Sensor Networks (WSNs) usually consist of battery-powered nodes. Therefore, once the batteries deplete, the networks collapse. Passive sensor nodes are immune to this kind of problem because they do not have batteries, but on the other hand, their range is significantly shorter. This paper shows that this range can be enhanced (in a noticeable manner) if the Radio Frequency (RF) source that powers the nodes is set up to radiate a multisine waveform instead of a pure sinusoid, considering the same average power. The passive sensor used to demonstrate the usefulness of combining multiple sinusoidal waveforms is based on a low-power 16-bit microcontroller, and includes circuits for bi-directional wireless binary communication (envelope detection for downlink, backscatter for uplink). The sensor also features a 50Ω antenna port and an interface for debugging and expansion composed of 26 pins. Considering a power source of 2W$_{erp}$, the maximum range of the wireless sensor (together with a half-wave dipole antenna) is 5.3 meters.**

I. Introduction

Current wireless sensor nodes include controllers optimized for low-power operation and a number of power switches that can interrupt the power supply to peripheral hardware modules whenever necessary. In addition, carefully designed software routines ensure that the node's energy consumption is always kept as low as possible, by disabling non-essential functional modules, and by making use of the controller's power-saving mechanisms. However, one of the most substantial challenges in the design of these devices is still increasing their lifetime without having to increase their size or weight (that would be the most likely outcome of using higher-capacity batteries to power the nodes). Further information regarding other design issues in Wireless Sensor Networks (WSNs) can be found, in the form of a survey, in [1].

The model that most sensor networks use assumes that the nodes are powered by disposable batteries. In fact, this model is suitable for small networks but it does not scale well, since maintenance costs rise quickly as more nodes are added. The need to replace batteries almost continuously creates a critical problem for any application.

Maintaing battery-operated sensor nodes in hard-to-service locations creates yet another significant challenge. In this (not so unrealistic) scenario, maintenance operations become much more difficult to accomplish and hence more expensive, thus adding a substantial cost to the already high cost of replacing batteries. In addition, this can even limit where the nodes are placed, therefore potentially reducing the effectiveness of the overall deployment. Also very importantly, for these networks to become ubiquitous, the size of the nodes has to decrease in a significant manner. Smaller batteries help minimize the size of the nodes, but generally contain less energy in comparison to their larger counterparts.

In short, the need shared by most wireless nodes for longer lifetimes and smaller sizes and the power density of currently available battery technology do not match, at least for the time being. In addition, even though substantial improvements have ocurred in other hardware modules, those improvements have not yet ocurred in battery technology, and no drastic changes are anticipated for now, according to [2]. This is precisely one of the reasons why the process of harvesting energy from the is becoming quite important.

Electromagnetic energy harvesting, frequently also referred to as Radio Frequency (RF) energy harvesting, allows sensors to be placed in inaccessible or hazardous areas, or in locations where battery replacements are impractical. With the capacity to power multiple devices from a single RF power source, this solution allows WSNs to scale by supplying maintenance-free power for hundreds of nodes, simultaneously. Additionally, in a solution based on electromagnetic energy harvesting, power can be replenished as desired. Other kinds of energy, such as solar, piezoelectric or thermal do not share this feature, since they rely on ambient energy sources that are generally beyond any control.

Passive sensor-enhanced wireless nodes are introduced and briefly decribed in the section that follows. In the subsequent sections, the passive node used in measurements is presented and the practical results are shown (and discussed).

II. Passive sensor devices

It is true that battery-powered sensor nodes usually outpace passive nodes in terms of maximum range. Yet, it is also true that passive nodes eliminate one of the most critical problems in sensor networks.

A. Wireless Passive Sensor Networks (WPSNs)

Unlike conventional wireless sensor nodes, wireless passive sensor nodes are fed remotely by an external RF power source and remain functioning as long as energy is delivered in. By definition, passive sensor nodes have no batteries (or any other disposable part) and use modulated backscatter to send data to sink devices, which can be the same devices that supply power to them or not. Moreover, there may be various power sources

978-1-4577-0027-9/11/$26.00 ©2011 IEEE

operating in a single network (advantages and disadvantages of different powering topologies and many other subjects related to this paradigm are discussed in [3]). If no RF power sources are active at a given moment of time, the energy accumulated in the passive sensor nodes eventually depletes, at which time they cease to function. Once a sufficient amount of energy is accumulated as a result of energy harvesting, the nodes begin to operate once again.

In terms of hardware design, a passive sensor node deviates from the typical sensor node on the power unit and transceiver but other than those there are no major differences. Instead of having a battery, passive sensors have an energy harvester, and instead of having an active transmitter, they have a backscatter modulator. It is worth to note that these new functional blocks are widely employed in the design of passive Radio Frequency IDentification (RFID) tags.

B. RFID Sensor Networks (RSNs)

The typical RFID system consists of one reader and a large number of tags. The reader interrogates the tags located within its range, in order to extract their identification codes (via RF waves). Since each tag is attached to a different object and all the codes are different, each object can be uniquely associated to a code.

The tags are usually battery-free, and therefore can be made reliable, paper-thin and often physically flexible. They have to be simple in order to be inexpensive (and therefore well suited for mass production). As a matter of fact, in RFID, nearly all complexity is at the reader's side. The tags extract energy from the radio waves radiated by the reader and use that energy to reply back, not by using active transmitters (since these would most likely deplete the tags' energy reserves in a short amount of time), but by using backscatter modulators. The latter enable the tags to send information back to the reader at little energy expense. Additional information regarding the basics of RFID can be found in [4].

While traditional passive tags find uses in a vast number of applications (where low price outweighs functionality), a new class of sensor-enhanced passive tags is emerging. These tags are able to report back to RFID readers not only their (static) identification numbers, but also the dynamic data collected by their sensors (some of the research challenges related to these networks are discussed in [5]).

C. Using multisines to improve range

Considering either passive wireless sensors or passive RFID tags, range is something of major importance. One method to increase it is to increase the power output at the transmitting antenna up to the threshold imposed by regulatory entities. A second method consists in designing the nodes (or tags) to be as efficient as possible in order to reduce power losses. A third method that can be used to increase range consists in shaping the amplitude of the transmitted RF signal in a way that takes advantage of the non-linear behavior of energy harvesters that are voltage multiplier-based. Multisine signals can be used for this purpose. As theoretically demonstrated in [6], if all of the frequency components of a multisine signal are phase-aligned and of equal power, the resulting non-constant envelope causes the energy harvesters to operate more efficiently, compared to a pure sinusoidal wave, for the same average power. In [7], it is shown that multisine signals can indeed improve the range of passive RFID systems.

III. System overview

The wireless node used in this work was designed to operate at a narrow band located between 865.6 and 867.7MHz. In this particular band, the maximum radiated power is higher (hence the choice), and set to 2W$_{erp}$. European RFID readers use this band as well (for the same reason). It is important to note that radio regulations can change in a significant manner from one country (or region) to another, as can be seen in [4]. The node is made of a 0.813mm thick RO4003C board and uses solely commercial off-the-shelf parts. The layout of the sensor node is shown in figure 1.

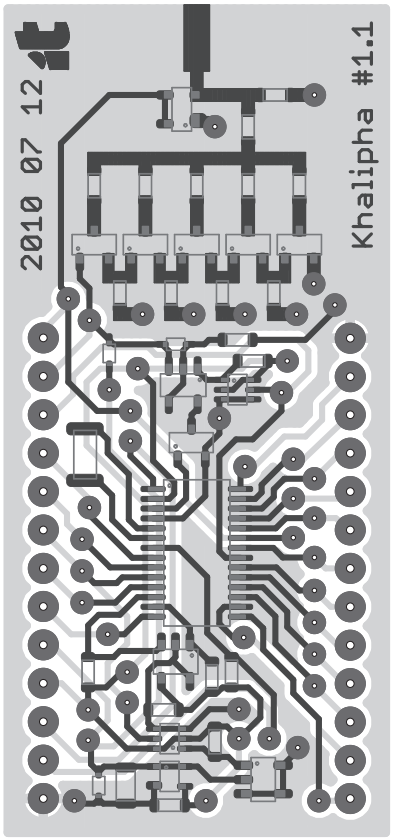

Fig. 1. Physical layout of the wireless node (shown on a 2:1 scale). In this layout, the dark-colored lines refer to the top copper layer, the lighter areas and lines refer to the bottom layer, and the round shapes represent vias. The remaining drawings identify the outlines of the components. At the top side of the layout is a wider line segment designed to accomodate an edge-mount 50Ω SMA connector. The larger vias were designed to be soldered to 2.54mm (0.1 inch) pitch pin headers.

At the center of the layout is a 28-pin flash microcontroller responsible for managing the entire node. The MSP430F2132 is able to operate in several modes, and consumes only 0.1μA at the deepest sleep mode. Furthermore, it can operate at up to

6MHz with a supply voltage of 1.8V and does not need much time to switch from a sleep state to a fully active mode. Other important features include 8kB of built-in flash memory and a very flexible clock system.

As the layout shows, the node integrates two rows of larger vias (containing 13 pins each). These allow the microcontroller to be programmed as desired, provide support for testing new hardware, and also facilitate access to key signals (something that is extremely useful for debugging).

A. Functional blocks

The block diagram of the wireless sensor node is shown in figure 2.

Once the sensor node's antenna captures a signal, that signal passes through the impedance matching block and then enters the energy harvester. The latter and the voltage regulator then convert the received energy into a regulated voltage to power the sensor. The energy harvester's output is also connected to the demodulator, so that a data stream can be extracted from the carrier wave. The baseband waveform at the output of the demodulator is then read by the microcontroller. Uplink data is sent via the backscatter modulator.

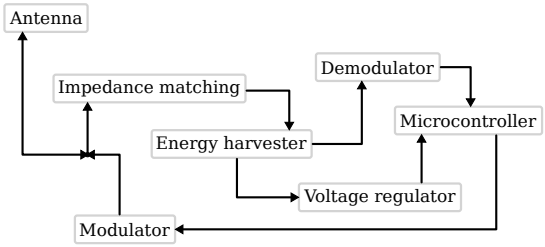

Fig. 2. Block diagram of the sensor node (in which the arrow tips indicate in which directions power, data, or both, depending on the context, are permitted to flow).

Additional functional modules that were integrated into the sensor node include:

- a voltage protection module based on a Transient Voltage Suppressor (TVS) diode, meant to protect sensitive parts from voltage spikes;
- an energy storage module, consisting on a single 6.8μF capacitor;
- a supply voltage supervisor, in order to guarantee that the node becomes active only when an appropriate voltage is accumulated at the storage capacitor;
- and a memory module based on an Electrically Erasable Programmable Read-Only Memory (EEPROM) memory chip of 1kB (since the flash built into the MSP430F2132 cannot be written to at 1.8V).

It should be noted that some circuits used in this node were based on the ones used in the Intel Wireless Identification and Sensing Platform (WISP). Further information on this project can be found in [8].

B. High frequency front-end

The front-end of the sensor node is composed of a matching network and a multi-stage voltage multiplier, several parasitic resistances, and a number of microstrip lines, as illustrated in figure 3.

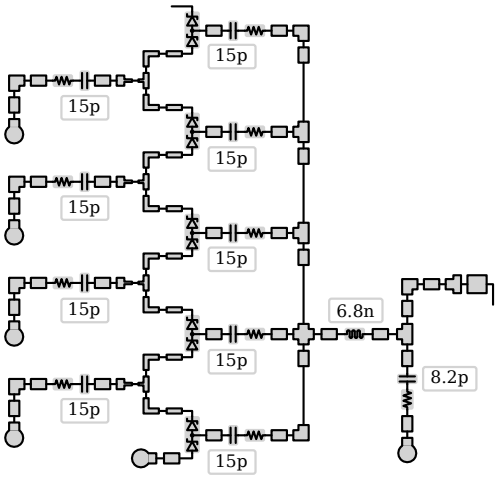

Fig. 3. Simulation model representing the front-end of the wireless sensor node, in which parasitic resistances are either added in the form of resistors (0.2Ω in case of the capacitors), or included directly into the components to which they refer to (4.11Ω in case of the inductor).

The values for the inductor and for the capacitors shown in the figure were determined via simulation, considering a load composed of the storage capacitor (mentioned earlier) placed in parallel with an ideal current source of 5μA. This particular value represents the estimated maximum current consumption of the entire node at the deepest sleep mode. The diodes used in the voltage multiplier were modeled as recommended in [9] and [10]. Furthermore, the matching network was designed so that the node would have an input impedance as close to 50Ω as possible.

C. Antenna

The node's antenna was based on the half-wave dipole, and its layout is shown in figure 4.

The antenna was designed to be highly efficient (for a 50Ω interface) and omnidireccional. The actual antenna is made of a 0.8mm thick FR4 layer. In simulation, an efficiency of 96% was obtained.

Fig. 4. Physical layout of the node's antenna (on a 1:2 scale). The antenna consists of a pair of radiating arms printed on a rectangular-shaped substrate board (one arm printed on each side).

Further information regarding this antenna or the described node is available in [11].

IV. Experimental results

Figure 5 shows the voltage harvested by the sensor node as a function of the RF input power.

In this test, the node was stimulated with a multisine signal with content located at 865.7, 866.3, 866.9 and 867.6MHz. In addition, the node was also tested with a pure sinusoidal wave

at 866.6MHz. For both signals, the power was varied from -15 to -1dBm and then from -1dBm back to -15dBm. It should be noted that during these tests the node was forced to remain at the deepest sleep mode.

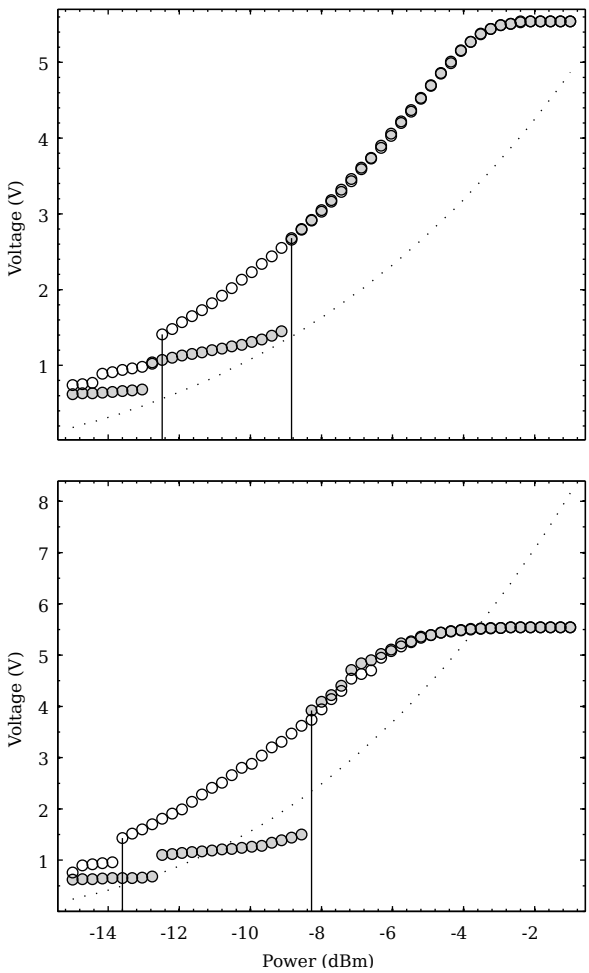

Fig. 5. Voltage measured at the storage capacitor inside the sensor node in function of increasing and decreasing input power levels (plotted with filled and empty circles, respectively), in comparison to the predicted results. The upper graph shows 1 tone data and the lower graph shows 4 tone data. Solid vertical lines were plotted to highlight points located at -13.60, -12.48, -8.84 and -8.28dBm.

The graphs illustrate a number of important aspects related to the behavior of the sensor node. First, the voltage measured in practice was higher than predicted. This was not a surprise since a worst-case scenario was assumed in the design of the node, in terms of quiescent currents and quality factors (both extracted from datasheets). Second, there is a clear hysteresis behavior, meaning that for a certain number of power levels the node can be either turned on or turned off, depending on its power history. Third, for higher power levels (more or less above -2dBm) the clamping effect of the TVS diode becomes clearly visible. The predicted curves does not exhibit that kind of behavior simply because the TVS diode was not taken into account in the simulation model. Finally, the graphs show that the use of 4 tones instead of 1 indeed increases the harvested voltage and decreases the turn off voltage threshold, yet it also increases (albeit slightly) the turn on voltage threshold (these thresholds are represented by the solid lines).

A. Operating distance in practice

The experimental setup utilized for measuring the range of the sensor node was comprised of a signal generator, a power amplifier and a circularly polarized patch antenna with a gain of 5.5dBil. The antenna was taken from a commercial passive RFID system. On the sensor's side, the firmware was changed and new hardware was added, in this case a LED. In order to cause the LED to flash once per second, the sensor node was programmed to switch to active mode twice per second (first to turn the LED on, then off). Under the described experimental conditions, the signal generator was configured to generate a 866.6MHz sine wave with enough power to produce 2W$_{\text{erp}}$ at the antenna. The sensor was then moved away from the power source until the LED stopped blinking, and the corresponding distance was measured. The maximum operating distance was also measured considering 4 tones at the output of the signal generator. In the first case, the sensor ceased to function at 4.1 meters. The use of 4 tones resulted in a maximum distance of 5.3 meters.

V. Conclusion

One of the most relevant disadvantages of battery-operated sensor nodes is that they cease to function once their batteries run out. Passive nodes are not affected by this problem (since they have no batteries), but their range is usually limited to a few meters. This paper has shown that the shape of the signal used to power the sensor nodes has a significant effect on the operating distance. Therefore, it is reasonable to conclude that the wireless range of passive nodes depends not only on how well they are designed (the more energy-efficient they are, the better), but also on how well the waveform that is radiated to them is able to exploit the non-linear behavior of their energy harvesting systems.

Acknowledgment

The authors would like to thank Fundação para a Ciência e Tecnologia (doctoral grant SFRH/BD/69392/2010 and project ID PTDC/EEA-TEL/099646/2008) and also Portugal Telecom Inovação (GreenTel project) for the financial support provided during the course of this work.

References

[1] I. Akyildiz, W. Su, Y. Sankarasubramaniam, and E. Cayirci, "A survey on sensor networks," *Communications Magazine, IEEE*, vol. 40, no. 8, pp. 102 – 114, aug 2002.

[2] R. Want, K. Farkas, and C. Narayanaswami, "Guest editors' introduction: Energy harvesting and conservation," *Pervasive Computing, IEEE*, vol. 4, no. 1, pp. 14 – 17, jan. 2005.

[3] O. Akan, M. Isik, and B. Baykal, "Wireless passive sensor networks," *Communications Magazine, IEEE*, vol. 47, no. 8, pp. 92 –99, august 2009.

[4] V. Chawla and D. S. Ha, "An overview of passive rfid," *Communications Magazine, IEEE*, vol. 45, no. 9, pp. 11 –17, september 2007.

[5] A. S. Michael Buettner, Ben Greenstein and J. R. Smith, "Revisiting smart dust with rfid sensor networks," in *Seventh ACM Workshop on Hot Topics in Networks (HotNets-VII)*, October 2008.
[6] A. S. Boaventura and N. B. Carvalho, "Maximizing dc power in energy harvesting circuits using multisine excitation," in *IEEE International Microwave Symposium*, Baltimore, USA, June 2011.
[7] M. Trotter, J. Griffin, and G. Durgin, "Power-optimized waveforms for improving the range and reliability of rfid systems," in *RFID, 2009 IEEE International Conference on*, 2009, pp. 80 –87.
[8] D. Yeager, P. Powledge, R. Prasad, D. Wetherall, and J. Smith, "Wirelessly-charged uhf tags for sensor data collection," apr. 2008, pp. 320 –327.
[9] *HSMS-2850 Series - Surface Mount Zero Bias Schottky Detector Diodes*, Agilent Technologies, 1999.
[10] *Application Note 1124 - Linear Models for Diode Surface Mount Packages*, Hewlett-Packard, 1997.
[11] R. D. Fernandes, "Design of a battery-free wireless sensor node," Master's thesis, Universidade de Aveiro, 2010.